NANOFIBROUS COMPOSITE MESHES FOR SURGICAL TISSUE REGENERATION

PhD thesis

Constantinos Voniatis

Doctoral School of Theoretical and Translational Medicine

Semmelweis University

Supervisors: Angéla Jedlovszky-Hajdú, Ph.D. Andrea Ferencz, MD, Ph.D

Official reviewers: Romána Zelkó, Ph.D, D.Sc
György Marosi, Ph.D, D.Sc

Head of the Complex Examination Committee: Alán Alpár, MD, Ph.D, D.Sc

Members of the Complex Examination Committee: László Cervenák, Ph.D
Mihály Kovács, Ph.D, D.Sc

Budapest
2022

Table of Contents

Abbreviations

AFM	Atom Force Microscopy
ATR/FTIR	Attenuated Total Reflection/Fourier-Transform Infrared Spectroscopy
CD	Cross-linking Degree
CL	Cross-linked
DAB	1,4-Diaminobuthane
DCM	Dichloromethane
DMAc	Dimethylacetamide/ N,N-Dimethylacetamide
DMF	Dimethylformamide/N,N- Dimethylformamide
DMSO	Dimethyl sulfoxide
DNA	Deoxyribonucleic acid
ECM	Extracellular Matrix
EtOH	Ethanol
GDA	Glutaraldehyde
Magn	Magnetite (Fe_3O_4)
PASP	Poly(aspartic acid)
PBS	Phosphate-buffered Saline
PCL	Polycaprolactone
PEG	Polyethylene Glycol
PGS	Poly(glycerol sebacate)
PLA	Poly(lactic acid)
PLGA	Poly(lactic-co-glycolic acid)
PLLA	Poly(lactic acid), D-lactide
PP	Polypropylene
PSI	Polysuccinimide
PTFE	Polytetrafluoroethylene
PVA	Poly(vinyl alcohol)
RNA	Ribonucleic acid
SEM	Scanning Electron Microscopy
THF	Tetrahydrofuran/Oxolane
UV	Ultraviolet Radiation
WCA	Water Contact Angle

Sample Designation and Nomenclature

Co-spun PSI/PVA	Co-electrospun Polysuccinimide/Poly(vinyl alcohol)
Co-spun PSI/PCL	Co-electrospun Polysuccinimide/Polycaprolactone
Blend-spun PSI/PCL	Blend electrospun Polysuccinimide/Polycaprolactone
Layer-spun PSI/PCL	Layered electrospun Polysuccinimide/Polycaprolactone
PSI/PVA-GDA	PSI/PVA Mesh with GDA CL PVA
PSI-DAB/PVA-GDA	PSI/PVA Mesh with DAB CL PSI and GDA CL PVA
PSI-DAB /PCL	PSI/PCL Mesh with DAB CL PSI
PSI-DAB-Magn	PSI Mesh with DAB CL and Magnetite Nanoparticles

1. Introduction

1.1 Foreword

Medicine is, and always has been, a multidisciplinary subject. Today, this is more evident than ever as due to the technological advancements of the past decades, medical research is now rapidly progressing with the simultaneous involvement of several different scientific fields. Researchers with different expertise cooperating and utilizing different methods, techniques and tactics is, what drives medicine forward. Compared to its early days, medicine is exceedingly advanced and together with the evolution of the civilised world had two major intertwined effects: increasing the average life expectancy and increasing the incidence of long-term complications of chronic diseases and disorders.

To solve, or at least manage the latter, medicine is steadily albeit slowly, progressing into the field of personalised and regenerative medicine. Personalised medicine (or precision medicine) aims to tailor treatment and management options specific to the patient's specific genome and molecular predisposition (1,2). Regenerative medicine on the contrary, focuses on the repair and regeneration of damaged or lost tissues following a more generalised approach (3–5).

Often perceived as medicine's ultimate goal, regeneration of tissues is a highly challenging, strenuous, and complex task (6,7). Various approaches, methods, and tactics are being researched and implemented. Amongst them, tissue engineering and the development of tissue scaffolds (i.e., tissue templates) has perhaps the greatest and most promising potential (8–10). A globally accepted effective and promising approach, is the fabrication of polymer-based membranes, meshes or mats composed nano-sized fibres (10,11). In the context of this thesis, membranes, meshes and mats are synonyms with no structural differences apart from an increase in thickness and fibre diameter (membrane < mesh < mat). These materials have a microstructure that resembles the body's innate extracellular matrix, a paramount structure found around almost every human cell and tissue. After implanting such membranes, native cells in the patient's body can adhere, proliferate, and even differentiate on them making them therefore excellent tissue scaffolds (10,12). However, as any material intended for medical and biomedical applications these membranes have serious prerequisites and criteria to fulfil (13).

Fabrication of polymer-based membranes or meshes can be achieved utilising electrospinning (14,15). This technique is commonly described as “simple and versatile” a phrase which rather readily summarises its advantages. While having innumerable options and modifications (14,16), electrospinning in its most basic form is the formation of fibres from polymer solutions via using an electrostatic force gained by a power supply. The most intriguing question however, is which polymer to use and for what application.

The theme of this work is the examination and possible combination of different polymers for the fabrication of advanced functional nanofibrous materials intended for surgical tissue regeneration.

1.2 Medical Devices, Biomaterials, and Implants

A medical device is an instrument, device, equipment, or tool intended to be utilising in patient care. The use of a medical device can be of a diagnostic or therapeutic nature, or in some cases both. Medical device is a broad and rather general term as it encompasses simple tools (e.g., a medical thermometer), disposable items (e.g., sterile gloves), more intricate devices (e.g., an operating room ventilator) and even computer software (e.g., CT or MRI image analysis software). Therefore, a classification system (17) is utilised to group medical devices based on the intended application and but more importantly, according to the risk for the patient (Figure 1).

Whilst this classification system provides a general insight to medical devices, it is rather a set of rules for the proper regulation and legislation of medical devices and does not provide criteria regarding the specific parameters of the devices i.e., biocompatibility standards as compared an ISO regulation (e.g., ISO 13485 ISO 10993, ISO 5832).

Biomaterial is the definition for any material designed, synthesised, and produced specifically intended to contact and in some form interact with a biological system (18). Furthermore, according to IUPAC definition (19) the biological system can be an organism, a living tissue, or even a microorganism. Definitely worth mentioning is the difference between biomaterials and biological materials, the latter originating from a biological source. In this regard biomaterials intended for *in vivo* applications can be Class I, II or III devices (according to EU regulations) depending on the duration of the usage/application and the invasiveness of the procedure.

An implant is defined as an object which is inserted and secured in the body to fulfil a specific purpose (20). In the biomedical field, an implant is a medical device (Class II or III by default) as well as a biomaterial (13,21). Another important distinction is the difference between implants (artificially produced) and transplants (biological materials). A transplant can be an autograft (transplanted from one part of the patient body to another), an allograft (transplanted from one patient to another) or a xenograft (transplanted from another species to a patient). Both implants and transplants have advantages and disadvantages and their application have been extensively discussed in relevant surgical literature. Most notably transplants are perfect as scaffold since the tissue transplanted is identical to the native tissue however, transplants are of limited supply and more often than expected have compatibility issues (host vs graft disease). Implants on the hand, can be mass produced and their compatibility as well their chemical and physical properties are reproducible and well documented. Nonetheless, one fundamental disparity is that implants, being artificially produced have more serious criteria to fulfil compared to transplants.

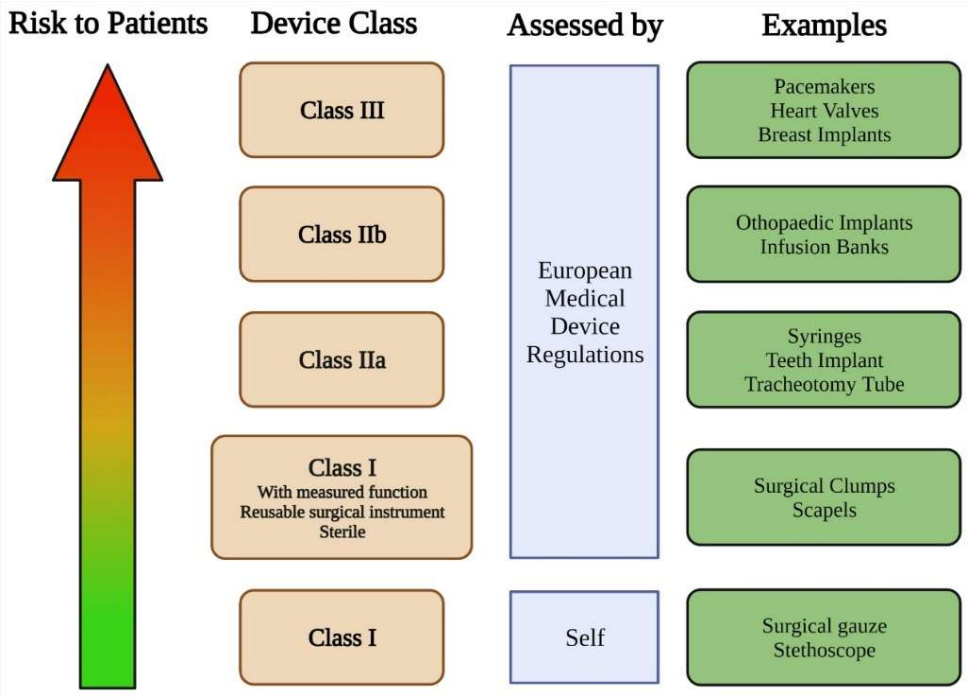

Figure 1. Classification of Medical Devices according to EU regulations.

1.3 Biomaterial Properties

Biomaterials intended to be surgically implanted, have several serious prerequisites to fulfil. Of course, according to the specific application these prerequisites or criteria change, nevertheless, whether polymer-based, metal or ceramic, some features are essential regardless of origin.

Biocompatibility

The most crucial and essential feature of any biomaterial is biocompatibility. Biocompatibility in general terms is the quality of materials to not induce unwanted side-effects e.g., injury, immune response, toxicity, cancer etc. However, the term is rather ambiguous and highly relative to the specific application. For example, while an inflammatory reaction is expected of surgical meshes used in hernia treatment (so that the abdominal wall defect is filled with connective tissue in the long-term and prevent hernia recurrence) (22,23), the same inflammatory reaction and fibrous capsule formation is a major disadvantage for breast implants (24). Therefore, several definitions exist for biocompatibility. Personally, I prefer the one expressed by Professor David F. Williams (25) "*The ability of a material to perform with an appropriate host response in a specific application" which was then extrapolated to "…the ability of a biomaterial to perform its desired function with respect to a medical therapy, without eliciting any undesirable local or systemic effects in the recipient or beneficiary of that therapy, but generating the most appropriate beneficial cellular or tissue response in that specific situation, and optimising the clinically relevant performance of that therapy*". In the context of this work, biocompatibility's definition aligns with Professor Williams's definition as although it seems lengthy, it perfectly summarizes that biocompatibility is relative and always specific to the application in question.

The most prominent paradigm of biocompatibility is the foreign body reaction (26,27). Implanting any material will cause an immune reaction (even the incision made by the surgeon does). The question rather, is how extensive this reaction is going to be. When a material is implanted the body's immune cells attack and attempt to degrade it as soon as possible. This process (Figure 2) progresses from protein adsorption to accumulation and infiltration of leukocytes to the infamous foreign body cell formation and finally if the degradation attempt is not effective a fibrotic capsule formation begins to surround and isolate the implant (28). These capsule formations can cause severe

complications as not only hinders the function of the implant but can also contract or even calcify (29,30). The chemical and biological background of this process is well documented, and it is evident that not only the origin of the materials that compose the implant are important but also the microstructure, surface morphology and physicochemical properties. Therefore, the design, synthesis and fabrication of biomaterials with good biocompatibility is quite complex and intricate.

Another essential consideration is the possibility of toxic, mutagenic, and carcinogenic effects. Non-toxicity is either incorporated in biocompatibility or by others regarded as a separate entity where non-toxic materials or their potential side-products do not induce, haemolysis, hepatotoxicity, mutagenic and carcinogenic effects. However, regarding non-toxicity as a separate entity is only relevant for *in vitro* applications as a biocompatible material should by default be non-toxic, non-haemolytic, non-mutagenic and non-carcinogenic whereas as a non-toxic material is not necessarily biocompatible or better put is not biocompatible until proven otherwise.

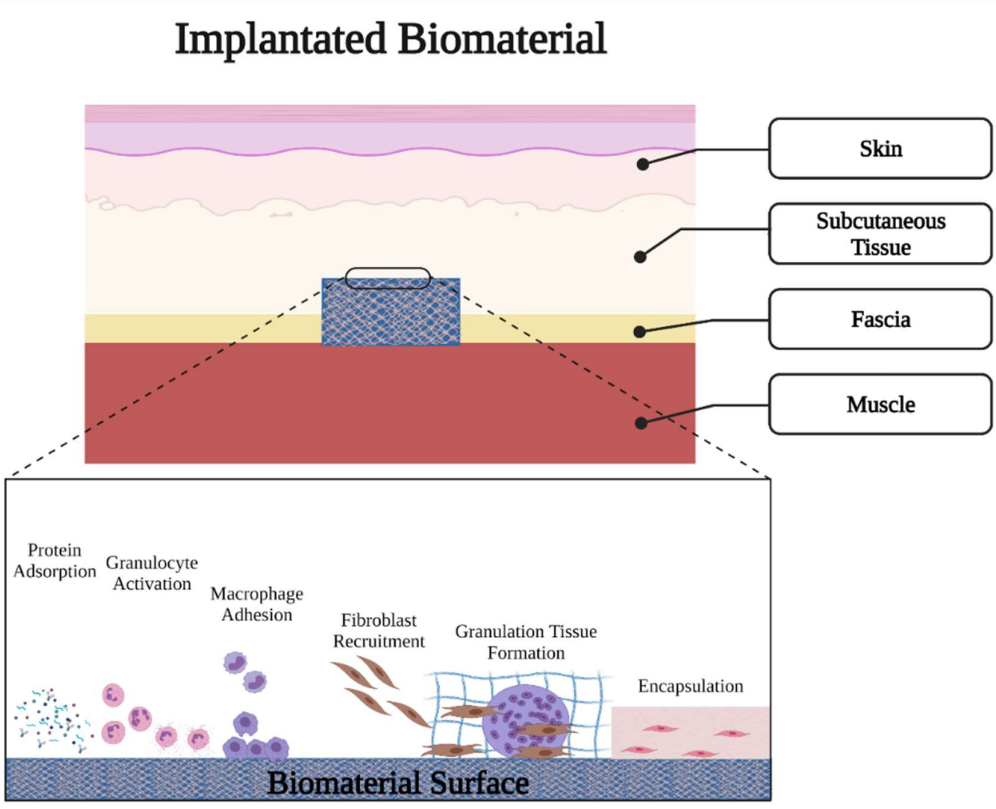

Figure 2. The foreign body reaction process

Bioabsorption

Contrary to biocompatibility, bioabsorption as a term is not that vague. This however is a property exclusive to polymeric materials. In this context absorbable, resorbable, and bioresorbable are synonymous epithets. A material is bioabsorbable when it is absorbed and can be eliminated through different pathways (e.g., expiration, urination, etc.). Two subgroups of bioabsorbable materials are biosoluble and biodegradable materials. Biosoluble polymers are bioabsorbed without requiring degradation as they can dissolve in the aqueous media and physiological environment of the tissues. Materials made from these polymers require cross-linking (i.e., the formation of chemical bonds between the polymer chains) to prevent an early and unwanted dissolution. On the other hand, biodegradable materials require degradation via an enzymatic or non-enzymatic pathway (19,31). Typically, polymer derived from a biological source (e.g., collagen, alginate) are degraded via an enzymatic process while synthetic biodegradable polymers (e.g., poly(glycolic acid), poly(lactic acid)) are degraded by a physicochemical degradation without requiring enzymatic assistant. In the end, materials from either class follows bioabsorption and excretion through either the lungs, kidneys or the bowels, therefore, bioabsorbable materials typically induce far less foreign body reactions and long-term complications.

Functionality

Normally, functionality would be considered as an elementary feature for any implant. Nevertheless, is always important to mention that biomaterials and especially implants should be functional or even multi-functional. Developing biomaterials is an exciting field and researchers sometimes neglect basic functional requirements for example physical and chemical stability or mechanical properties. These are essential regarding the practical usage and implementation of implants. As good as a material may be in theory, if it cannot be implanted properly (e.g., implant hard to manipulate surgically, implant unsuitable for fixation) or if the implantation process increases the risk of the procedure it would results in waste of materials, experimental animals and other resources. Therefore, functionality and practicality should always be kept in consideration.

Sterilization, Storage and Cost-effectiveness

Without the ability to be properly sterilized, an implant's applicability is severely limited. The sterilization method always depends on the physical and chemical composition of the biomaterial in question. Of course, a more effective sterilization method (e.g., autoclave, UV or other ionization radiation etc.) is preferable as long as the biomaterial's integrity is not compromised. Lighter sterilization methods utilising weaker chemicals have been documented without presenting any issues. Nevertheless, sterilization should be as strong as possible not only in terms of intensity but in terms of sterility duration as well. For this reason, biomaterials are sterilised according to their respective ISO standards (e.g., ISO 17664, 17665).

In addition, storage might seem as a non-significant matter however, in practical terms (especially if the biomaterial in question aspires to reach the market one day) this can lead to sever limitations and simultaneously waste of resources. If a biomaterial's storage is limited, and it can only be implanted or applied within a specific window, can be a major disadvantage as it would normally entail waste of resources. Furthermore, complicating storage and implementation only increases the risk for mistakes by doctors and other health care workers. Therefore, simplicity in storage is crucial.

Finally, cost-effectiveness is rather self-explanatory. Biomaterials should be as cost effective as possible, not only to increase a company's profits per se but more importantly to increase the application frequency and use on patients, which not only will help more people but also initiate a feedback for improvement and modifications.

1.4 Polymers for Regenerative Medicine

Polymers have been regularly used for the synthesis, fabrication, and production of biomaterials. The term polymers originating from the Greek word *πολυμερή* (*πολύς*"polis" meaning many and *μέρος* "meros" meaning part). As their name suggests they are a type of macromolecule composed of myriads of connected repeating subunits named monomers. Polymers can be found ubiquitously in nature; from rubber and silk to glycogen and collagen, to the very basis of life itself (i.e., DNA and RNA), polymers possess advantageous features making them versatile reliable materials which have been used for centuries, even before their very structure was identified. These include general advantages for example reproducibility, versatility, simplicity and cost-effectiveness of production. Or more specific ones according to the type of polymer for example:

resistance to chemicals, heat and oxidation, variable biodegradation, reactive functionalisation, and others.

They can be classified and grouped according to their structure, architecture, composition, physico-chemical properties and of course origin. In terms of medical and biomedical applications, the most crucial parameter is probably the origin i.e., whether the material is derived from nature (natural polymer or biopolymer) or artificially synthesised by using a synthetic or a natural monomer (a monomer found in nature, but the polymer itself is artificial).

Natural polymers also known as biopolymers have three subgroups: Proteins (e.g., collagen, fibrinogen), Polysaccharides (e.g., cellulose, dextran) and Polynucleotides (DNA and RNA). While they are non-toxic, biocompatible, and biodegradable making them perfect candidates for biomedical applications, they also have issues. Natural polymers, especially those derived from animal tissues possess antigenicity and therefore can elicit serious immune reactions leading to implant rejection. In addition, they are typically heat- and pH-labile making them rather unstable and difficult to store, whilst their sterilisation can also be problematic. Furthermore, reproducibility and poor mechanical performance are also well-known issues limiting their applicability.

To solve these issues, researchers started modified natural polymers utilising synthetic cross-linking agents (creating natural origin polymers) aiming to make natural polymer-based materials more robust and stable. However, typically these types of works become a double-edge knife as due to the chemical modification, biocompatibility and biodegradability is compromised. Furthermore, natural polymers are well known for being harder to work with while they also suffer from having poor mechanical properties and limited sterilisation possibilities as they cannot withstand harder sterilizing methods.

Synthetic polymers on the contrary, are typically cheaper, simpler and rather straightforward to produce (compared to the extraction process used for natural polymers) or modify. They are also more physico-chemically stable and reproducible while possessing better mechanical properties and chemical resistance. However not all synthetic polymers are biocompatible or biodegradable and some can even be toxic therefore, a comprehensive examination is required before utilising them as biomaterials.

Polymer cross-linking is a very effective method to enhance biomaterials. Both natural and synthetic polymers can undergo cross-linking. The benefits of cross-linking

include, enhanced tensile strength, prolonged biodegradation and if the selected polymer is hydrophilic, it can even make the biomaterial absorb surrounding liquid and therefore become a hydrogel. Gel-based biomaterials resemble the body tissues in terms of density. making them excellent scaffolds. In addition, they possess features of both solids and liquids making them implantable but also able to transfer water and other molecules through diffusion.

Whether composed of natural, synthetic or both, polymer-based biomaterials have been used in several areas of regenerative medicine. Notable examples include specialised wound dressings, surgical meshes for hernia repair, stents and graft (Figure 3).

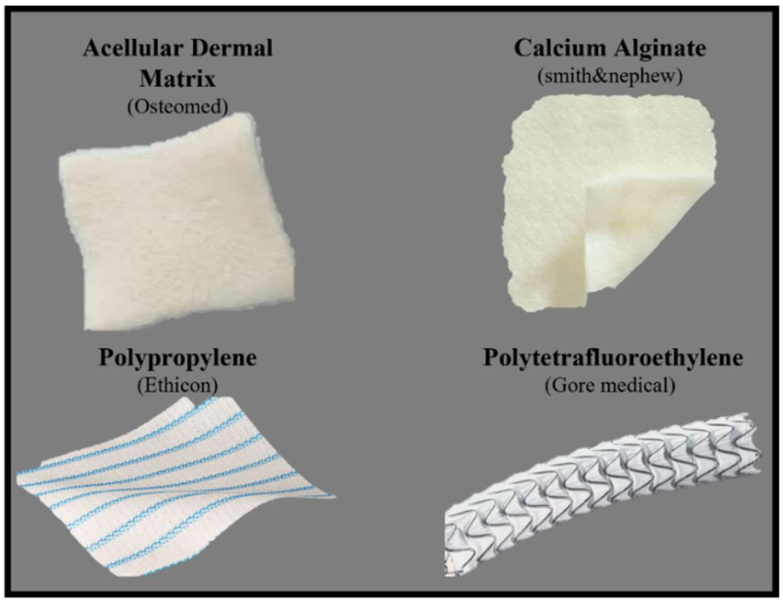

Figure 3. Examples of natural (top two) and synthetic (bottom two polymer-based implants in regenerative medicine

In the frame of the current work, one synthetic and two natural origin but artificially synthesised polymers are investigated: poly(vinyl alcohol) (PVA), polycaprolactone (PCL) and poly(succinimide) (PSI). PVA is a well-known polymer which is regularly used in medical and biomedical applications. For example, it has been used as a drug binder and drug capsule material, a prominent component of contact lenses and eye drops, a component of cartilage replacement material but also a component of embolic agents. Without a doubt PVA had a significant role in the development of biomaterials. PCL on the other hand, is a highly versatile polymer, currently approved by the FDA as component of dental night guards and root canal fillings, surgical sutures,

anti-adhesive membranes and even drug carrier systems. Research is currently strong on the utilisation of PCL in dermal fillers, tissue engineering and biomaterial fabrication for different applications due to the polymer's many favourable features. Finally, PSI is a recently developed polymer. It is synthesised via the thermal polycondensation of L-aspartic acid. It has been utilised in environmental, filter and sensor applications. Literature on its biomedical applications is rather limited however, the current results show great potential, however a biomedical application is not on the market yet. Due to its easily modifiable structure PSI can be used as a functionalizing component to currently utilised systems. Being a poly(amino acid), it is biocompatible and biodegradable therefore it should be utilized for biomedical applications without any issues.

1.5 Electrospinning as a Nanotechnological Fabrication System

Electrospinning is a method to produce fibres composed of diameter ranging between a few nanometres and a couple of micrometres. The method has been used for decades and has been explored, modified, and improved resulting several setups producing different types of fibrous systems. In its most basic form however, the setup only requires a needle attached to a polymer solution filed syringe, a syringe pump, a high voltage power supply and a grounded collector. During electrospinning, two crucial forces are in play: the polymer solution's surface tension and the electrostatic force provided by the power supply. As the polymer solution is pushed through, a droplet is formed on the end of the needle which retains its position until the surface tension is overcome by either the droplet's weight (causing it to spill) or the electrostatic force oriented to the collector. Normally the droplet would fall however, when the electrostatic force is applied the droplet first elongates; then, after reaching a critical point (forming the so called "Taylor Cone") the solution is expelled towards the grounded collector (Figure 4). The fibre producing stream or jet has two main phases. A first short linear phase where the fibres themselves are produced, and a second longer randomly whipping phase where the polymer fibres elongate while the solvent evaporates (Figure 4). Finally, the fibres attached on to the grounded collector and due to the second phase produces the classic randomly oriented fibres. The resulted membranes, meshes or mats can then be extracted from the collector.

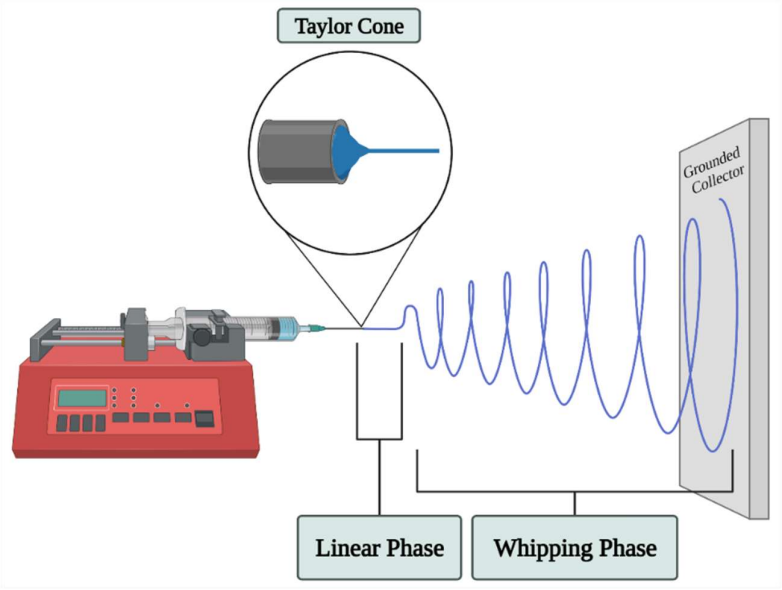

Figure 4. Electrospinning process

Electrospinning Parameters

Electrospinning is regularly described as a straightforward and versatile method. While the statement initially seems true, several parameters must be adjusted and optimised to reach the desired result.

Electrospinning parameters can be classified in to three groups:

a) Polymer solution parameters: including polymer type, polymer concentration and solution viscosity, conductivity, evaporation rate, surface tension.
b) Electrospinning setup parameters for example voltage, flow rate, needle size, collector distance.
c) Ambient parameters: ambient temperature and humidity.

Most of these parameters are not static and exhibit co-dependent correlations. In other words, altering or adjusting one will almost definitely requires modifying another (Figure 5.). For example, increasing the polymer solution's viscosity typically increases the fibre diameter, while increasing the voltage would decrease it. However, electrospinning of higher viscosity solutions requires higher voltages as the surface tensions are higher. This balance between the parameters is what makes optimisation of an electrospinning process for a given polymer time consuming. Even more so when additional elements are included in the fabrication (e.g., addition polymers, incorporation of drugs or other molecules, etc.). Therefore, a thorough investigation where typically

one or two parameters are gradually adjusted is a common and accepted strategy. Simultaneously adjusting more parameters results in hard to interpret results and mistakes. Recently, the use of simulation software has gained some attraction as it reduces time spend on the optimisation phase. Simulations have been implemented to investigate which parameters are critical and how should they be adjusted to achieve the desired fibre quality. Results seem promising nevertheless, simulations are best used for already utilised, un-modified polymers with no additional elements.

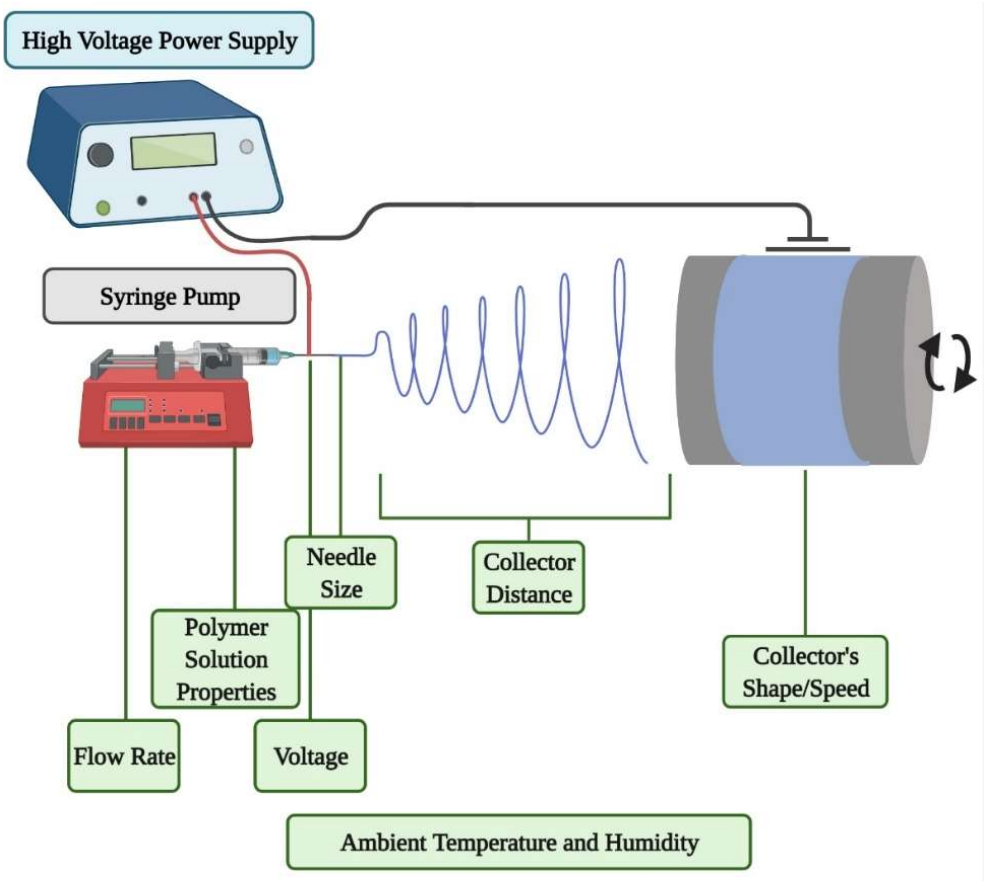

Figure 5. Electrospinning parameters

Electrospinning Configurations and Setups

While the basic electrospinning setup is quite elementary, several advances have been made since the early days of electrospinning. These included the implementation of additional needles, changing the shape and size of the collector, implementing heat or air to assist the fibre formation and many others. The following examples are some of the innovations made in the field which are most relevant to the topic of the thesis.

Rotating Cylindrical Collector

A rotating cylindrical collector is utilised to equally distribute the polymer fibres. Using a flat static collector results in circular samples which are thickest in the centre then become thinner towards the periphery (thus upon extraction the periphery tears away or is impossible to remove) (Figure 6 upper schematic). In contrast the cylindrical collector results in a sample whose thickness distribution has a lower variance but rectangle shape which is more efficient for in later usage (Figure 6 lower schematic). Therefore, the cylindrical collector not only makes mesh fabrication more reproducible but also decrease material waste. In addition, it has been documented that increasing the rotating speed of the collector will result in a mechanically induced alignment of the fibres.

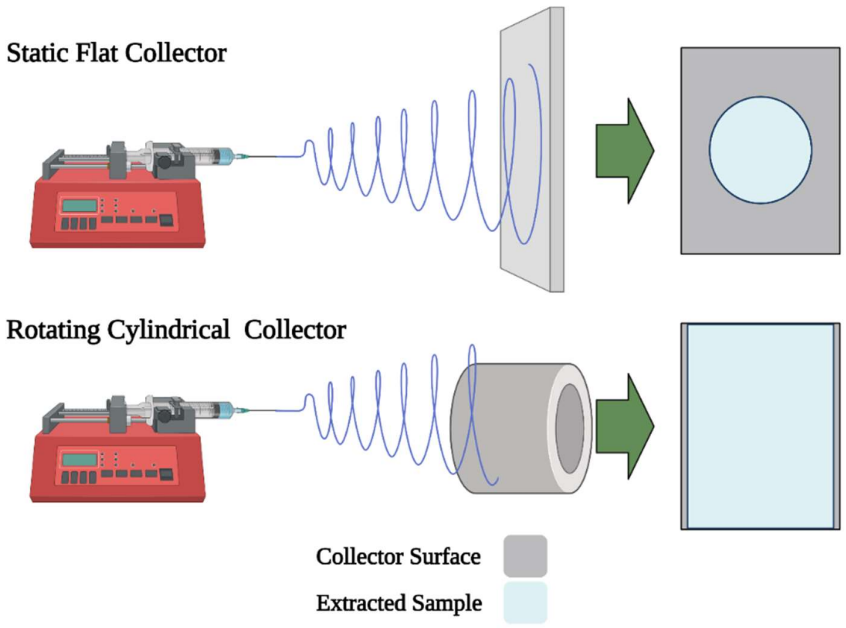

Figure 6. Effect of collector difference on post-electrospinning sample size

Layered Electrospinning

Layered electrospinning is a minor alteration. It is a sequential process where different polymers are electrospun one after the other on the same collector (Figure 7.). This results in a composite mesh composed of two or more distinct layers of polymer fibres. The advantage here is the addition of a secondary polymer which can enhance the system properties (e.g., mechanical performance). In addition, a mesh composed of two sides with different chemical or physical compositions can serve two separate function and therefore can be used in cases where the biomaterial is placed between two different tissues (e.g., bone-cartilage implants, surgical mesh) or must separate two compartments (e.g., wound dressing, anti-adhesion membrane) from freely communicating.

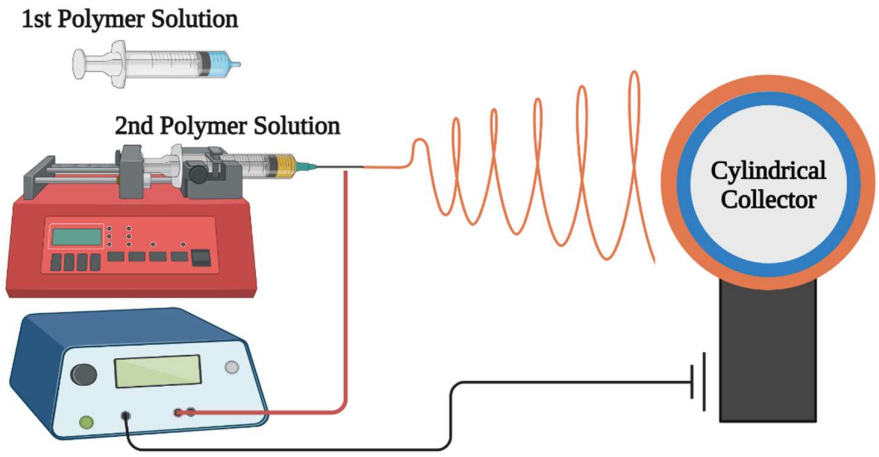

Figure 7. Layered-electrospinning with rotating cylindrical collector

Co-electrospinning and Coaxial Electrospinning

While having similar names, these processes are entirely different. Co-electrospinning refers to the concurrent electrospinning of two or more polymer solutions upon the same collector (typically a rotating cylinder) (Figure 8 A).

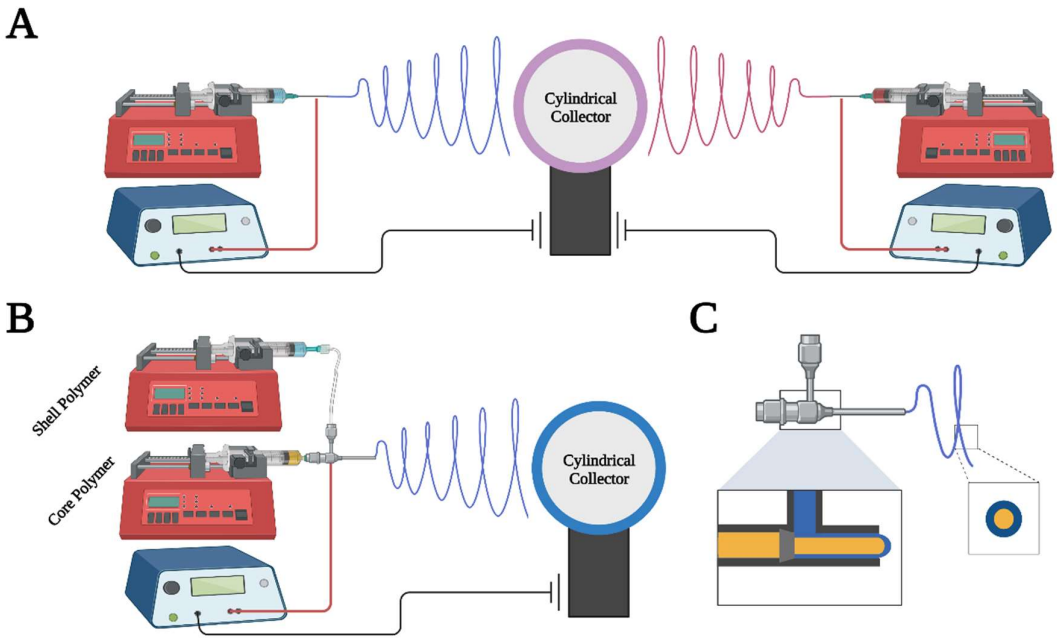

Figure 8. Co-electrospinning(A) and coaxial (B) electrospinning configurations

While coaxial electrospinning is the electrospinning of two polymer solutions by utilizing a coaxial needle (i.e., a needle within a needle system) (Figure 8 B and C). While the end result may be identical in terms of overall chemical composition the two meshes will have fundamentally different microstructures. Co-electrospinning results in a mesh composed of two or more polymer fibre types whereas coaxial electrospinning results in core-shell fibres, where one fibre is composed of an inner and outer layer according to which polymer solution was used with the coaxial needle (Figure 9 C).This will result in the membranes having different physical, chemical, mechanical or even biological features.

Blend and Emulsion Electrospinning

The two methods are identical in terms of practical execution however the resulted mesh structure depends on the solutions used. If two miscible polymer solutions are used, the mesh will be comprised of fibres composed of two polymers (blend electrospinning). On the contrary if the two solutions are not miscible enough the mesh will be comprised of either (version a) core-shell fibres (albeit the process and optimisation being significantly harder than using a coaxial needle) or (version b) twin fibres composed of the two solutions (Figure 9.). These results are highly dependent on the polymer solution properties and the used polymer itself.

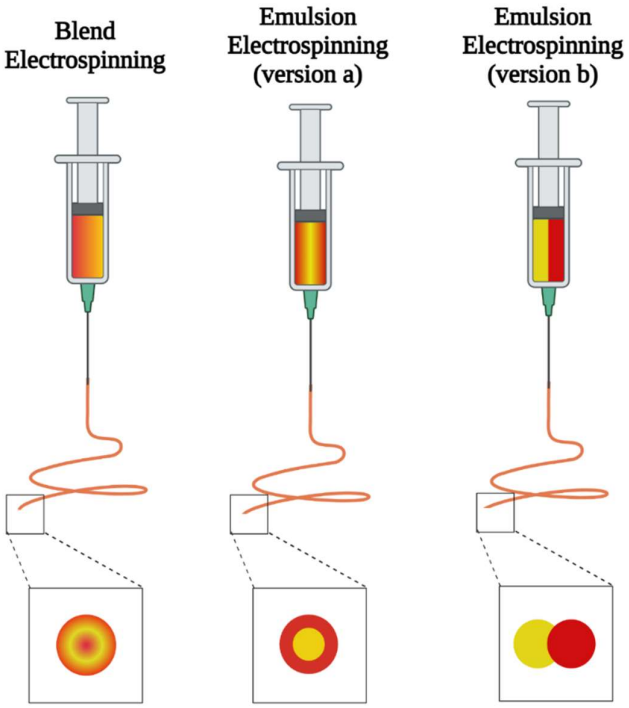

Figure 9. Comparative result of fibre structure according to the used configuration

1.6 Surgical Tissue Regeneration and Tissue Engineering

Surgical tissue regeneration is not a widespread definition. In the context of this work, it refers to the usage of biomaterials that can be used to treat or manage disorder and conditions typically seen in surgical wards; or biomaterials that require surgical handling, implantation, and fixation to serve their purpose. Potential applications for these electrospun meshes include wound dressings for diabetic legs and decubitus, surgical meshes for hernia treatment, anti-adhesive membranes and other implants to repair damaged or lost tissue conditions.

Tissue engineering is the science of regenerating and creating new tissues. It has three main frames:

1. Administration of pharmaceuticals, drugs or other molecules to enhance tissue regeneration *in vivo* and *in situ.*

2. Synthesis of materials for cell proliferation and tissue formation *ex vivo* which will later be implanted back to the patient.

3. Fabrication of biomaterials that will be implanted directly in the patient, providing innate cells a template for attachment, proliferation, and differentiation resulting in the formation of new tissue.

These frames or approaches are not strictly separate. Today these tactics are mixed, resulting in advanced complex approaches utilising biomaterials and cells concurrently to achieve the best results possible.

Fabrication of biomaterials includes different tactics. For example, fabrication of meshes or bulk materials, synthesis of hydrogels or tissue extraction and processing (e.g., acellular grafts). Electrospun meshes however are highly promising candidates as they can withstand surgical handling and fixation compared to other soft materials (e.g., hydrogels) while also retaining an advantageous microstructure compared to bulk materials.

Electrospun nanofibrous membranes have several advantages and have been utilised in numerous scientific fields and applications. Nevertheless, their advantageous features are prominently based on the membrane's structure and the huge surface area to

volume ratio. Firstly, having a structure similar to the extracellular matrix makes them perfect scaffolds. Secondly, their mechanical performance is enhanced as the traction between the nanofibres also adds to the overall tensile strength of the materials themselves. Furthermore, incorporations of nanoparticles, drugs or other chemicals is greatly enhanced by the enormous specific surface area which allows for increased and tuneable active ingredient release over short or longer periods. Finally, addition of supplementary components and the fabrication of composite materials using the electrospinning method is not only feasible but well documented.

Composite materials are materials where two or more different components are incorporated in the same system. In terms of electrospun membranes, composite materials have been fabricated and utilised for different applications. Typically, the addition of a material enhances the systems mechanical properties, improves biocompatibility, or gives the system additional features and functions. The current tissue engineering research trend is concentrated on fabricating multi-functional and smart materials as it is always advantageous to implant a material that can serve two or more functions therefore eliminating the use of additional materials and procedures (Figure 10).

An exciting component to incorporate in electrospun meshes are nanoparticles resulting in advanced polymer nanocomposites. Nanoparticles are particles whose size falls under 100 nm in all three dimensions. Nanoparticles are very useful due to their two prominent features: a) their immense specific surface and b) quantum size also known as quantum confinement effect. While the specific surface makes nanomaterials advantageous as tissue engineering and drug delivery materials the quantum size effect gives them optical properties useful in contrast assisted imaging. Nanoparticles are utilised in a broad range of applications including biomedical. Most common applications include MRI and fluorescent imaging contrast agents, drug carriers and antibacterial additives to wound dressing or other medical equipment (32–36).

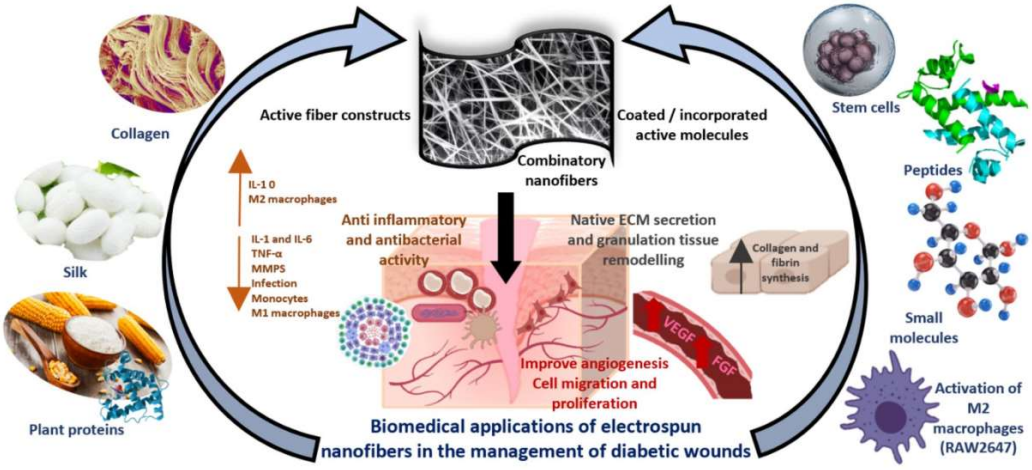

Figure 10. Example of electrospun membrane possibilities for biomedical applications (37)

Several types of polymers have been combined to composites and nanocomposite materials and the relative literature is quite extensive. The following pages present the polymers (Figure 11) and composite systems most relevant to the theme of the thesis.

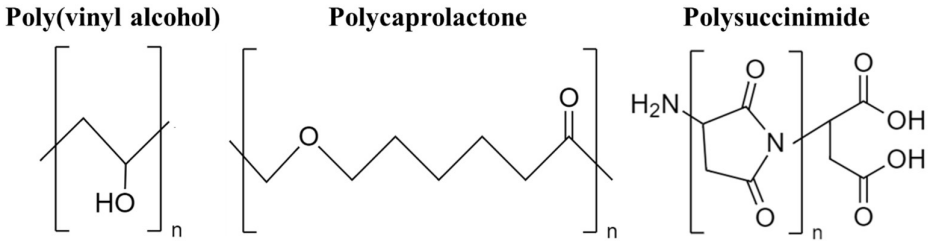

Figure 11 Chemical structure of utilised polymers in this thesis work

Poly(vinyl alcohol)

Poly(vinyl alcohol) (PVA) is a well-known polymer found in numerous even daily-used materials. It is a colourless, odourless, and water-soluble synthetic polymer typically produced by hydrolysing of polyvinyl acetate. It has a melting point 210-260 ºC a glass transition temperature 30 and 45 °C depending on the molecular weight and negligible vapour pressure. Being chemically inert, non-toxic, biocompatible while also exhibiting low tendency for protein adhesion it has been extensively used in medical and biomedical applications. Without a doubt PVA had a significant role in the development of biomaterials evident by its prominent use.

In this regard, electrospun PVA membranes have a huge advantage compared to other polymer membranes as fibre formation can be achieved by using water instead of more volatile and hazardous solvents. It is noteworthy mentioning that very few polymers

can be electrospun using water. Compared to other organic solvents, water is not a good solvent for most polymers, has low conductivity (especially ultrapure water) and does not evaporate as fast therefore it presents difficulties in fibre formation. This issue might require the usage of a binary solvent (e.g., Water-Ethanol) or addition of salts (e.g., NaCl).

Furthermore, being water soluble, makes any PVA-based material bioabsorbable under physiological conditions (19,31). Bioabsorbance highly depends on the molecular weight of PVA. If the molecular weight falls under 10 000 g/mol it can be excreted through the kidneys, if not it is eliminated through the gastrointestinal tract. In some cases, this can be beneficial (e.g., drug carrier systems,) for some applications (e.g., implants) however, the crosslinking of the system is essential to prevent this early and unwanted dissolution of the system.

Crosslinking of PVA can be achieved by either physical (e.g., heat treatment, freeze thawing, radiation mediated) or chemical (i.e., addition of cross-linker) However, as aforementioned, for long-term implants, cross-linking is necessary. Different physical and chemical cross-linking methods have been examined in the past. The two methodologies as expected have both advantages and disadvantages. Physically cross-linked system using heat treatments, freeze -thawing or even UV radiation have the advantage of not using cross-linking agents which as chemicals could potentially be toxic or cause other unwanted side effects. While these methods do indeed successfully induce cross-links in a PVA system they are more suitable for bulk hydrogel formation or other additive manufacturing based produced materials. Unfortunately for physical cross-linking typically alters the fibrous microstructure of electrospun meshes, either deforming the fibres or melting them, forming a uniform amorphous layer thus eliminating their main advantage. In addition, according to swelling profiles, physically cross-linked systems swell less than their chemically cross-linked counterparts. On the other hand, chemical cross-linking does require chemical agents which could potentially decrease the biocompatibility of the system. Several agents have been investigated e.g., boric acid, citric acid, maleic acid, glutaraldehyde etc. While acidic compounds (e.g., citric acid, maleic acid) require heat to induce cross-link formation, glutaraldehyde require a low pH typically gained by HCL which is introduced to the system by either immersion (of the mesh in a HCL solution) or vapours. Although the predisposition is that these chemically

cross-linked systems would have biocompatibility issues several studies demonstrated that the meshes are non-toxic, cytocompatible and biocompatible (38–41,43,45).

PVA composite systems are of great interest. Both natural and synthetic polymers, small molecules, nanoparticles and other components have been combined with PVA to fabricate advanced functional materials. The aim was to overcome PVA drawbacks such as limited hydrophilicity, insufficient mechanical properties, slow biodegradability (due to cross-linking) etc. or enhance the system features (e.g., cell adhesion, antibacterial properties etc.). Although many systems can be found in the relevant literature a few of examples of most relevance can be found in Table 1.

Table 1. Examples of PVA composite systems intended for biomedical applications

System Composition	Application	System Advantages	Author and Reference
PVA/Egg White	Wound Dressing	Enhanced Regeneration	T. Lu et al. (42)
PVA/PLGA-Chitosan	Skin Reconstruction	Enhanced Fibroblast Attachment/Proliferation	B. Duan et al. (44)
PVA/Silk Fibroin	Heart Patch	Enhanced Mechanical Strength and Cell Attachment/Proliferation	M. Sayed et al. (46)
PVA/PLA	General Tissue Regeneration	Enhanced Surface Wetting, Mechanical Properties and Cell Attachment/Proliferation	H. Alharbi et al. (47)
PVA/Chitosan/Graphene	Cartilage Regeneration	Enhanced Mechanical Properties and Cell Growth	L. Cao et al. (48)
PVA/Hydroxyethyl Cellulose	Bone Regeneration	Enhanced Cell Infiltration	S. Chahal et al. (49)
PVA/Collagen	Artificial Cornea	Enhanced Mechanical Properties and Light Transmittance	Z. Wu et al. (50)

Polycaprolactone

Polycaprolactone is probably one of the most popular polymers researchers have been focused on in recent years (Table 2.). It is semi-crystalline, aliphatic polyester, synthesized by ring-opening polymerization of ε-caprolactone. In contrast to PVA, PCL is not dissolvable in water but is nevertheless biocompatible and biodegradable. Additionally, by being dissolvable even at room temperatures in a range of organic solvents (e.g., DMF, THF, DCM, etc.), possessing a low melting temperature (60^{o}C) and glass transition temperature (-60^{o}C), it exhibits an extraordinary potential to form blends with other polymers. Furthermore, it has relatively good physicochemical properties especially when compared to other biodegradable polymers possessing a chemical resistant to water, oil and solvent, and an excellent tensile strength which varies according to its molecular weight and degree of crystallinity. In this regard, biodegradability (via hydrolysis of its ester linkages) also closely correlates to the molecular weight therefore, according to the specific application a different molecular weight is used (for biomedical applications typically 30 – 80 kD).

Table 2. Examples of PCL composites systems intended for biomedical applications

System Composition	Application	System Advantages	Author and Reference
PCL/Chitosan + NGF	Nerve Regeneration	Enhanced Mechanical Properties, Surface Morphology, Cell attachment/proliferation	H. Afrash et al. (51)
PCL/PVA	Wound Dressing	Dual Drug Release with Antibacterial properties	X. Lan et al (52)
PCL/PLGA/Dextran	Annulus Fibrosus Regeneration	Enhanced Mechanical Properties, Biodegradation, Anti-inflammatory effect	X. Wuang et al. (53)
PCL/ Decellularized Matrix	Bladder Muscle Regeneration	Enhanced Regeneration with Excellent Mechanical Properties	C. Wang et al. (54)
PCL/PGS	Bone Regeneration	Enhanced Cell Attachment/Proliferation/Differentiation	Al. Rezk et al. (55)
PCL/Alginate/Chitosan	Periosteum Regeneration	Enhanced Osteogenesis	F. Tao et al (56)
PCL/Silk Fibroin	Abdominal Wall Regeneration	Enhanced Regeneration	D. Yang et al (57)

Unsurprisingly, PCL composite systems have also been exploited to produce advanced functional materials. Due to its versatile nature, it has been extensively combined with both natural and synthetic polymers to fabricate electrospun hernia meshes, bone scaffolds and other implantable biomaterials.

Polysuccinimide

Polysuccinimide (PSI) which is also known as polyanhydroaspartic acid or polyaspartimide is a recently developed polymer. Its production is quite simple, produced by the thermal polycondensation of L-aspartic acid in the presence a catalyst (e.g., phosphoric acid). PSI has been gaining the attention of researchers as due to its reactive nature (58,59) it is a versatile, potential component for functionalised systems. An easily modifiable polymer (due to the imide-ring opening even under mild conditions) PSI has been utilized to produce for example thermal and pH reactive or magnetic nanoparticle incorporating systems (58,60–63,67). PSI is hydrolysed in slightly alkaline media and water (albeit quite slowly in the latter) and recent studies have already demonstrated its cyto- and potential biocompatibility (64–66) therefore it could be considered as a promising candidate for biomedical applications. Nevertheless, it has two main weaknesses: a poor mechanical performance and rapid a biodegradation time (68,69).

Compared to PVA and PCL, the literature on PSI-based electrospun membranes and meshes is extremely limited (manuscripts number ranging in the single digits). Even more so, PSI composite meshes have not been documented at all.

2. Objectives

The need for biocompatible, biodegradable, and functional materials is grave. In this regard, electrospun nanofibrous meshes are advantageous for several reasons. When fabricating electrospun meshes, the choice of polymer is crucial. Poly(amino acid) based meshes should be promising candidate for surgical tissue regeneration as being composed of amino acid monomers they should be biocompatible and biodegradable.

The first objective of this thesis was the optimisation of poly(amino acid) based and more specifically polysuccinimide fibrous meshes and the enhancement of their biomedically relevant features. The second and third objective was the development and characterisation of composite meshes by combining polysuccinimide with poly(vinyl alcohol) and polycaprolactone respectively. The aim here was to overcome PSI weaknesses and explore the possibility of creating composite meshes with different features. Finally, the incorporation of nanoparticles and fabrication of functionalised composite meshes was explored.

The work of the thesis can be divided into four frames:

A. Optimisation of PSI electrospun membranes.
An optimisation of its parameters for example fibre size and mechanical properties will enhance biomedically relevant features and increase its applicability spectrum.

B. Fabrication and characterisation of co-electrospun polysuccinimide/poly(vinyl alcohol) meshes.

C. Fabrication and characterisation of layered-electrospun, co-electrospun and blend electrospun polysuccinimide/polycaprolactone meshes.

D. Functionalization of PSI and PSI composite electrospun meshes with magnetite nanoparticles.

One important aspect of this work was to attempt and include the entire biomaterial development process including synthesis and fabrication, and the characterisation of parameters (chemical, physical, mechanical, biological) relevant to surgical tissue regeneration.

3. Materials and Methods

3.1 Materials

3.1.1 List of Chemicals and Solvents

L-Aspartic Acid (reagent grade ≥ 98 %, Mw ~133, Sigma Aldrich, USA), Orthophosphoric Acid (reagent grade ≥ 99 %, Mw ~98, Sigma Aldrich, USA), Poly(Vinyl Alcohol) (Mowiol® 10–98, Mw ~61,000, Sigma Aldrich, USA), Glutaraldehyde (25%, Merck, Germany), Hydrochloric Acid (37%, Reanal Labor, Hungary), Polycaprolactone (Mw ~80,000, Sigma Aldrich, USA), L-Aspartic Acid (Reagent Grade ≥ 98%, Mw ~133, Sigma Aldrich, USA), Acetone Puriss (reagent grade ≥ 99.5 %, Lach:ner, Czech Republic), Acetonitrile (reagent grade ≥99.5%, AnalaR NORMAPUR® ACS, VWR Chemicals BDH®, VWR International, USA), Acetic Acid (reagent grade ≥ 99.7 %, Sigma Aldrich, USA), Dichloromethane (reagent grade ≥99.5% stabilised with 2% ethanol, AnalaR NORMAPUR®, VWR Chemicals BDH®, VWR International USA), N,N-Dimethylacetamide (reagent grade ≥ 99.8%, technical, VWR Chemicals BDH®, VWR International, USA), N,N-Dimethylformamide (reagent grade ≥ 99.8%, AnalaR NORMAPUR®, VWR Chemicals BDH®, VWR International, USA), Dimethyl sulfoxide (reagent grade ≥99.5%, dehydrated max. 0.03% H_2O, AnalaR NORMAPUR®, VWR Chemicals BDH®, VWR International, USA), Ethanol (reagent grade ≥99.5 %, Honeywell USA), Ethylene Glycol (reagent grade ≥ 99.8 %, Sigma Aldrich, USA), Methanol (reagent grade ≥ 99.9 %, Chromasolv®, Sigma Aldrich, USA), Methyl Ethyl Ketone (reagent grade ≥99.0% ACS, VWR Chemicals BDH®, VWR International, USA), Propanol-1 (≥99.5%, AnalaR NORMAPUR® Reag. Ph. Eur. analytical reagent, VWR International, USA), Cyclohexane Puriss (reagent grade ≥99.5 %, Riedel-de Haën®, Honeywell USA), 1-Octanol (reagent grade ≥ 99 %, anhydrous, Sigma Aldrich, USA), Tetrahydrofuran (anhydrous, inhibitor free, Reagent Grade ≥99%, Sigma Aldrich, USA), Toluene (≥99.5%, AnalaR NORMAPUR®, VWR Chemicals BDH®, VWR International, USA), Ultrapure Water (Water Purification System, Zaneer), Imidazole (ACS Reagent, ≥99%, Sigma-Aldrich), Citric-acid*H_2O (ACS Reagent, ≥99.9%, VWR), Sodium Chloride (99-100.5%, Sigma-Aldrich), Phosphate Buffer Saline (PBS) (Tablet, Sigma), Sodium hydroxide (VWR International, USA), 5,5'-ditio-bis-(2-nitrobenzoic acid) (Aldrich, ≥99%), Ethylene-Diamino-Tetra Acetic Acid (Aldrich, ≥99%),

Ammonium Iron (II) Sulphate Hexahydrate (VWR Chemicals), Iron (II) Chloride Tetrahydrate (VWR Chemicals), Iron (III) Chloride (97%, Sigma-Aldrich), Potassium Permanganate (Reanal Labor , Hungary), Hydroxylamine Hydrochloride (ACS Reagent, Acros Organics), Ammonium Acetate (Ultra-Pure, VWR Life Science, AMRESCO), Phosphate-Buffered Saline (Sigma Aldrich, USA), Sodium-azid (Sigma Aldrich, USA), Chlorine Dioxide (3350 Ppm, Solvocid, Hungary), Nile Blue A Stain (Dye Content ≥75%, Sigma Aldrich, USA).

3.1.2 List of Reagents and Solutions for the Cell Studes

Minimal Essential Medium Eagle (Gibco, USA), foetal bovine serum (FBS) (Gibco, USA), L-glutamine (Gibco, USA), penicillin (Gibco, USA), streptomycin (Gibco, USA), Non Essential Amino Acids (NEAA) (Gibco, USA), Minimal Essential Medium, no glutamine, no phenol red (Gibco, USA), WST-1 [2-(4-Iodophenyl)-3-(4-nitrophenyl)-5-(2,4-disulfophenyl)-2H- tetrazolium] (Roche, Switzerland), Vybrant DiD (Molecular Probes, USA), trypsin-EDTA (Gibco, USA), paraformaldehyde (PFA) (Sigma-Aldrich, USA), Dulbecco's Phosphate Buffered Saline (Lonza, Switzerland), 155 BR human fibroblast cells were purchased from European Collection of Authenticated Cell Cultures (Sigma Aldrich, USA). The cells were maintained in a humidified incubator (Nuaire, USA) in tissue culture flasks under standard culture conditions (37 °C, 5% CO_2, 100% humidity). The culture medium consisted of Eagle's Minimal Essential Medium supplemented with 10 v/v % foetal bovine serum (Gibco, USA), 2 mM L-glutamine and 1 v% Non-Essential Amino Acids (Gibco, USA), 100 units/ml penicillin and 100 mg/ml streptomycin (Gibco, USA).

3.1.3 List of Materials and Chemicals for the Animal Experiments

Polycarbonate Cage type IIL (Innovo Kft, Hungary), Polycarbonate Cage type IV (Innovo Kft, Hungary), Polycarbonate water bottle (500ml, Innovo Kft, Hungary), Polysulfone water bottle (500ml, Innovo Kft, Hungary), SAFE® MK3500 (natural vegetable granules bedding material SAFE, France), SAFE® Crincklets Natural (paper nesting material, SAFE®, Innovo Kft, Hungary), SAFE® Tube M (Innovo Kft, Hungary), SAFE® Tube L (Innovo Kft, Hungary), SAFE® A05 food pellets (Innovo Kft, Hungary), 5 ml Syringe (Chirana, Slovakia), Needles (23G, Becton Dickinson, USA), Ketamine (Calypsol 50 mg/ml , Richter Gedeon, Hungary), Xylazine (CP-Xylazine 2 %, Medicus

Partner, Hungary), Formaldehyde (35 w/v %, VWR International, USA), Ethanol (Reagent grade ≥99.5 %, Honeywell USA), Xylol (Puriss, Reanal Labor, Hungary), Paraffin (Puriss, Reanal Labor, Hungary), Eosin (Puriss, Reanal Labor, Hungary), Haematoxylin (Puriss, Reanal Labor, Hungary), Glass slides (Surgipath, Leica, USA).

3.2 Synthesis of Polysuccinimide

L-aspartic acid and phosphoric acid were mixed at a 1:1 mass ratio and mixed in a rotary vacuum evaporator system (RV10 digital rotary evaporator, IKA, Germany). The mixture was heated to 180 °C while the pressure inside the flask was decreased to 5 mbar at a predetermined gradual rate (Figure 12A). The entire synthesis lasted 8 hours. After the synthesis, PSI was dissolved in approximately 200 ml of DMF (Figure 12B). Subsequently, PSI was precipitated and thoroughly washed by pouring it in poured in to stirred water (Figure 12 C) before filtration using a G3 type glass filter (Figure 12D). After 5 wash and filtration cycles (Figure 12D) (when the supernatant became neutral), the resulted white PSI powder was dried at 40 ºC for 5 days in a dehydrator (Figure 12E).The details of the chemical reaction can be found in Figure 13. Reproducibility of the synthesised batches was examined similarly to other researchers work (70,71).

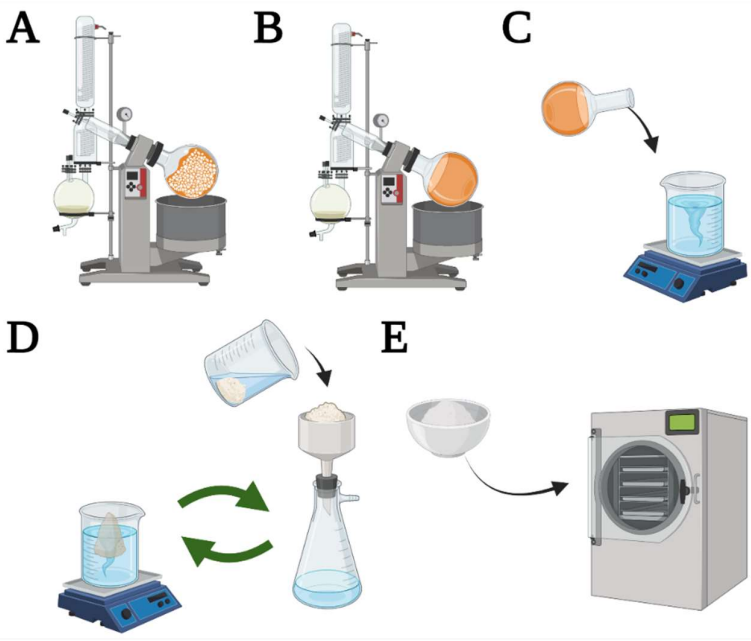

Figure 12. Synthesis and preparation of Polysuccinimide: A. PSI Synthesis, B. Dissolution in DMF, C. Precipitation distilled water, D. Washing and Filtration cycles. E. Dehydration

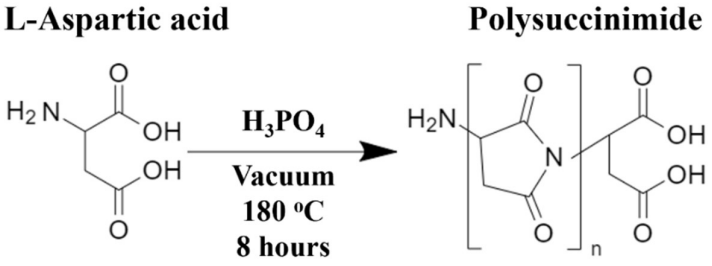

Figure 13. Thermal polycondensation of L-Aspartic Acid

3.3 Polysuccinimide Solubility Study

The information on PSI solubility is quite limited. To investigate any additional electrospinning possibilities, a selection of solvents (typically used for electrospinning – Acetone, Acetic Acid, Acetonitrile, Cyclohexane, dH_2O DMAc, DCM, DMF, DMSO EtOH, Ethylene Glycol, Methanol, Methyl Ketone, Propanol, Octanol, THF, Toluene) was selected, and solubility studies were performed. Polymer concentration was set at 10 w/w % (0.1 g PSI + 0.9 g Solvent). Solutions were prepared with a magnetic stirrer at room temperature.

3.4 Polysuccinimide Viscosity and Conductivity Studies

Viscosity and conductivity are essential parameters for fibre formation during electrospinning. Therefore, viscosity and conductivity of the polymer solutions were determined, which were able to dissolve the 10 w/w % PSI concentration. Viscosity studies were performed with a SV-10 Vibrational Viscometer (A&D Company, Limited, Japan) for the specific and a MFR 2100 Micro Fourier Rheometer (GBC Scientific Equipment Pty Ltd, Australia) for relative measurements. An Orion Star™ Series Meter (Thermo Fisher Scientific, USA) was then used for conductivity assessments. All measurements were performed in ambient laboratory conditions (Temperature: 25 ±1.5 ^{o}C, Humidity: 30 ±5 %).

3.5 Fabrication of PSI and PSI Composite Meshes

3.5.1 Electrospinning and Optimisation of PSI Meshes

The feasibility of PSI electrospinning has been documented before by our own research group as well as a few others (59,72). However, no actual data can be found about which electrospinning parameters influence fibre quality and size the most.

Optimising the electrospinning parameters could result in smaller fibre diameters, which subsequently could result in scaffolds with enhanced mechanical and biological features. The starting parameters were similar to previous works. From there, a comprehensive investigation was performed examining different solvent types, polymer concentrations, needle sizes, flow rates, voltages, collector distances and speeds. The parameters of the PSI electrospun meshes presented in the thesis can be found in Tables 3 and 4 (full optimalisation was performed, however not all parameters can be included in the thesis due to thesis length limitations).

Table 3. Polymer Solvents PSI Electrospinning

PSI Concentration (w/w %)	**Solvent**	**Voltage (kV)**	**Flow Rate (ml/h)**	**Needle Size (G)**	**Collector Distance (cm)**	**Collector Speed (rpm)**
25	DMAc	13	1	18	15	60
	DMF					
	DMSO					

Table 4. Electrospinning parameters of PSI mesh fabrication

PSI Concentration (w/w %)	**Voltage (kV)**	**Flow Rate (ml/h)**	**Needle Diameter (G/mm)**	**Collector Distance (cm)**	**Collector Speed (rpm)**
22.5 25	13 15	0.25 0.5 1	18 / 0.838 30 / 0.159	10 20 25	60 500 2000 4000 6000

Polymer solutions were transferred to 5 ml Luer slip-syringes (Chirana, Slovakia) equipped with customized blunt needles of various diameters (Becton Dickinson, USA). Polymer solutions were delivered by an infusion pump (KDS100, KD Scientific, USA). The electric potential was provided by a high voltage DC supply (73030P series, Genvolt, UK). The grounded collector was a custom-made rotating cylinder (Width: 10 cm, Diameter: 8 cm).

3.5.2 Electrospinning of PSI/PVA Composite Meshes

To produce co-electrospun meshes, two polymer solutions were concurrently electrospun on the same collector as depicted in Figure 8. PSI and PVA solutions were prepared at 25 w/w % and 15 w/w % using DMF and UP water, respectively. To produce entirely 1 – 1 mass ratio meshes the solutions were always prepared using the same polymer mass (i.e., 1 g PSI and 1g PVA), in addition flow rates were adjusted to equalize fibre distribution along the mesh. Furthermore, 454 μL of 1M glutaraldehyde was added to the PVA solutions as a cross-linking agent. The cross-linking density was set to 50 (where in theory every 50th monomer is cross-linked). Control PVA meshes were fabricated with exactly the same electrospinning parameters. Details can be found in Table 5.

Table 5. PSI/PVA Co-electrospun mesh parameters

Polymer	Concentration (w/w %)	Voltage (kV)	Flow Rate (ml/h)	Needle Diameter (G/mm)	Collector Distance (cm)	Collector Speed (rpm)
PSI	25	14.5	0.7	18 / 0.838	20	500
PVA	15	17.5	1			

3.5.3 Electrospinning of PSI/PCL Composite Meshes

PSI/PCL composite meshes were fabricated in three different configurations. Bilayer meshes were fabricated by layered electrospinning, co-electrospun meshes by co-electrospinning and blend meshes by blend electrospinning. In the same manner to the PSI/PVA meshes, fabrication was performed resulting in 1 – 1 polymer mass ratio meshes.

Table 6. PSI/PCL composite meshes electrospinning parameters

Mesh	Polymer Concentration (w/w %)	Voltage (kV)	Flow Rate (ml/h)	Distance (cm)	Collector Speed (RPM)
PCL	15	12.5	1	20	500
Layered PSI/PCL	15 / 25	12.5 /13.5	1/1		
Co-spun PSI/PCL	15 / 25	12.5 / 13.5	1/0.6		
Blend-spun PSI/PCL	15 +25	13	1		

3.6 Mechanichal Treatment of PSI and PSI Composite Meshes

3.6.1 Mechanical Reinforcement of PSI meshes

To reinforce PSI meshes from different directions. 10 x 10 cm samples were cut from the electrospun meshes then stacked on each other. Different arrangements were prepared with layers having different fibre orientations (Figure 14). Samples were then compressed along their entire surface with 5 t of pressure with a hydraulic press (RH-97331 Hydraulic Press, Shanghai Reach Automotive, China) (Figure 15).

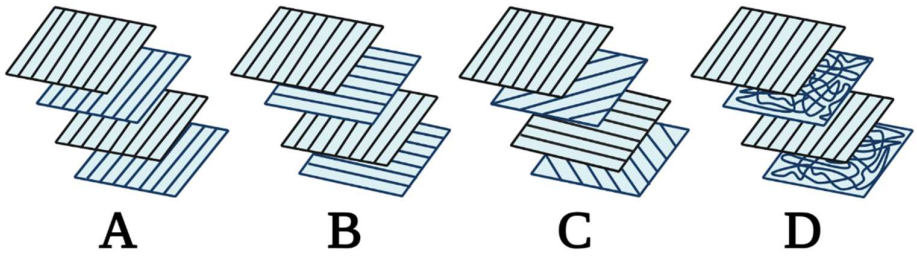

Figure 14. Mechanical Treatment of PSI meshes: 4 x 0°, B: 0°+90° variation, C: 0°+45° +90° +135°, D: 0°+ non oriented fibre layer variation

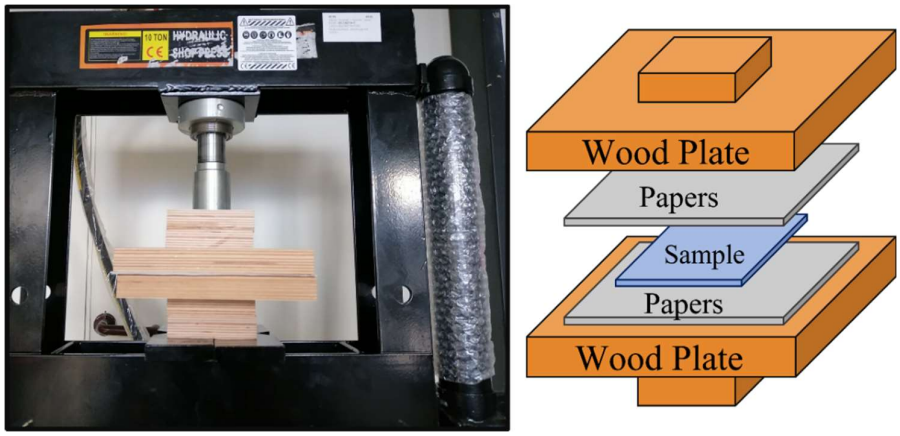

Figure 15. Mesh compression using a hydraulic press

3.6.2 Mechanical Reinforcement of PSI Composite Meshes

Due to the lack of an industrial device and setup, the mesh fabrication has its limit. For this reason, the produced meshes were quite thin and fragile (i.e., less than 0.5 mm) thus measuring thickness with a calliper was not deemed trustworthy). The folding technique was performed keeping the direction of the collector the same throughout the folding (Figure 16). Subsequently, composite samples were compressed (at room temperature and humidity) in the same manner as the PSI samples (Figure 15).

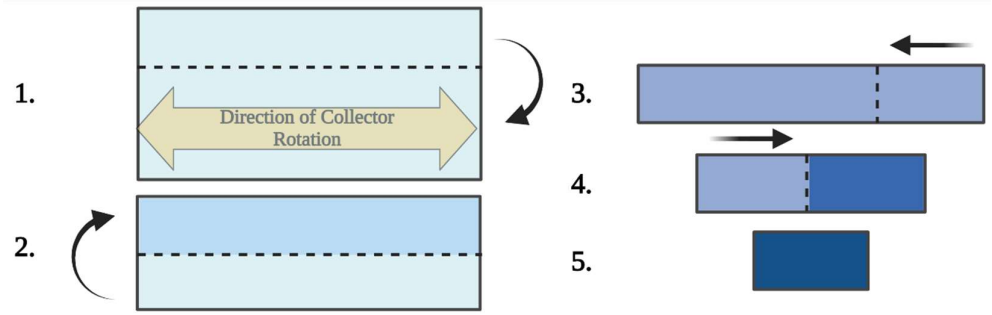

Figure 16. Folding technique for PSI composite meshes

3.7 Chemical Treatment of PSI and PSI Composite Meshes

Theoretically polysuccinimide is rapidly hydrolysed *in vivo* to polyaspartic acid in 2 – 3 days. To prevent this quick degradation. Chemically induced post-electrospinning cross-linking was performed. PSI and PSI/PCL composite meshes were immersed in a 0.5 M DAB/EtOH Solution for 1 hour(at room temperature). The chemical reaction can be observed in Figure 17.

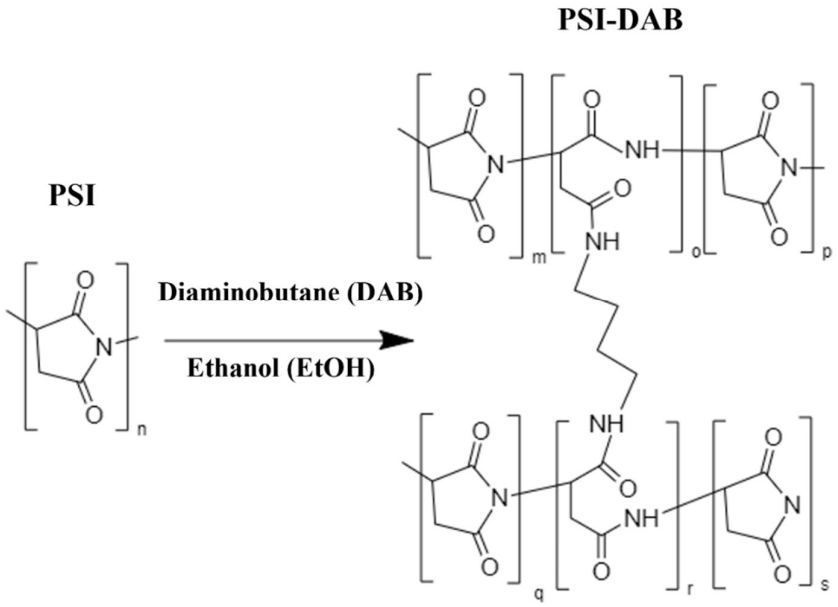

Figure 17. Chemical cross-linking of PSI by immersion in DAB/EtOH

In addition, PVA also requires cross-linking to prevent its immediate dissolution. PVA and PSI/PVA meshes were cross-linked by GDA. The GDA was added to the polymer solution pre-electrospinning however, to induce the cross-linking reaction a low pH is required. Thus, PVA and PSI/PVA meshes were immersed in 2M HCL for 1 hour (at room temperature). The chemical reaction can be seen in Figure 18.

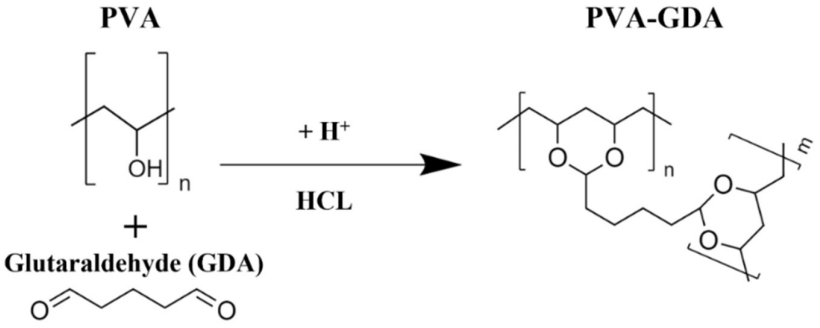

Figure 18. PVA cross-linking chemical reaction

In the case of the PSI-DAB/PVA composite meshes, a three-step cross-linking process was performed comprised of:

1) GDA Cross-linking (immersion in HCL)
2) Thorough washing in UP water until the pH becomes neutral
3) DAB cross-linking (immersion in DAB-/EtOH)

All chemically treated meshes and samples were thoroughly washed with UP water before storage.

3.8 Functionalisation of PSI and PSI Composite meshes

Magnetic nanoparticles were incorporated into PSI and PSI/PCL composite meshes (PSI-DAB). 1.5 x 1.5 cm square samples were cut and immersed in a 0.5 M DAB/EtOH solution. Subsequently, to synthesize magnetite inside the fibres, the membranes were first immersed in a Fe(II)-Fe(III)-chloride solution (14,92 g $FeCl_3$ and 12,6 g $FeCl_2$ x 4 H_2O dissolved in 30 ml UP water) then in a 3 M NaOH solution (2.37 g solid NaOH dissolved in 25 ml UP water). The immersion duration was 1 hour, 30 minutes and 30 minutes, respectively.

3.9 Sterilization and Storage

Samples before chemical treatment and functionalisation were stored dry in airtight boxes. After the chemical treatment, samples were always thoroughly washed with UP water then storage in UP Water or PBS (pH=7.4, I=150mM) with added Na-azide (0.1 w/w %,) and Chlorine Dioxide (10 w/v %) under refrigeration.

3.10 Chemical Characterisation of PSI and PSI Composite Meshes

Chemical analysis of the electrospun fibrous meshes was performed using an FTIR spectrophotometer (4700 series type A, JASCO, Japan), equipped with a diamond ATR head (ATR Pro One, JASCO, Japan). All measurements were carried out in a mid-infrared range of wavelength (4000 – 400 cm^{-1}), with 2 cm^{-1} resolutions and 126 total number of scans. Prior to starting the analysis, background spectra (H_2O, CO_2, ATR Head exclusion) were obtained on a clean and dry diamond crystal and were subtracted from the sample spectra. All samples were examined dry (chemically treated samples were extensively dried in a dehydrator first).

3.11 Physical Characterisation of PSI and PSI Composite Meshes

3.11.1 Scanning Electron Microscopy

To examine the fibre quality and size scanning electron microscopy was utilised. Small (10 mm^2) samples were taken from meshes before and after the chemical treatment. In the case of the treated samples, freezing and lyophilization was necessary before imaging. Images were taken with a JSM 6380LA scanning electron microscope (JEOL, Japan). After securing them on an adaptor with conductive stickers, samples were coated with a thin layer of gold using a JFC-1200 Sputter Coating System (JEOL, Japan). The applied voltage was 15 kV and micrographs were obtained at a 1000x, 2500x and 5000x magnifications. Average fibre diameter and size distribution were determined by measuring 100 individual fibres. All measurements and studies were performed using Fiji software (Open-Source Software) and a non-parametric one-way analysis (Kruskal-Wallis test, $p<0.05$) was performed using STATISTICA 10 software (TIBCO Software Inc, USA).

3.11.2 Two Photon Excitation Microscopy

In order to examine the fibre distribution of the composite meshes two-photon excitation microscopy was utilized. PSI fibres can be observed as produced without staining, due to their auto-fluorescent nature. PVA and PCL fibres were stained with Nile Blue A stain (0.5 w/w % of Polymer). A Femto2D series (Femtonics, Hungary) two-photon microscope was used. Photo-activity of samples was induced with a DeepSee™ laser (Spectra Physics, United States), with a excitation wavelength of 800 nm. Images

were taken with a 10× and 60× objectives through the low-green (emission wavelength: 490-560 nm) and low-red (emission wavelength: 600-700 nm) channels.

3.11.3 Fluorescence Microscopy

Fluorescence microscopy was utilised to examine difference between composite meshes, namely co-electropsun and blend-electropsun PSI/PCl composties. A Nikon Eclipse E600 Fluorescence Microscope (Nikon, Japan) equipped with a Prime BSI Scientific CMOS (Teledyne Photometrics, USA) was utilised. In order to distinguish the PCL from the PSI fibres, Nile Blue stain was thoroughly mixed over 72 h (0.5 w/w %) with the PCL solutions at 40 ºC. In the case of blend electrospinning, the dyed PCL solution was mixed with the PSI solution just 5 minutes before electrospinning. A small sample was collected during electrospinning which then was observed under the microscope at a 340 nm excitation wavelength. Images were taken with a 20× and 40× objectives through two different channels (380 and 480 nm wavelength).

3.11.4 Water Contact Angle

Assessment of wettability was performed on small circular samples (d = 1.6 cm) from each mesh. Distilled water was transferred to a 50 µl Hamilton syringe equipped with a needle (d = 0.56 mm) then, a droplet (5 µl) was carefully placed on the centre of the samples. Assessments were performed using a contact angle meter with a built-in camera (OCA 15 Plus, Dataphysics, Germany). Initial water angles (θ) were measured as well as absorption times (t) when applicable. In the case of the layered samples, the contact angle was measured on both sides. All samples were examined in a dry condition (pre-dehydrated).

3.11.5 Transmission Electron Microscopy

Magnetite nanoparticles were examined by TEM studies performed on the soaking solution of the PSI-DAB-Magn. After washing out some magnetic particles from the mesh membrane (using with ultrapure water for that), the particles were dropped on a CF200-as Cu TEM grid in a highly diluted way and dried on it. The grid was placed in a Philips CM20 (accelerating voltage: 200 kV, LaB6-filament). The maximum resolution of the instrument is 0.2 nm.

3.12 Mechanical Studies of PSI and PSI Composite Meshes

To assess the mechanical parameters of the meshes, samples (1.5 cm x 6 cm) were taken from every mesh in both a vertical (N = 5) and horizontal (N = 5) orientation (to that of the collector's axis of rotation) direction (Figure 19). A uniaxial mechanical tester (4952, Instron, USA) was utilised. The mesh samples were pulled until tearing at a pulling speed of 1 mm/minute. The highest load registered was regarded as the maximal sustained load.

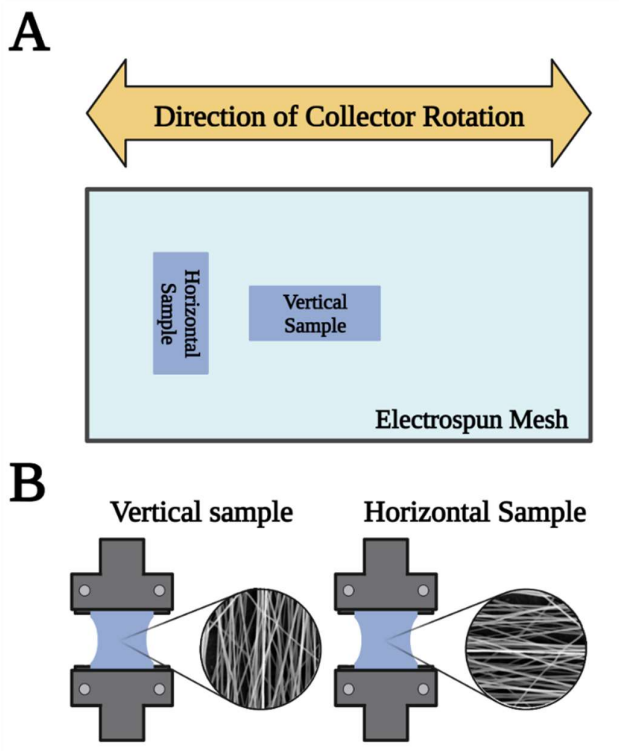

Figure 19. Vertical and horizontal sample concept

Mechanical assessment of soft biomaterials is quite complex as a defect or deformation is always created upon clamping or fixation. To be as comprehensive and objective as possible, the surface area and the mass of the samples were both taken into consideration. A specific loading capacity was calculated using the following formula:

$$\textbf{Specific Load Capacity}\ (\frac{\boldsymbol{N\ m^2}}{\boldsymbol{g}}) = \frac{Maximal\ Sustained\ Load\ (N)}{Area\ Density\ \left(\frac{g}{m^2}\right)}$$

where

$$\textbf{Area Density}\ (\frac{\boldsymbol{g}}{\boldsymbol{m^2}}) = \frac{Sample\ Mass\ (g)}{Sample\ Surface\ Area\ (m^2)}$$

Generally, biomaterial mechanical assessment is performed in air, however, as these samples are intended for implantation replicating the surrounding environment could give further insight to the in vivo performance of the biomaterials. Therefore, samples were assessed in air (Figure 20 A) and under liquid (physiological saline, temperature: 25 ºC) (Figure 20 B).

Figure 20. Uniaxial mechanical measurement in air and under liquid

3.13 Cell Studies of PSI and PSI Composite Meshes

3.13.1 Preparation of 155BR cell line

155BR adherent human skin fibroblast cells (ECACC 90011809) were purchased from European Collection of Authenticated Cell Cultures. The cells were maintained in a humidified incubator (Nuaire, USA) in tissue culture flasks under standard culture conditions (37 °C, 5% CO_2, 100% humidity). The culture medium consisted of Eagle's Minimal Essential Medium supplemented with 15 v/v % FBS, 2 mM L-glutamine, 1 v/v % Non-Essential Amino Acids (NEAA), 100 units/ml penicillin and 100 mg/ml streptomycin.

3.13.2 Cell viability assay and cell morphology studies

To investigate the incidental toxicity of the fibrous samples, first, disk shaped) samples (Diameter: 0.16 mm were sterilised by immersion in a ClO_2/PBS mixture for 1 hour. Subsequently samples were left immersed in the cell culture medium (1 ml/disk) overnight before the examination.

10 000 cells/cm^2 were seeded in 100 µl cell culture medium in wells of 96 well plates. After culturing for 1 day, the cells were treated with the rinsed fibrous disk

samples. After 24 and 72 hours of the treatment, the WST-1 [2-(4-Iodophenyl)-3-(4-nitrophenyl)-5-(2,4-disulfophenyl)-2H-tetrazolium] cell proliferation reagent was applied. This reagent contains water soluble tetrazolium salts, which are cleaved to formazan molecules by mitochondrial enzymes in the living cells. 100 µl of 1:20 dilution of WST-1 reagent with Minimal Essential Medium without Phenol Red was applied in each well for 4 h at 37 °C. After the incubation, the absorbance of the formazan molecules was detected by a microplate reader (Model 3550, Bio-Rad Laboratories, Japan) at 450 nm with 650 nm reference wavelength. Wells containing only the reagent, but no cells were used as blank and untreated cells were used as control.

To visualize the level of confluency and the morphology of the cells after the treatment, cell cultures were observed under a phase contrast microscope (Nikon Eclipse TS100, Nikon, Japan) with a 4x objective. Images were taken with a high-performance CCD camera (COHU, USA) applying the Scion imaging software.

3.13.3 Cell adhesion and morphology studies

For observation of cell adhesion, disk shaped fibrous samples (d = 16 mm) were sterilised by immersion in ClO_2/PBS mixture for 1 hour then rinsed in cell culture medium (4 ml/disk) twice the day before cell seeding.

On the following day the disks were rinsed in a fresh cell culture medium for 2 hours. Cells were labelled with fluorescent vital dye Vybrant DiD before seeding onto the fibrous samples. During this experiment, 6 well plates were used for seeding the cells at 20 000 cells/cm^2. The fibrous disks were placed onto round glass coverslips in the wells. Cloning rings were used to keep the fibrous disks on the bottom of the wells. Wells containing cells seeded on glass coverslips were used as control.

After 24 and 48 hours the medium was changed to fresh cell culture medium (5,5 ml). After 72 hours of seeding, samples were washed with tempered PBS (37 °C) then fixed with 4% para-formaldehyde (PFA) at room temperature for 20 min, which was followed by another wash in PBS. stored at 4 °C until examination under a Femto2d two-photon microscope (Femtonics, Hungary). A Spectra Physics Deep See laser was used with 800 nm wavelength to induce the photoactive stain. Pictures were taken using a 10x objective applying the MES4.4v program.

3.14 Animal Experiments and Biocompatibility Investigation of PSI and PSI Composite Meshes

3.14.1 Animal Model

In order to examine a biomaterials biocompatibility and biodegradability profile, *in vivo* animal experiments are required. For this purpose, Wistar rats were chosen as the animal model according to the European Union's 2010/63/EU and EU 2019/1010 directive on the protection of animals used for scientific purposes. Rats possess the size, blood volume, and easy handling properties required for the study. Male rats (average weight: 225-250 g) were acquired (Toxicoop Zrt., Hungary) and kept in groups of four. Animals were then randomly selected. Sample and Termination dates can be found in Table 7. The experimental protocol adhered to rules laid down by the Directive of the European Parliament and of the Council on the protection of animals used for scientific purposes and was approved by the Semmelweis University's Institutional Animal Care and Use Committee. The animal experiment registration number is PE/EA/93-7/2021. The accreditation number of the animal experiment facility is 22.1/1244/3/2015.

Table 7. Sample and termination dates for in vivo experiments

Animal Name	Sample 1	Sample 2	Termination
PSI 1-4	PSI	PSI-DAB	2 Weeks
PCL 1-3	PSI/PCL co-spun	PSI-DAB/PCL co-spun	
PCL 4	PSI/PCL co-spun	PCL	
PCL 5	PSI-DAB/PCL co-spun	PCL	
PCL 6-8	PSI/PCL blend-spun	PSI-DAB/PCL blend-spun	
PCL 9	PSI/PCL blend-spun	PCL	
PCL 10	PSI-DAB/PCL blend-spun	PCL	
PVA 1-3	PSI/PVA-GDA	PSI-DAB/PVA-GDA	
PVA 4	PSI/PVA-GDA	PVA	
PVA 5	PSI-DAB/PVA-GDA	PVA	
PSI-Magn 1-3	PSI-DAB-Magn	1 Day, 8 Days	1 Day, 8 Days

3.14.2 Surgical Procedure

Surgical anaesthesia and analgesia were performed by intraperitoneal injection of a 4:1 Ketamine (70 mg/bodyweight kg) and Xylazine (10 mg/bodyweight kg). Before implantation, the samples were sterilized by immersion in a PBS/ClO_2 solution for 30 minutes. The surgical procedure was entirely aseptic. Surgical instruments and equipment were sterilised by a Kronos Class B autoclave (Unimet Kft, Hungary). Two samples (1.5 x 1.5 cm) were implanted in every animal After a dorsal median 5 – 6 cm incision (Figure 211 A, B) on the back along the nuchal ligament the subcutaneous tissue was bluntly dissected to ensure enough space for the samples. Samples were fixated along the dorsal median line on the underlying fascia and muscle with a simple interrupted stich (21 C, Figure 222B). Non-cross-linked samples were fixated cranially while cross-linked ones were always secured caudally. Skin closure was performed with an intracutaneous suture technique (Figure 2121 D, Figure 222C). For both fixation and skin closure an Atramat 4-0 polyglycolic acid absorbable suture material was used.

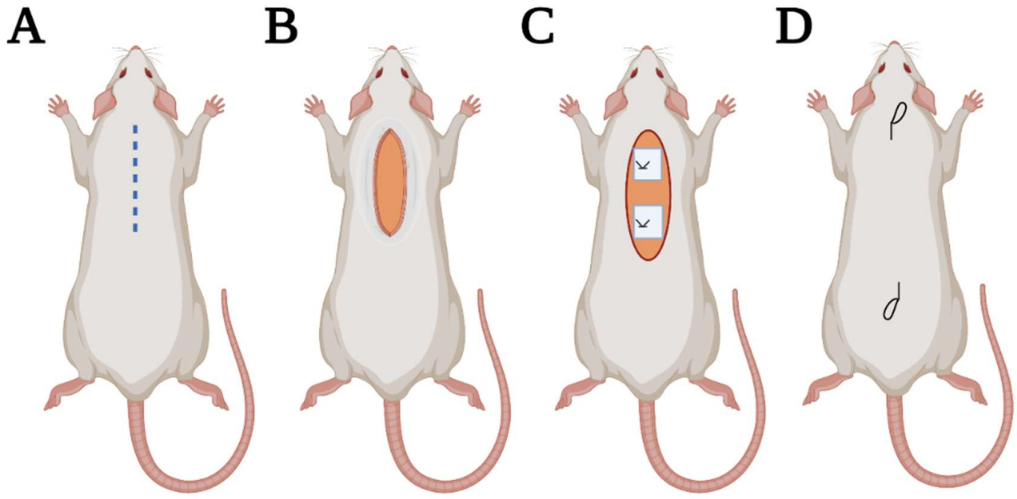

Figure 21. Surgical Procedure: A. Dorsal Midline Incision, B Dissection, C. Sample Implantation and fixation, D. Skin closure with intracutaneous technique

In the case of the PSI-DAB-Magn investigation only one sample (1x1 cm) was implanted in a similar manner to prevent sample interference issues during the MRI examination.

Control animals were not designated According to the in the 2010/63/EU guideline of the European Union, the number of animals used should be reduced as low as reasonably possible. In this regard, the surgical procedure for the control animals would

just involve the same incision proceeded by the skin closure. This would almost certainly result in a standard, physiological wound healing process that is comprehensively documented in peer-reviewed literature, surgery, and pathology books.

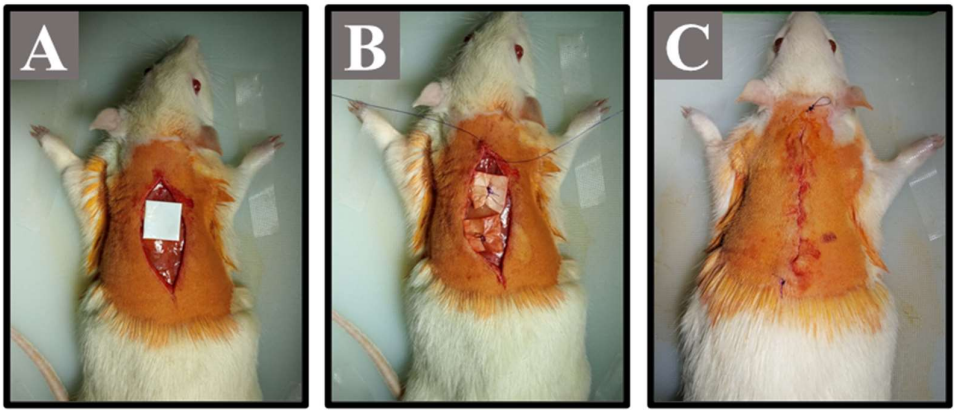

Figure 22. Implantation Procedure: A. After Incision and dissection, B. Samples fixated by a simple interrupted suture, C. Intracutaneous skin closure

3.14.3 Animal Housing

Post-operatively animals were kept in individual cages (Polycarbonate Cage type IIL), for one week in order to prevent animal interactions and wound suture disturbance. After one week, animals were kept in groups of 4 (Polycarbonate Cage type IV) (Figure 23 A). Environment enrichment was ensured by paper tunnels, paper nesting material and paper sheets (Figure 23 B-C).

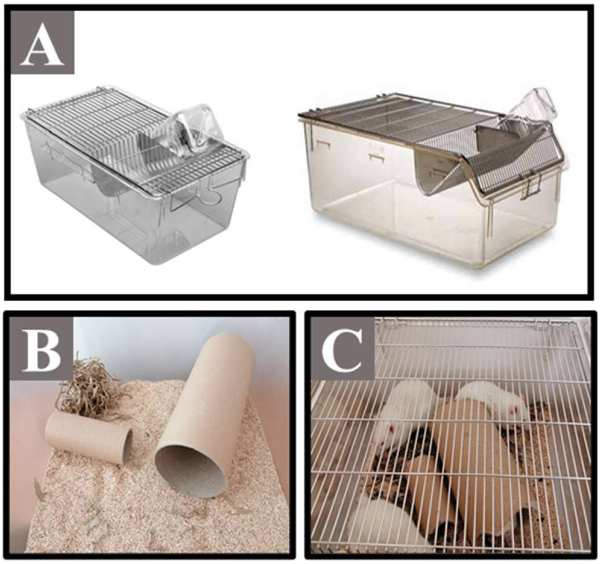

Figure 23. Animal housing during the experiments Polycarbonate Type IIL (left) and IV(right), B. Environment enrichment, C. Animals exploring the housing

3.14.4 Animal Monitoring

Animals were observed daily for evidence of wound complications, such as skin dehiscence, seroma, hematoma, or infection. If applicable, wound cleaning and disinfection was applied. Grimace scale and animal weights were documented. Grimace scale documentation (orbital tightening, nose flattening, ear changes) was performed daily for five days. Animal weight was documented on the first three post-operative days, then weekly.

3.14.5 Haematocompatibility Examination

Blood sampling was performed before every assigned termination. Blood samples were collected from the retro-orbital plexus and cardiac puncture using glass capillaries and needles respectively. Blood samples were then evaluated with an Abacus Vet 5 (Diatron Zrt., Hungary). Results values for each sample were averaged (e.g., leukocyte count, thrombocyte count etc.) then, averaged once again for each mesh type.

3.14.6 MRI Imaging

PSI-DAB-Magn meshes were examined by MRI. On the 1st and 7th postoperative day, animals were placed in a nanoScan PET/MR (Mediso, Hungary) instrument equipped with a 1T permanent field magnet, 450 mT/m gradient system and volume transmit/receive coil with a diameter of 60 mm. Examination parameters were: axial orientation, 0.5 mm slice thickness, 128 slices, and with a pixel size of 0.5 mm. T2 relaxation was determined in 3 animals parallel.

3.14.7 Termination and Sample Retrieval

Termination dates can be found in table. Termination was performed by providing anaesthesia and analgesia by an intraperitoneal injection of Ketamine-Xylazine followed by an intracardiac KCl injection. Samples were extracted by dissection the overlying skin and underlying muscular layer. then preserved in a 10 w/w % formaldehyde solution for 48 hours.

3.14.8 Histopathology Examination

Samples cut and transferred to tissue cassetes, After sample immersion in the PBS solution, samples were processed in a Leica TP1020 tissue processor. The process involved sample immersion and transferring in the following solutions:

1. 70 % Ethanol – 2x1 hour
2. 80 % Ethanol – 2x1 hour
3. 95 % Ethanol – 2x1 hour
4. Absolute Ethanol – 1 hour
5. Xylol – 2x1 hour
6. Paraffin 56-60 ºC – 1 hour

Paraffin embedding was then performed using a Leica Histoscore Arcadia H and Leica Histoscore Arcadia C. Slices of 8 µm thickness were cut (Histo Core Cut RM 2245, Leica, USA). Slices were transferred to microscope glass slides (Surgipath, Leica, USA) with the help of a H1210 water heater (Leica, USA).

The Haematoxylin-Eosin staining was performed with according to the following protocol:

1. De-paraffinization
    - Xylol – 2x 10 minutes
2. Hydration
    - Absolute Ethanol – 2 x 5 minutes
    - 95 % Ethanol – 5 minutes
    - 80 % Ethanol – 5 minutes
    - 70 %Ethanol – 5 minutes
    - Distilled water – 1 minutes, then 5 minutes
3. Nuclear Staining
    - Harris Haematoxylin – 5 minutes
    - Distilled Water – 10 minutes
4. Differentiation
    - 1 % Acid Alcohol – 30 seconds
    - Distilled Water – 10 minutes
5. Counterstaining
    - 95 % Ethanol – 10 seconds
    - Eosin – 1 minute
6. Dehydration
    - Absolute Ethanol – 2x1 minute

- 95 % Ethanol – 2x1 minute

7. Clearing
    - Xylol – 2x5 minutes

Finally, microscope slide examination was perforemd using a Leica RM2245 Microscope. Samples were evaluated according to the ISO 10993-6 guideline for histpopathoglogy examination of implanted biomaterials.

Table 8. Biocompatibility evaluation according to ISO-10993-6

Cell Type/ Tissue Response	**Score per High Power**				
	0	**1**	**2**	**3**	**4**
Polymorphonuclear Cells	0	Rare 1 – 5 phf	5 – 10 phf	Heavy infiltrate	Packed
Lymphocytes	0	Rare 1 – 5 phf	5 – 10 phf	Heavy infiltrate	Packed
Plasma Cells	0	Rare 1 – 5 phf	5 – 10 phf	Heavy infiltrate	Packed
Macrophages	0	Rare 1 – 5 phf	5 – 10 phf	Heavy infiltrate	Packed
Giant Cells	0	Rare 1 – 5 phf	5 – 10 phf	Heavy infiltrate	Packed
Necrosis	0	Minimal	Mild	Moderated	Severe
Neovascularization	0	Minimal 1-3 buds	Mild 4-7 with supporting fibrotic structures	Broad band	Extensive band
Fibrosis	0	Narrow Band	Moderate Band	Broad band	Extensive band
Fatty Infiltrate	0	Minimal	Several layers of fat and fibrosis	Elongated and broad accumulation of fat cells	Extensive fat completely surrounding the implant
Collagen Elastin	0	Minimal	Mild	Moderated	Extensive
Traumatic Necrosis	0	Minimal	Mild	Moderated	Severe
Foreign Debris	0	Minimal	Mild	Moderated	Severe

3.15 Statistical Analysis

When applicable statistical analysis was performed using STATISTICA 10 software (TIBCO Software Inc, USA) ($p<0.05$). The type of statistical test (e.g. T-Test, Kruskal-Wallis test etc.) was decided according to the predictor and outcome variable and reference literature.

4. Results

4.1 Optimisation of electrospun polysuccinimide meshes

4.1.1 Synthesis of Polysuccinimide and Solubility Study

The synthesis was reproducible and the produced PSI batches were always macroscopically identical. Details about the PSI synthesis evaluation can be found in the relevant literature. PSI can be dissolved in dimethylacetamide (DMAc), dimethylformamide (DMF) and dimethyl sulfoxide (DMSO) (Figure 244). In addition, PSI dissolution in DMF was quite fast occurring even at room temperatures without requiring assistance. Although PSI can be dissolved in DMAc and DMSO, this occurs at slower rates unless assisted heating (40-50 ºC) is implemented. Furthermore, the colour of the polymer solution darkens as the polymer concertation increases. At 10 w/w% its yellow and almost transparent while at 25 w/w % it becomes dark amber (Figure 25).

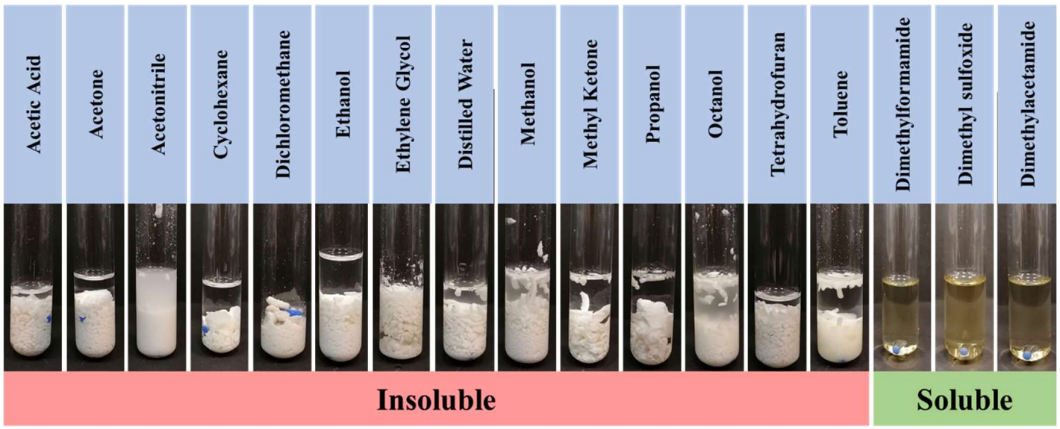

Figure 24. Solubility study results of 10 w/w % PSI solutions

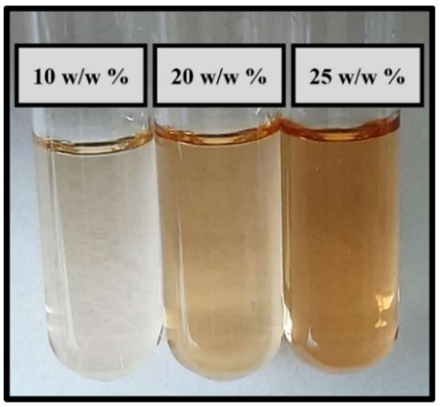

Figure 25. PSI polymer solution colorimetric differences at increasing concentrations

4.1.2 Viscosity and Conductivity Studies

Viscosity and conductivity investigation was performed on polymer solutions that were able to dissolve the PSI. The concentration was 25 w/w % as this concentration has been used for PSI electrospinning thus far. DMSO and DMF solutions proved to be the most viscous and least viscous solutions, respectively (Table 9). Furthermore, DMF proved to be the most conductive (Table 9). Relevant data for the used solvents can be found in Table 10.

Table 9. Viscosity and conductivity measurements results using different solvents at 25 w/w % PSI

Note: Presented values are average results along with their standard deviations

Sample	Temperature (°C)	Viscosity (mPas)	Conductivity (µS/cm)
DMAc	24 ±1	3150±10	3.316 ±0.03
DMF		2810±25	20.748 ±0.04
DMSO		8020±50	4.625 ±0.04

Table 10. Properties of the used organic solvents according to the chemical data banks (HSDB, ICSC, CAMEO Chemicals)

Solution	Density (g/ml)	Viscosity (mPas)	Vapor Pressure (mm Hg)	Dielectric Constant
DMAc	0.936	0.945	2.00	37.8
DMF	0.944	0.920	3.87	36.7
DMSO	1.100	1.987	0.60	46.7

Viscosity and conductivity of PSI-DMF solutions was further examined. A correlation can be observed as decreasing the concentration results in a decrease in viscosity and increase in conductivity (Table 11).

Table 11. PSI/DMF solution viscosity and conductivity

Note: Presented values are average results along with their standard deviations

Sample	Temperature (°C)	Viscosity (mPas)	Conductivity (µS/cm)
25 w/w% (DMF)	24 ±0.5	2810±10	20.748 ±0.04
22.5 w/w% (DMF)		716±5	21.453 ±0.04
20 w/w% (DMF)		320±2	22.318 ±0.03

Relative viscosity measurements concluded that increasing frequency decreases the viscosity in all three PSI/DMF solutions (Figure 26).

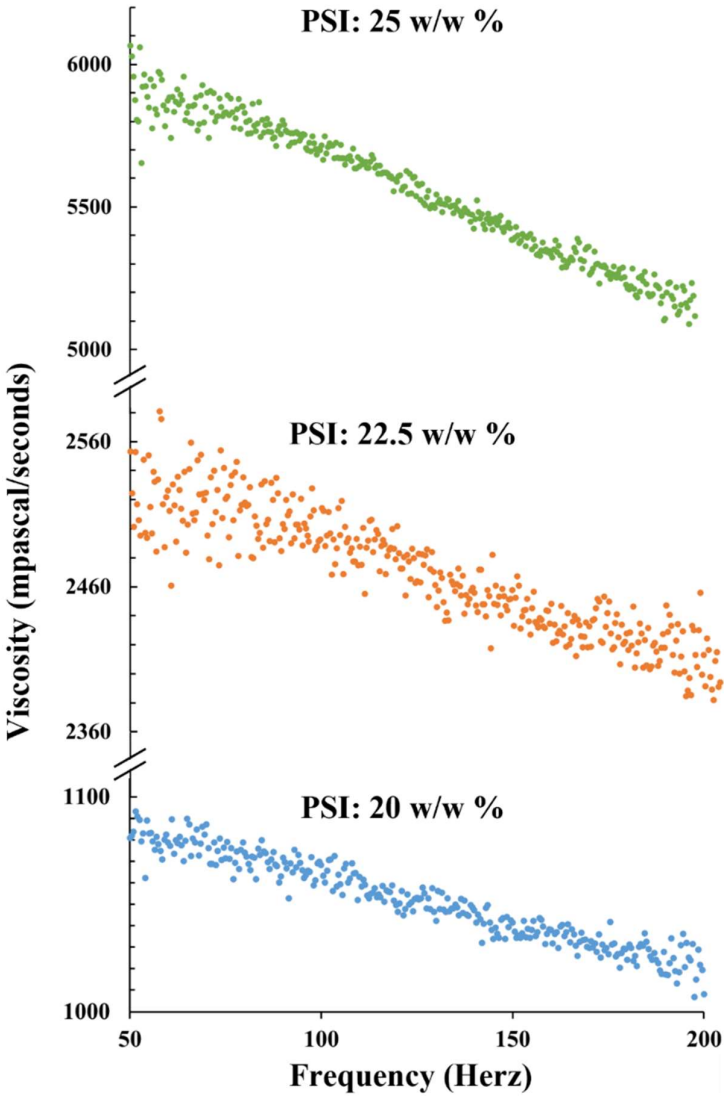

Figure 26. Relative viscosity comparison of PSI solutions

4.1.3 Fibre Quality and Diameter Optimization

Effect of Solvents

DMF proved to be the best solvent option as not only the polymer solution preparation was achieved with the least effort, but the produced fibres are evidently the best in terms of quality (Figure 27). In contrast DMAc and DMSO based solutions produced fibres containing beads and other artefacts (Figure 27).

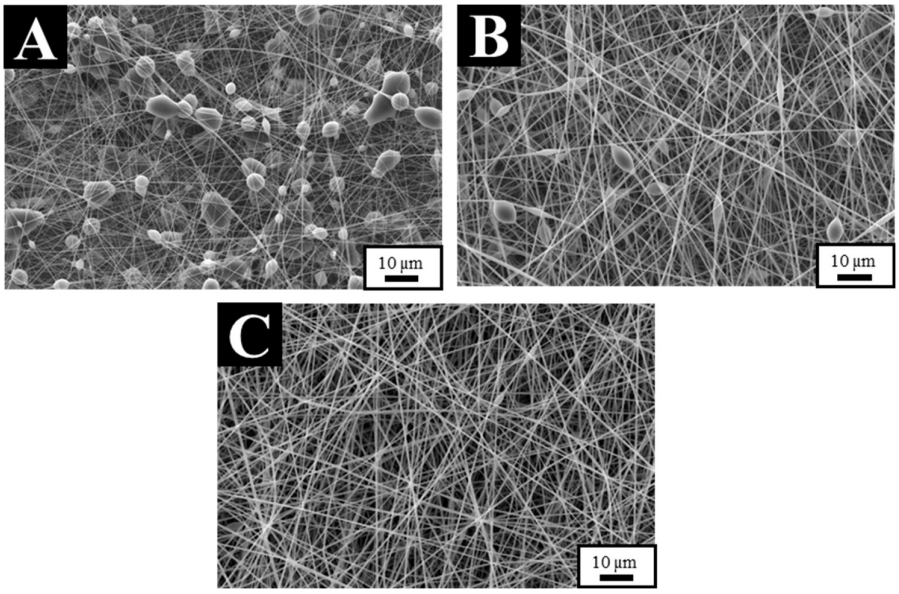

Figure 27. Electrospun meshes produced with 25 w/w % PSI in A. DMSO, B. DMAc, and C. DMF.

Note: Exact electrospinning parameters can be found in Table 11

Comparing the IR spectra of the PSI meshes produced by using different solvents while the characteristic peaks concur with ones found in other works (59,63,73) ; no significant difference can be seen when using different solvents (**Error! Reference source not found.**). Examining them in detail; the peaks depict the asymmetric stretching vibration (1705 cm^{-1}), the stretching bending vibration (1385 cm^{-1}) for the imide ring, the C—N stretching vibration (1159 cm^{-1}), the C=C (835 cm^{-1}) and C-H (697 cm^{-1}) bending vibration.

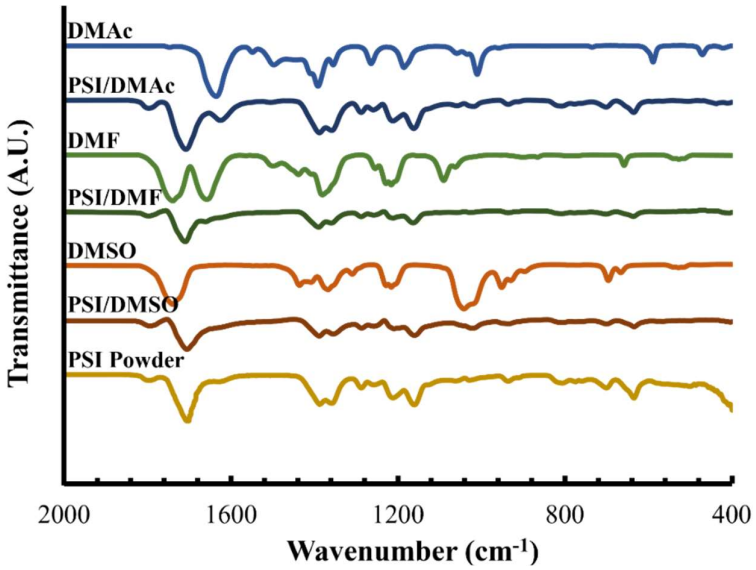

Figure 28. ATR-FTIR analysis of meshes produced with 25 w/w % PSI

Effect of Collector Speed and Distance

Increasing the rotation speed of the collector had one prominent effect, increasing fibre alignment. In Figure 29 (A-D) the correlation of collector speed and fibre alignment can be visually as well as quantitatively observed. Regarding fibre size, the influence of the collector speed was deemed insignificant as the fibre size changes were within the standard deviation and statistically not significant. In addition, collector distance was also proven to be a non-significant parameter as neither fibre size nor orientation was influenced.

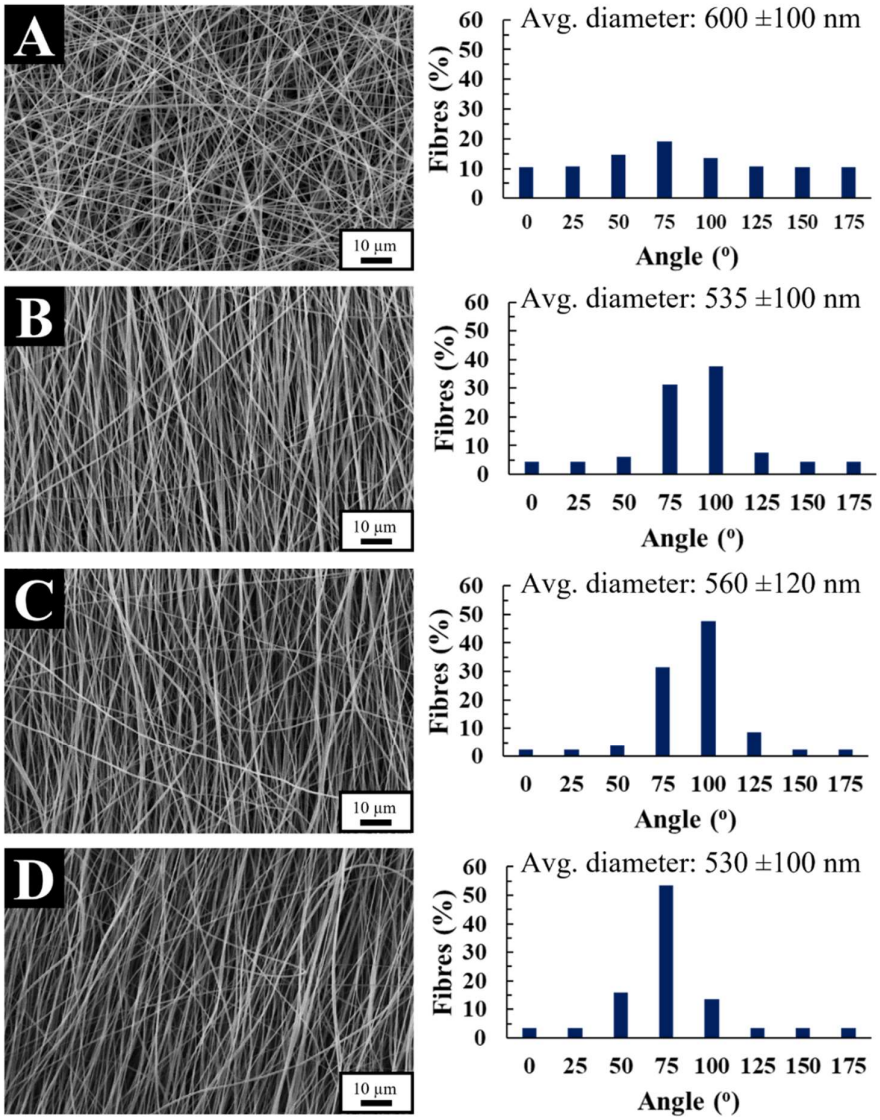

Figure 29. Effect of collector speed on fibre alignment: A: 60 RPM, B:2000 RPM, C: 4000 RPM, D: 6000 RPM

Note: Zero angle is aligned along the X axis of the SEM micrograph. Average diameters are given with standard deviation

Effect of Needle Size and Flow Rate

Needle size and flow rate adjusted together significantly decreased the fibre diameter of the meshes. The combined effect of these two parameters was able to produce a significant 130 nm decrease in fibre size (from 550 ±120 to 420 ± 60, $p < 0.0005$) but also narrow the fibre size deviation from the mean, making these meshes not only composed of thinner but more uniform fibres. Decreasing the flow rate was not significant only in two occasions (Figure *30*30). Additional results depicting all investigated needle sizes and flow rates can be found in the Supplementary Information.

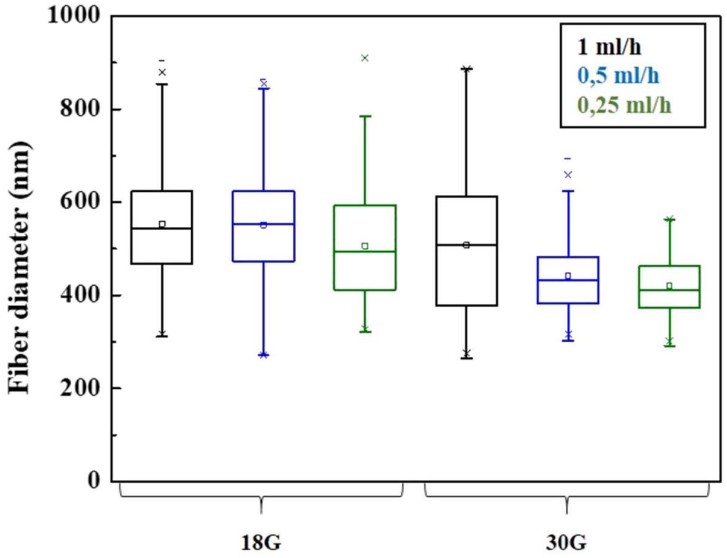

Figure 30. Effect of decreasing needle diameter and flow rate (electrospinning parameters: 13 kV, 25cm, 6000 rpm)

Note: the inner diameter of the 18 and 30 G needles are 0.838 and 0.159 mm respectively

Effect of Polymer Concentration and Voltage

Polymer concentration and voltage are also two parameters which are rather closely connected as they are typically adjusted together. The lowest PSI concentration producing fibres without defects was 22.5 w/w % (Figure 31 A). At lower concentrations (22 and 21 w/w %) bead formation was visible (yellow arrows, Figure *31*31 B, C). Furthermore, the upper voltage limit was 15 kV as by further increasing it, the jet becomes unstable, hindering uniform fibre formation.

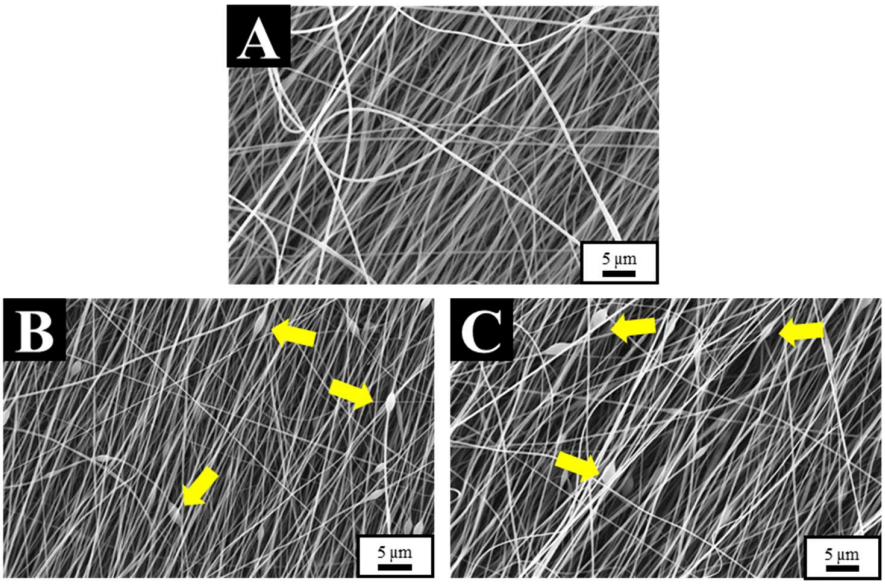

Figure 31. Effect of polymer concentration on fibre quality: A.25 w/w % -15 kV, B .22 w/w % - 15 kV, C .21 w/w % -15 kV

Increasing the voltage did not decrease the fibre dimeter although it decreased the standard deviation of the average fibre size. In contrast, the added adjustment of concentration to the previously optimized parameters produced fibres of 280 ± 50 nm diameter and had statistically the most significant effect ($p < 0.0005$) (Figure 322).

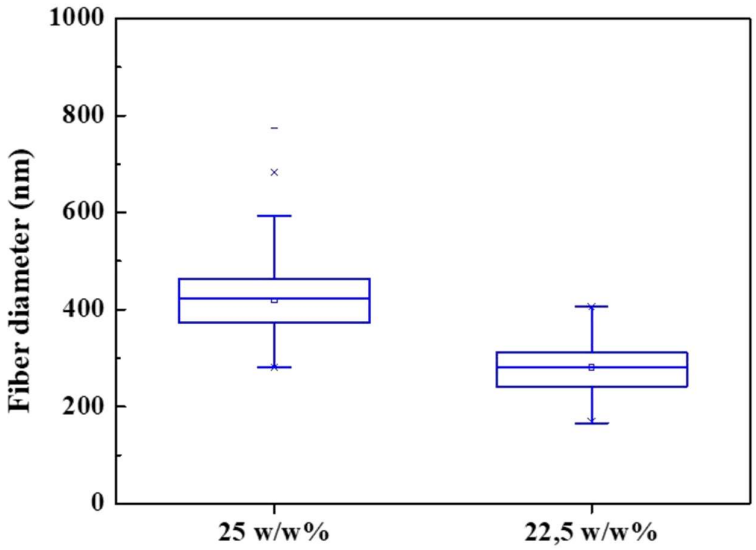

Figure 32. Decrease of fibre diameter after concentration adjustments (Electrospinning parameters15 kV,0.25 ml/h, 25 cm, 6000 rpm)

4.1.4 Mechanical Studies and Mesh Reinforcement

Effect of Fibre Alignment

As depicted in Figure 333 an increase in fibre alignment increases the specific loading capacity. In contrast, when fibres are pulled from direction 90° to that of their alignment the mesh performs poorly. No significant difference was documented in the specific loading capacity of 4000 rpm ($p = 0.51$) and 6000 ($p = 0.27$) rpm samples compared to the 2000 rpm samples or between the 4000 rpm and 6000 rpm samples ($p = 0.51$) while a significant difference as observed in the corresponding horizontal samples ($p < 0.05$) (Figure 333).

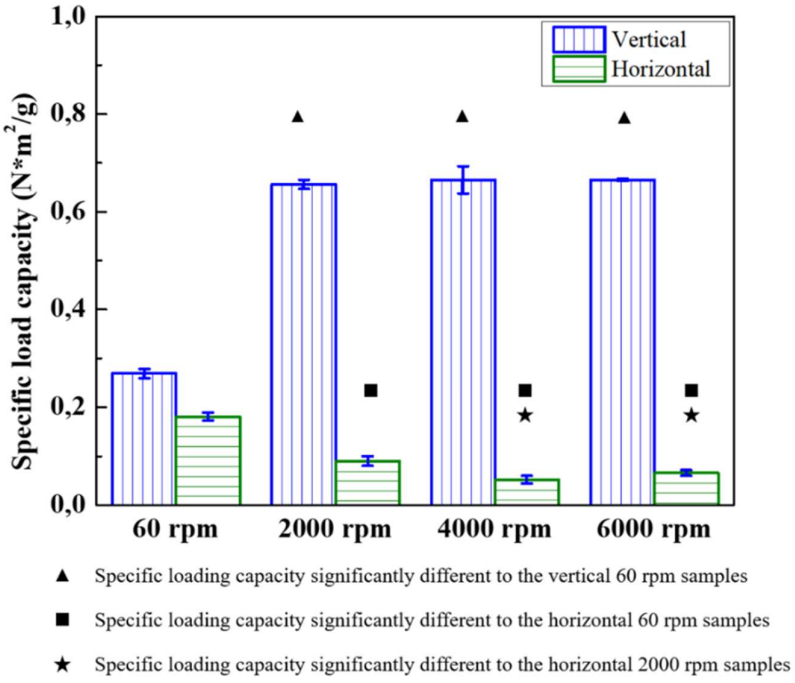

Figure 33. Effect of collector speed/ on the mechanical properties of the meshes

Fibre Diameter Correlations

Meshes composed of thinner fibres (d = 280 ±50 nm) were significantly weaker ($p < 0.0005$) than ones with thicker fibres (d = 615 ±105 nm) (Figure 34).

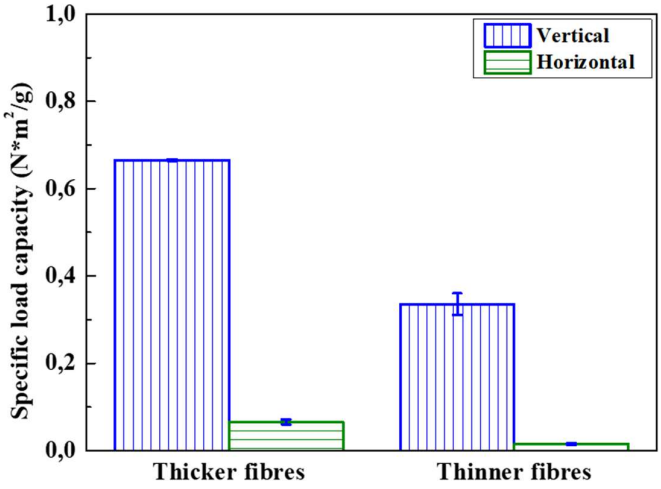

Figure 34. Fibre diameter and mechanical performance correlation
Note: Thicker fibres = 615 ±105 nm, Thinner fibres = 280±50 nm

Multi-layer Compression

The technique was successful in enhancing the biaxial mechanical performance of the meshes (both vertical and horizontal directions). In

Figure *35*, representative stress-strain curves of the different mesh layer configuration as well as their specific loading capacity is presented. Examining the results, it is evident that when alignment is kept in parallel as expected, no change is observed in the horizontal direction. In contrast, in a configuration where the layers placed with 90° alternating directions the mechanical performance of the mesh is significantly improved from either direction ($p = 0.04$). When the mesh is configured having 45° alternating directions a similar effect is observed, however the specific loading capacity is significantly less ($p = 0.04$). The fourth configuration with the aligned and randomly oriented layers performed better than expected but not as well as the aligned meshes with 90° alternating directions. In addition, while the difference may seem small, aligned meshes are more uniform as shown by their stress-strain curves (

Figure *35*) and therefore their performance can be predicted which in practical terms means they will be trustworthy during application.

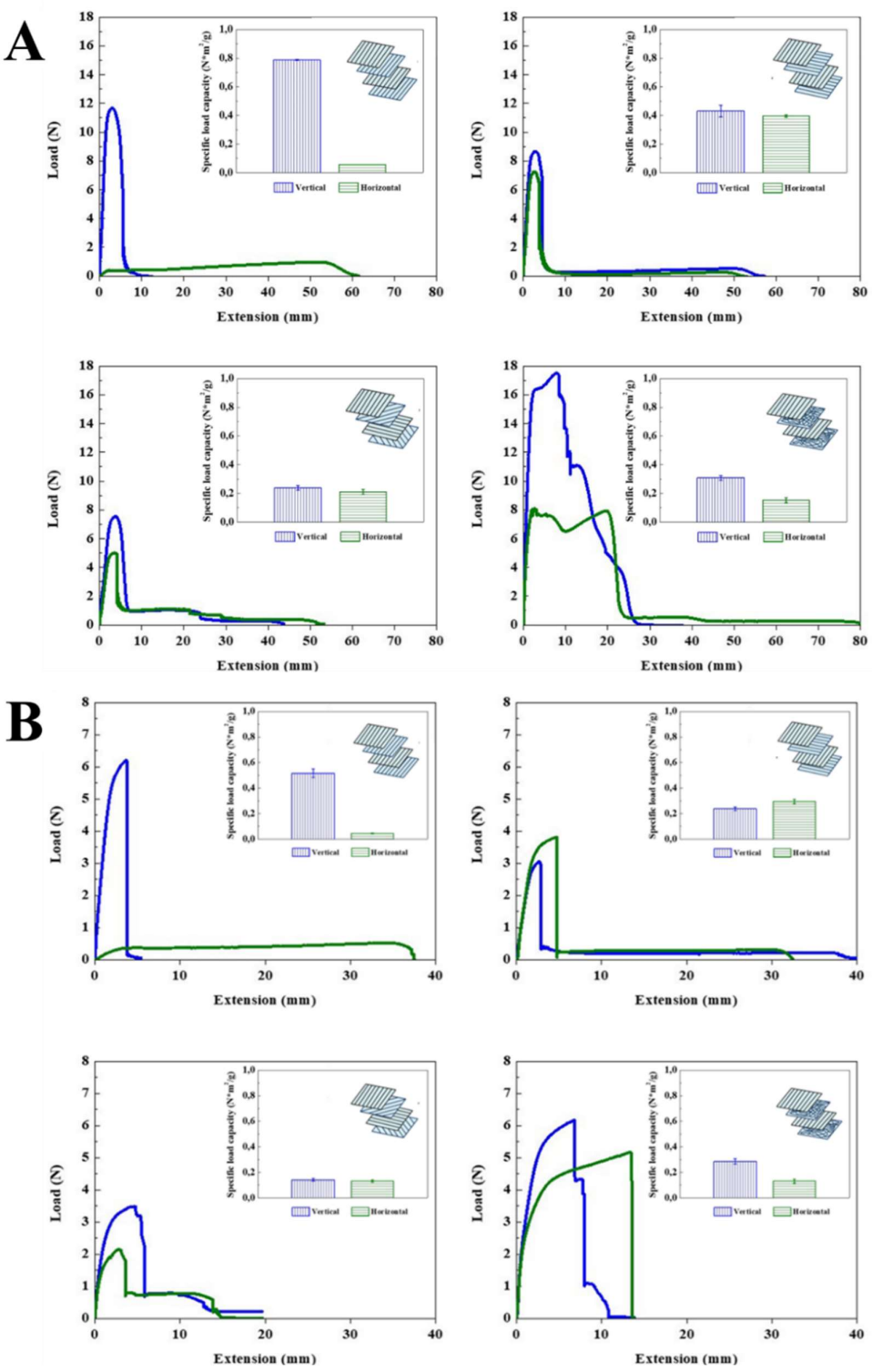

Figure 35. Mechanical evaluation of multi-layer meshes:

A. Avg. Diameter: 615 ±105 nm, B. Avg. Diameter:280±50 nm (pulling rate at 1mm/minute)

4.2 Cross-linked PSI-DAB Meshes

4.2.1 Macroscopical and Microscopical Changes

The cross-linking was successfully performed as previously documented. Details regarding the cross-linking can be found in the research group's papers (70). PSI-DAB while retaining the original white colour is no longer fleecy or adhesive due to charge. Due to the cross-linking PSI-DAB fibres absorbed the surrounding liquid and swelled (Figure 36). Average fibre diameter decreased from an initial 550 ± 130 nm to 440 ± 115 through the cross-linking reaction. Furthermore, the fibre alignment seems to have decreased as the chemical reactions seem to interfere and curl the fibres (Figure 37).

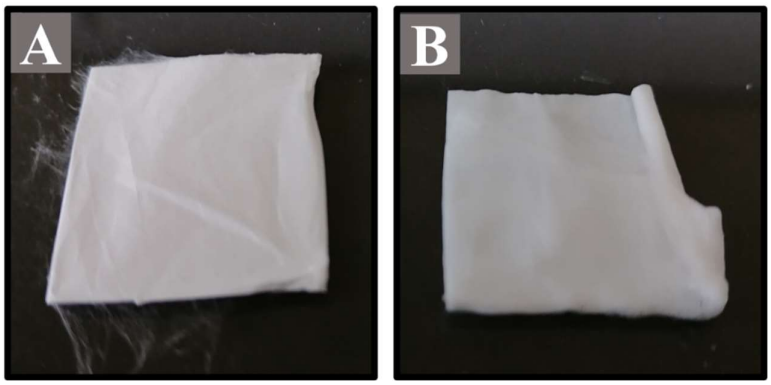

Figure 36. PSI (A) and PSI-DAB (B) mesh
Note: Sample size 1.5 x 1.5 cm

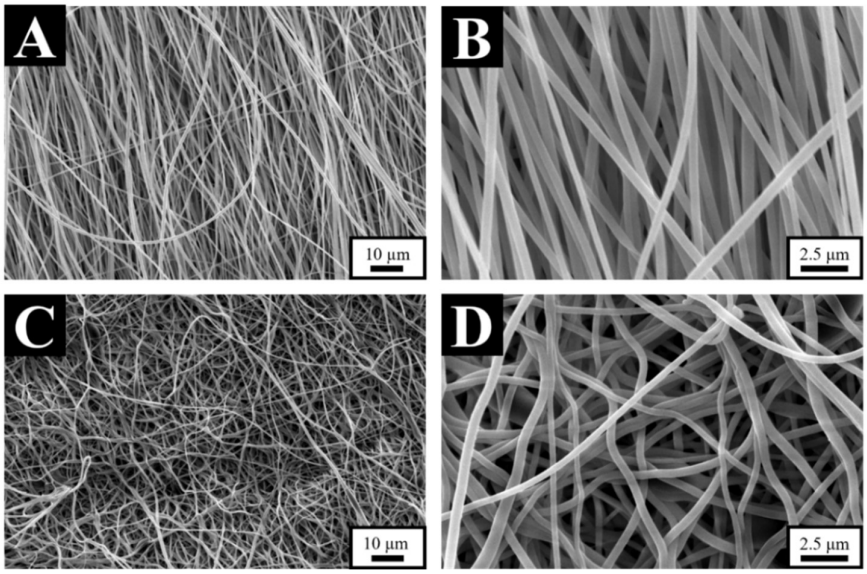

Figure 37. Scanning electron microscopy of PSI (A, B) and PSI-DAB (C, D)

4.2.2 Wettability

Wettability is a crucial parameter in biomedical applications. Although PSI is non-soluble in water according to the wettability assessment is very hydrophilic ($\theta = 31.7^{o}$) as water passed through it almost instantly (Table 12) with only an initial water angle estimation being possible. However, this is caused by a capillary effect which draws water into the mesh, a quite unique feature as PSI itself is non-water soluble. The cross-linking increases the initial water angle and prolongs the water absorption as well (Figure 388).

Table 12. Wettability of PSI and PSI-DAB meshes
Note: Presented values are average results along with their standard deviations

Mesh	Contact angle (°)	Absorption time (s)
PSI-Mesh	31.7 ± 2.0	1.41 ± 2.37
PSI-DAB	71.4 ± 6.2	28.7 ± 14.4

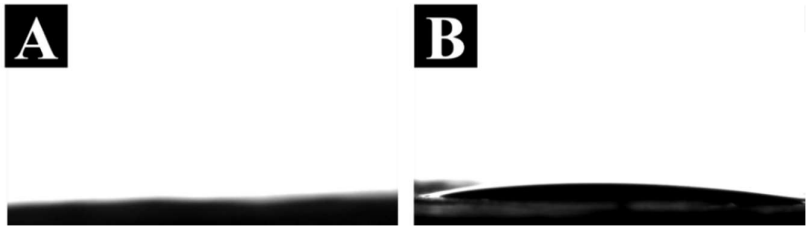

Figure 38. Wettability assessment of PSI (A) and PSI-DAB (B) meshes

4.2.3 Mechanical Properties, Cell and Animal Studies

The mechanical properties, cell studies including cytotoxicity, morphology, and cell adhesion, as well the animal studies are presented in the next two chapters along with the PSI/PVA and PSI/PCL composite meshes to provide better comparison between the different meshes.

4.3 Polysuccinimide/Poly(vinyl alcohol) Composite Meshes

4.3.1 PSI/PVA Co-electrospinning

No issues were observed with either polymer during the co-electrospinning. The single polymer meshes (PSI, PVA) (Figure 36A, Figure 399A) and the composite co-spun PSI/PVA meshes (Figure 399B) are macroscopically identical, a difference can only be identified in texture, as the composite meshes are fleecier. Macroscopical differences were documented only after the chemical treatment. PVA meshes after the chemical treatment typically become opaque (Figure 39 B). Co-spun PSI/PVA-GDA meshes remain white but swell (Figure 39 C). When comparing the co-spun PSI/PVA-GDA (Figure 39C) and co-spun PSI-DAB/PVA-GDA (Figure 39D), the latter seems to better retain its structure.

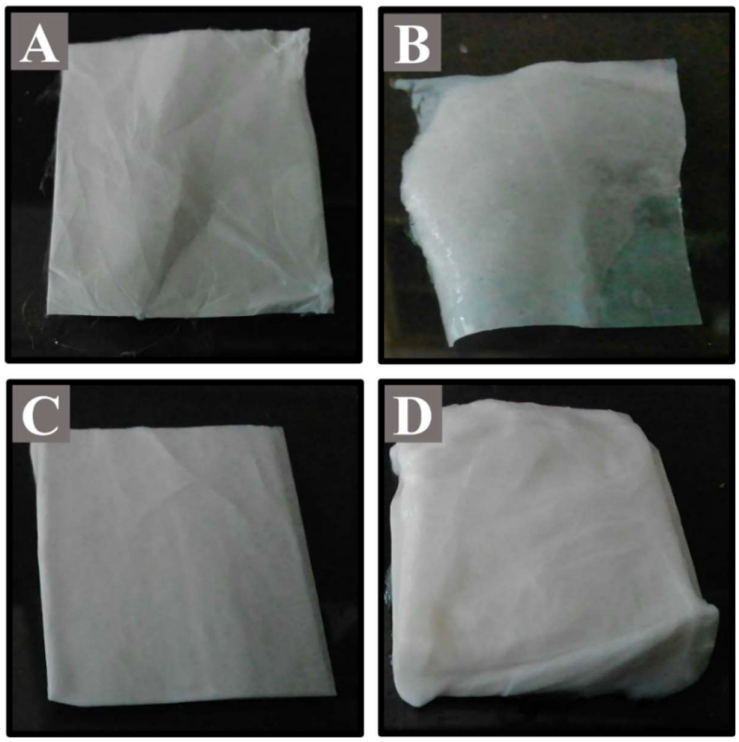

Figure 39. Samples before and after chemical treatment: A. PVA, B. PVA-GDA, C. Co-spun PSI/PVA-GDA, D. Co-spun PSI-DAB/PVA-GDA
Note: Sample size 1.5 x 1.5 cm

4.3.2 Microstructure and Nanofibre Diameter

The fibrous microstructure was present in all the meshes (PVA, cospun PSI/PVA) and remained unaltered (Figure 40, Figure 41) throughout the mechanical and chemical treatment (Sections 4.6 and 4.7). After the cross-linking, PVA fibres absorb surrounding liquid and become gel fibres (Figure 40). In the case of the PSI/PVA co-electrospun meshes polymer fibre type cannot be objectively identified by scanning electron microscopy (Figure 41). The average fibre diameters can be found in Table 13.

Table 13. Average fibre diameter and standard deviation of control PSI and PSI/PVA composite meshes

Mesh Type	Average Fibre Diameter (nm)
PSI	550 ± 100
PVA	250 ± 50
PVA-GDA	600 ± 150
Co-spun PSI/PVA	360 ± 70
Co-spun PSI/PVA-GDA	790 ± 100
Co-spun PSI-DAB/PVA-GDA	690 ± 130

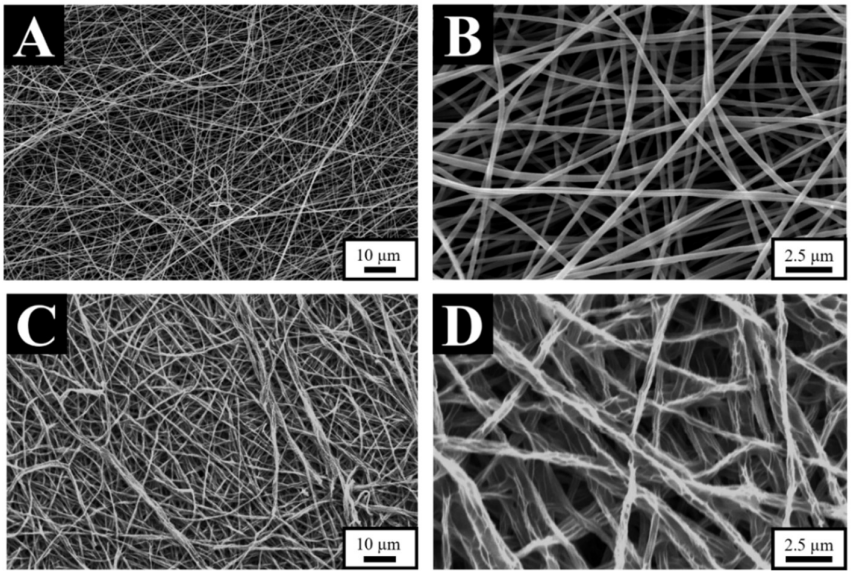

Figure 40. Electrospun PVA mesh before (A, B) and after (C.D) cross-linking with GDA (initiated with pH = 2)

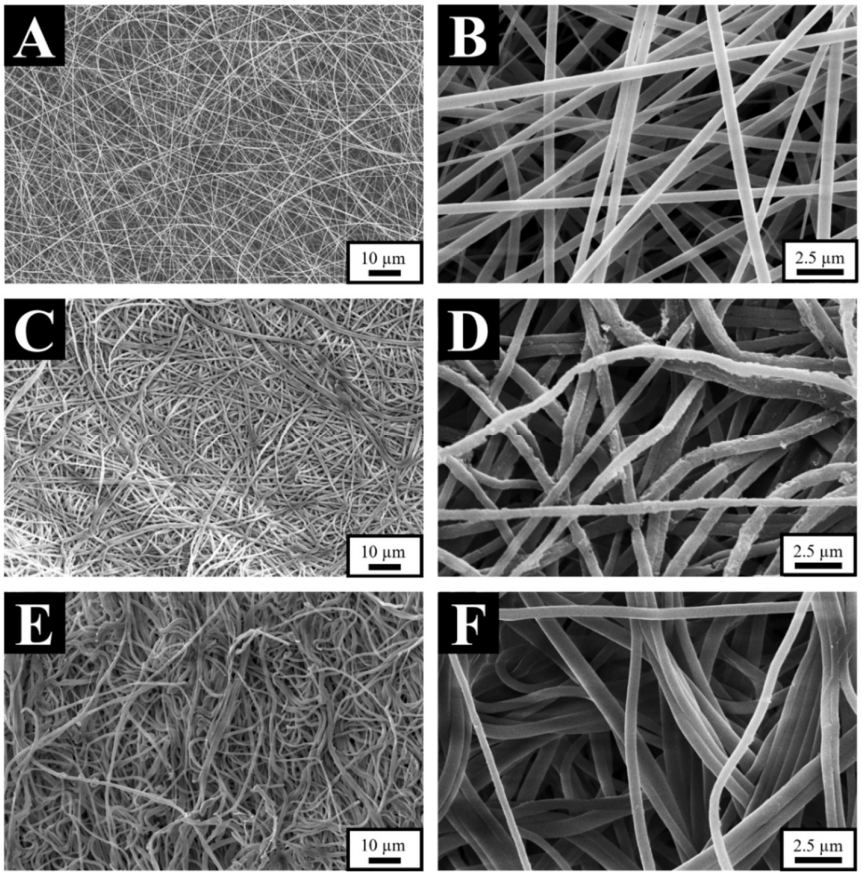

Figure 41. Co-electrospun PSI/PVA (A,B), PSI/PVA-GDA(C, D) and PSI-DAB/PVA-GDA (E,F)

Two photon excitation microscopy was successfully utilised to visualise the randomly distributed PSI and PVA fibres along the PSI/PVA composite meshes. The dyed PVA fibres were well visible next to the auto-fluorescent PSI ones (Figure 42).

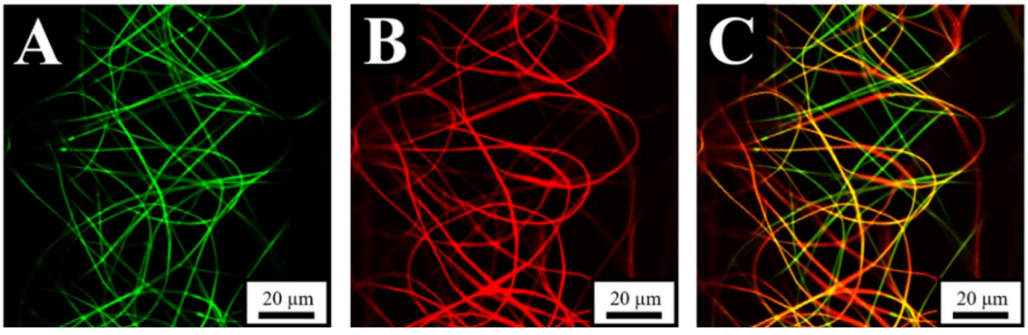

Figure 42. TPEM micrographs of co-electrospun PSI/PVA meshes: A. PSI fibres – low green channel, B.PVA fibres - low red channel C. PSI/PVA fibres both channels

4.3.3 Chemical Composition Differences and Changes

Examining the spectra of the PVA samples it can be clearly seen how the OH peak at 3303 cm^{-1} decreases after the chemical treatment as the GDA crosslinking takes place (Figure 43). Additionally, peaks at 2905 cm^{-1}, 1418 cm^{-11} and 1076 cm^{-1} mark the C-H, C=O and C-O-C bonds respectively and remain unaffected. The spectra of the PSI/PVA composite mesh demonstrate characteristic peaks of both polymers. Furthermore, the GDA crosslinking (and the resulted OH group decrease) as in the case of the PVA-GDA can be seen on the PSI/PVA-GDA spectrum. Finally, the PSI-DAB/PVA-GDA bares characteristics of both PSI-DAB and PVA-GDA spectra.

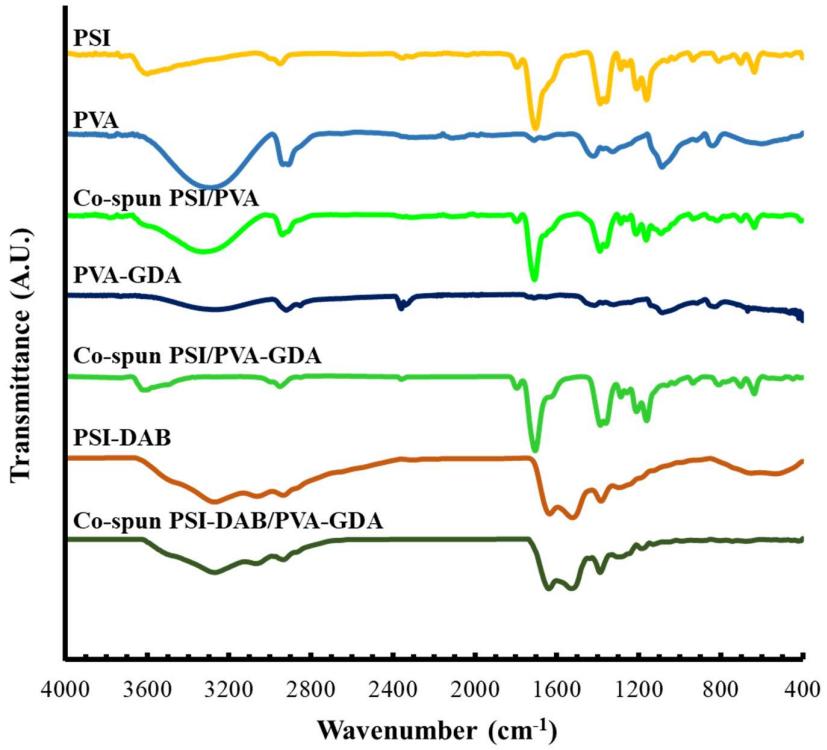

Figure 43. ATR/FTIR Analysis of co-electrospun PSI/PVA composite meshes and the resulted changes

4.3.4 Wettability

Water contact angle examination was performed on PSI/PVA co-electrospun meshes before and after cross-linking chemical treatment. Compared to PSI meshes, PVA-GDA exhibited higher water contact angles (Table 14, Figure 44). As expected, crosslinking increases contact water angles and absorption times (Table 14, Figure 44).

Table 14. Wettability of co-electrospun PSI/PVA composite meshes

Mesh	Contact Angle (°)	Absorption time (s)
PVA-GDA	60 ± 10.9	-
Co-spun PSI/PVA	48.7 ± 6.1	3.75 ± 0.90
Co-spun PSI/PVA-GDA	60.3 ± 2.8	12.8 ± 3.3
Co-spun PSI-DAB/PVA-GDA	71.1 ± 11.9	17.4 ± 8.5

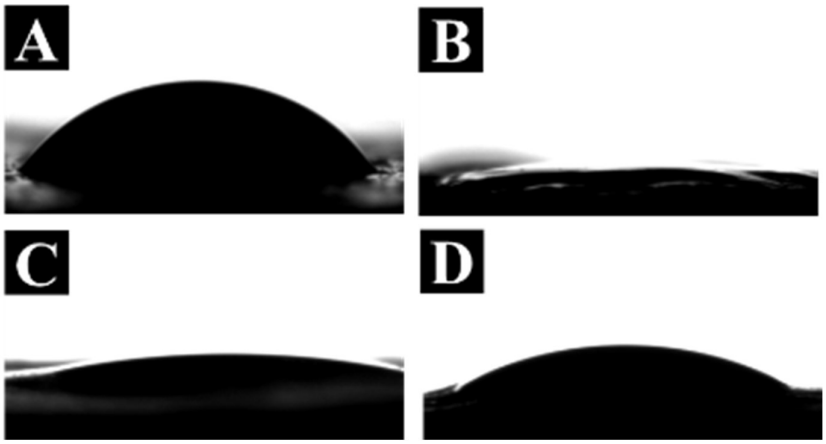

Figure 44. Wettability assessment of co-electrospun PSI/PVA meshes: A. PVA-GDA, B. Co-spun PSI/PVA, C. Co-spun PSI-PVA-GDA, D. Co-spun PSI-DAB/PVA-GDA

4.3.5 Mechanical Properties

According to the uniaxial mechanical assessment dry (pre-cross-linked) PVA meshes are stronger than PSI ones. The specific loading capacity tensile of the untreated dry (pre-cross-linked) PSI/PVA composite meshes as expected falls somewhere between the PSI and PVA meshes. No synergistic effect was observed suggesting that no chemical

bonding occurred between the two polymers only physical fibre to fibre contact. Although DAB cross-linking improved PSI mesh performance under liquid, when comparing them to PVA-GDA meshes they proved significantly weaker. Surprisingly, PSI/PVA-GDA meshes proved mechanically stronger than PSI-DAB/PVA-GDA meshes. Specific loading capacities can be found in Table 15. Representative stress-strain curves (not incorporating sample mass) of the PSI, PVA and co-spun PSI/PVA meshes can be found below in Figure 45.

Table 15. Specific loading capacity of PSI/PVA composite meshes
Note: Presented values are average results along with their standard deviations

Mesh Type	**Specific Loading Capacity (N m^2/g)**	
	Vertical	**Horizontal**
PSI (in air)	0.310 ±0.500	0.240 ±0.500
PSI (under liquid)	0.080 ±0.500	0.010 ±0.007
PSI-DAB (under liquid)	0.037 ±0.008	0.005± 0.001
PVA (in air)	0.237 ±0.035	0.207 ±0.023
PVA-GDA (under liquid)	0.418 ±0.260	0.366 ±0.025
Co-spun PSI/PVA (in air)	0.325 ±0.003	0.255 ± 0.02
Co-spun PSI/PVA-GDA (under liquid)	0.164 ±0.016	0.056 ±0.023
Co-spun PSI-DAB/PVA-GDA (under liquid)	0.058 ±0.013	0.023 ±0.005

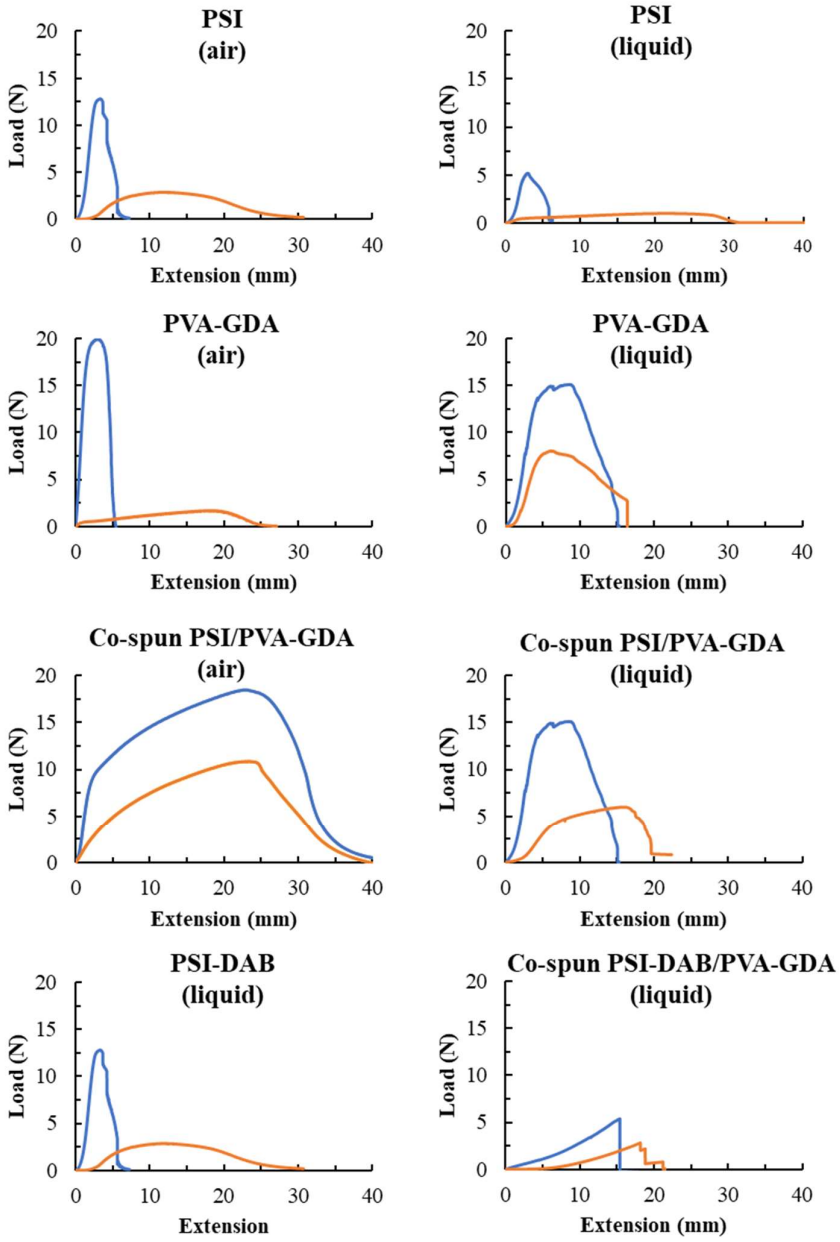

Figure 45. Stress-Strain curves of PSI, PVA and co-spun PSI/PVA meshes
Note I: Blue curves indicate vertical samples, orange curves indicate horizontal samples
Note II: The curves do not take surface density into account

4.3.6 Cytotoxicity, Morphology and Cell Adhesion

Cytotoxicity

According to the cell studies PVA-GDA meshes are not cytotoxic (Figure 466). On the contrary PSI meshes did not perform as well. Cell viability of the PSI meshes decreased after 24 and 72 hours as well the composite PSI/PVA-GDA meshes followed a similar pattern (Figure 46). After cross-linking the PSI, the issue resolves as PSI-DAB meshes exhibited a non-cytotoxic nature as after 72 hours cell viability is largely increased (Figure 477). The double cross-linked PSI-DAB/PVA-GDA mesh followed accordingly (Figure 477).

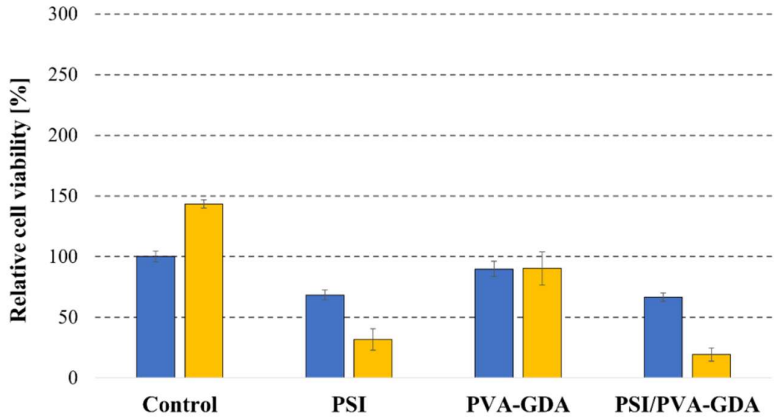

Figure 46. Cell Viability of PSI, PVA-GDA and PSI/PVA-GDA, and meshes
Note: Blue – 24 hours, Yellow – 72 hours

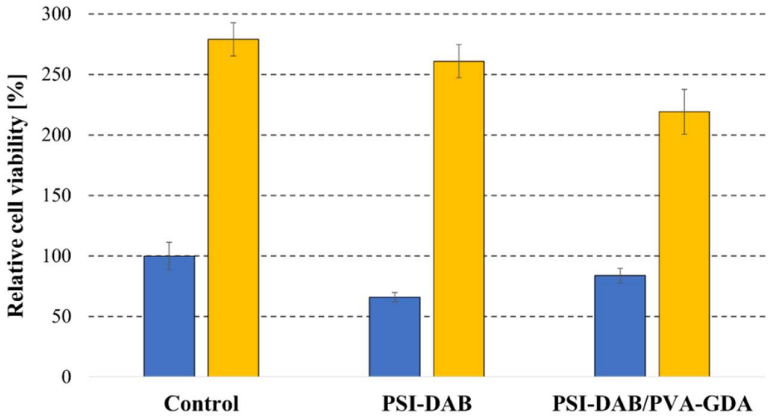

Figure 47. Cell Viability of PSI-DAB and PSI-DAB/PVA-GDA meshes
Note: Blue – 24 hours, Yellow – 72 hours

Morphology

In terms of cell, morphology, cell retained their original fibroblast shape with no evidence of differentiation. A few apoptotic cells can also be seen in the control and almost every sample (Figure 488, Figure 499).

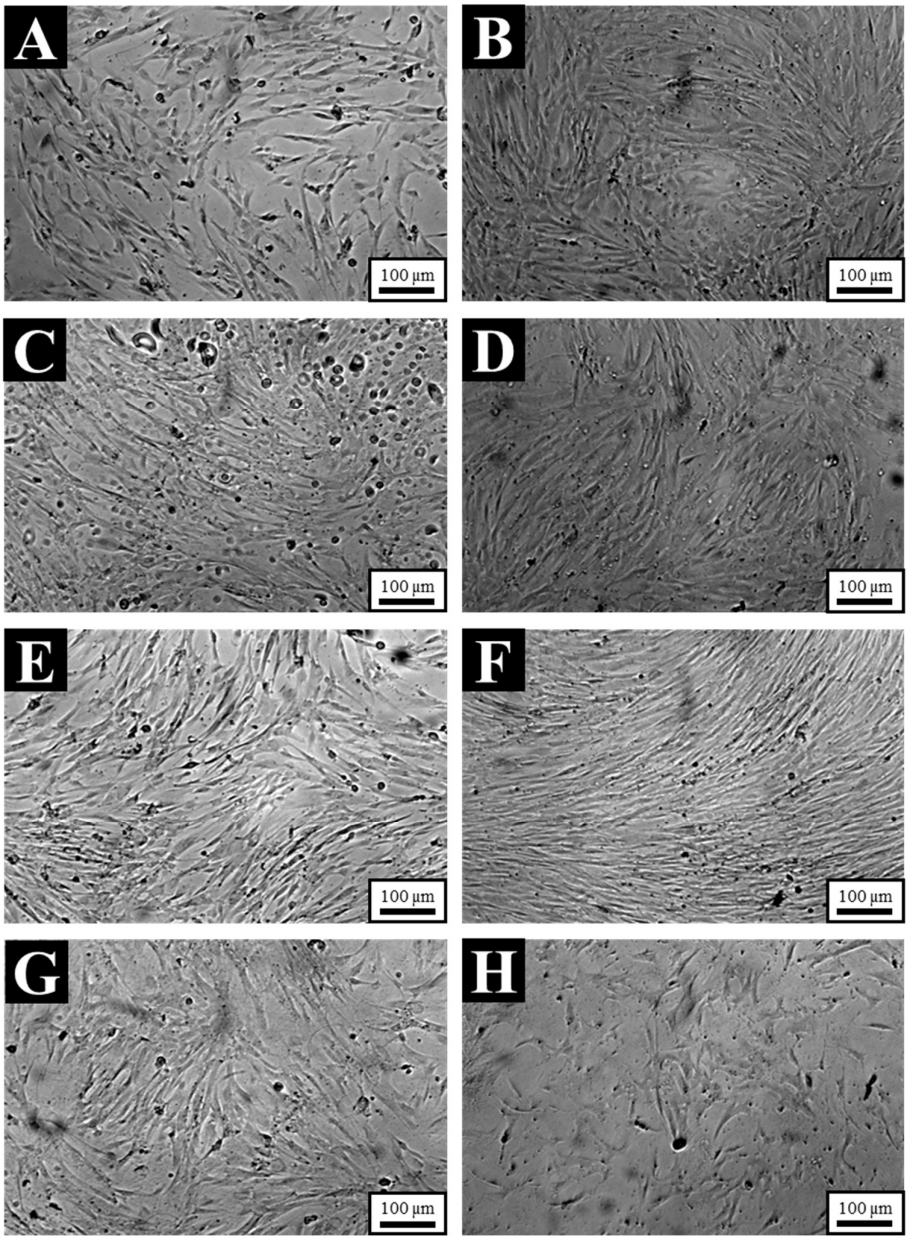

Figure 48. Phase contrast microscopy of fibroblast cell study A. 24h Control, B. 72h Control, C. 24h PSI, D. 72h PSI, E. 24h PVA-GDA, F. 72h PVA-GDA, G. 24h PSI/PVA-GDA, F.72h PSI/PVA-GDA

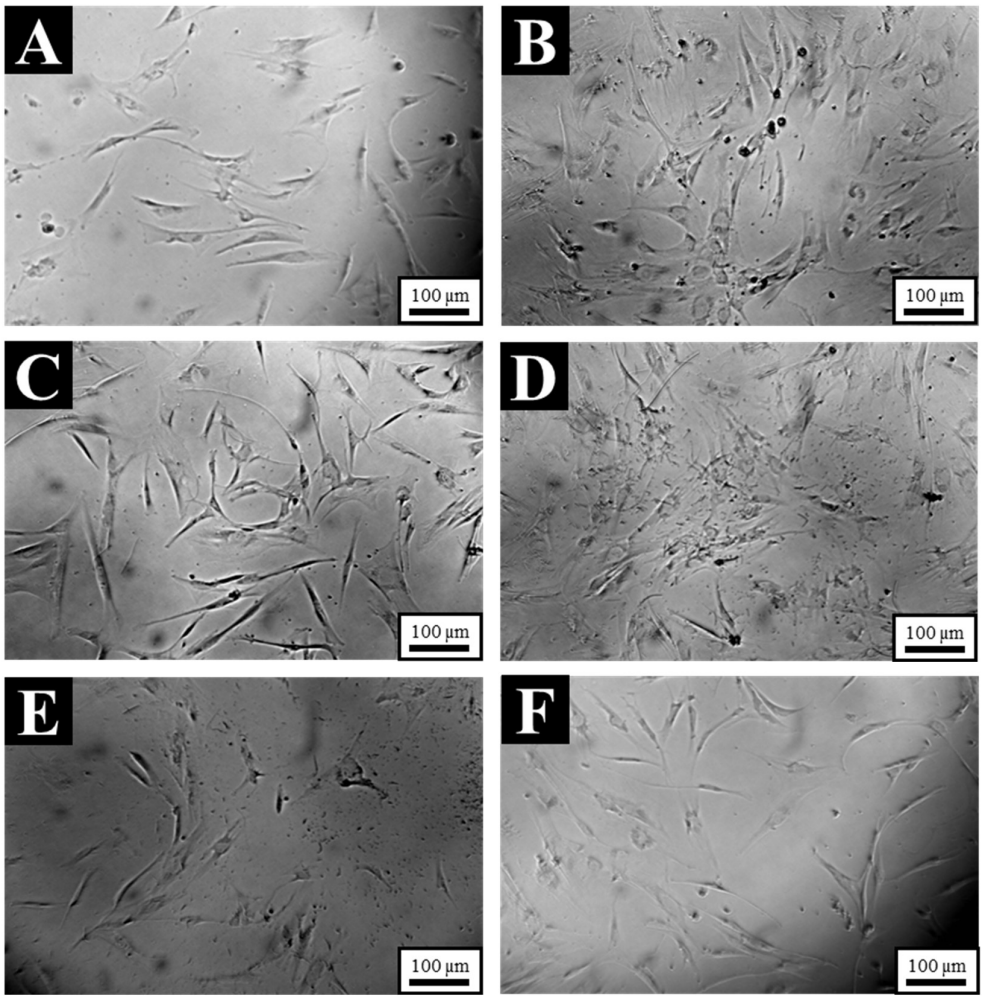

Figure 49. Phase contrast microscopy of fibroblast cell study A. 24 h control, B. 72h control, C. 24h PSI-DAB, D. 72h PSI-DAB, E. 24h PSI-DAB/PVA-GDA, F. 72h PSI-DAB/PVA-GDA

Cell adhesion

Regarding cell adhesion, according to two photon excitation microscopy imaging PVA-GDA hinders cell attachment. The addition of PSI increased cell adhesion at least visually. As seen in Figure 5050, mesh samples are fluorescent green while cell found on their surface are red due to the Vybrant-DiD staining.

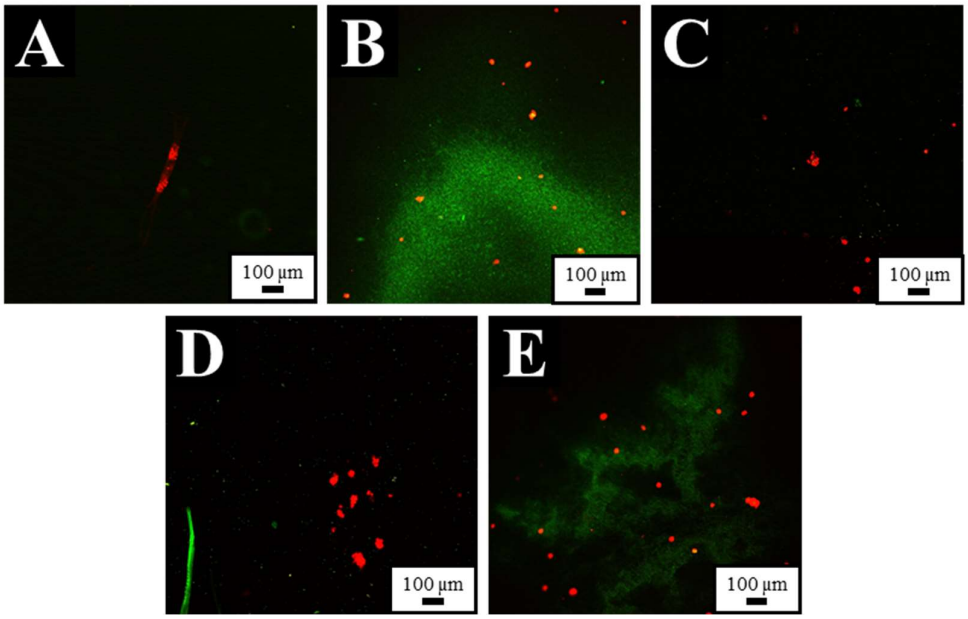

Figure 50. Two photon excitation microscopy imaging of cells placed on A. PSI, B. PSI-DAB, C. PVA-GDA, D. PSI/PVA-GDA and E. PSI-DAB/PVA-GDA
Note: Red: Cells, Green: Mesh surface

4.3.7 Animal Experiments and Biocompatibility Study

Operative Experience

During the surgical procedure, no difficulties were documented in either surgical handling or fixation. Samples were easily fixated and sample tearing due to suturing or knotting was not observed.

Animal Monitoring

During the postoperative period, two animals exhibited signs of mild postoperative discomfort while the rest did not demonstrate pain or irritation scoring low on the grimace scale (

Table 16). Animals as expected lost some of their appetite for 1-2 days (

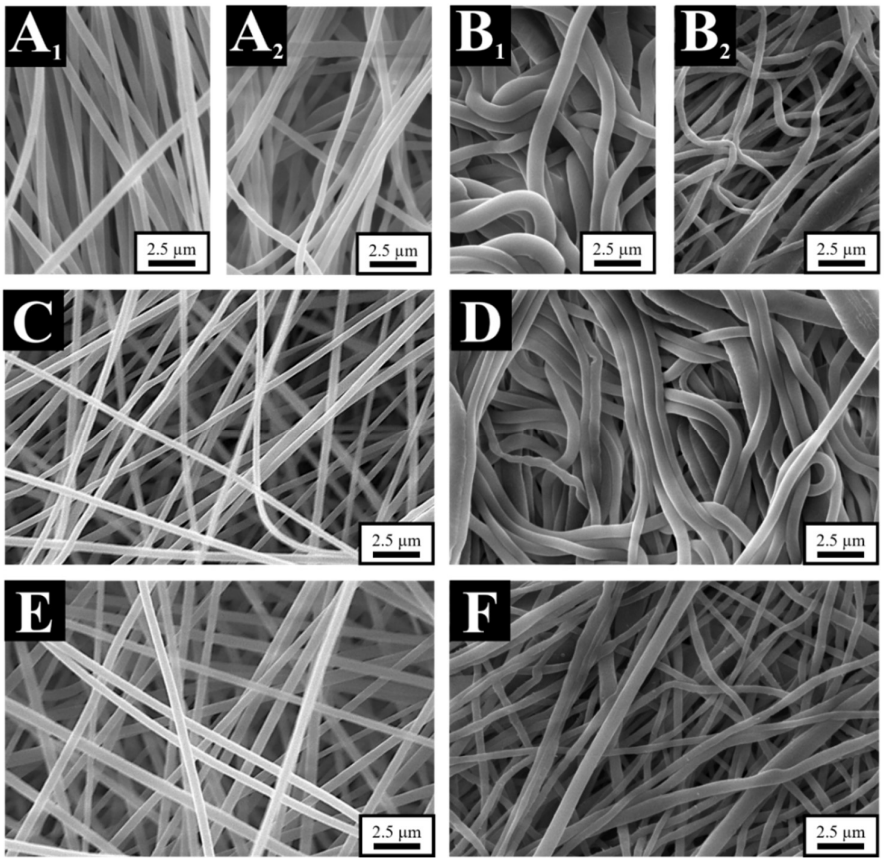

Figure 57) after which they regained normal habitual behaviour (i.e., food intake, bowl movement, mobility) (Figure 52 A) and weight (Figure 51) while also showing curious behaviour about the environment enrichment (Figure 52 B). While animals were kept individually for 5 days to prevent suture interference, two animals managed to reach their sutures and tear them thus additional sutures were placed to prevent wound dehiscence. The rest of the animals exhibited a physiological wound healing (Figure 52 C).

Table 16. Post-operative Grimace scale. Points are given in the following manner: 0 – Not present, 1 Moderately present, 2. Obviously present

Day	Average Orbital Tightening	Average Nose/Cheek Flattening	Average Ear Changes
Day 1	0.22 ±0.42	0.11 ±0.31	0.11 ±0.31
Day 2	0.22 ±0.42	0.11 ±0.31	0.11 ±0.31
Day 3	0.11 ±0.31	0.11 ±0.31	0.00
Day 4	0.00	0.00	0.00

Day 5	0.00	0.00	0.00

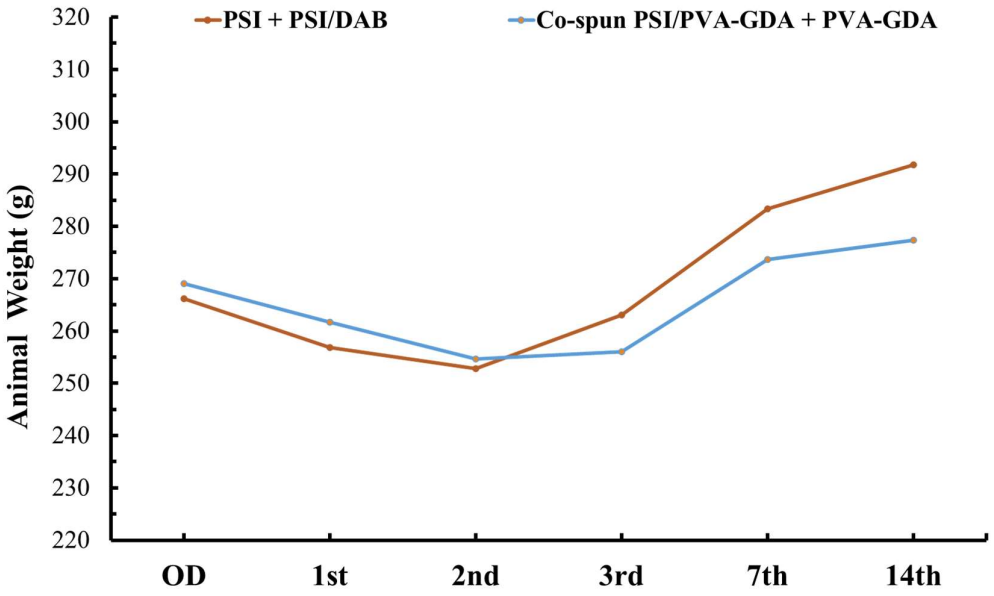

Figure 51. Animal weight changes during the Operative Day (OD) and the 1st, 2nd, 3rd, 7th, and 14th Operative Day

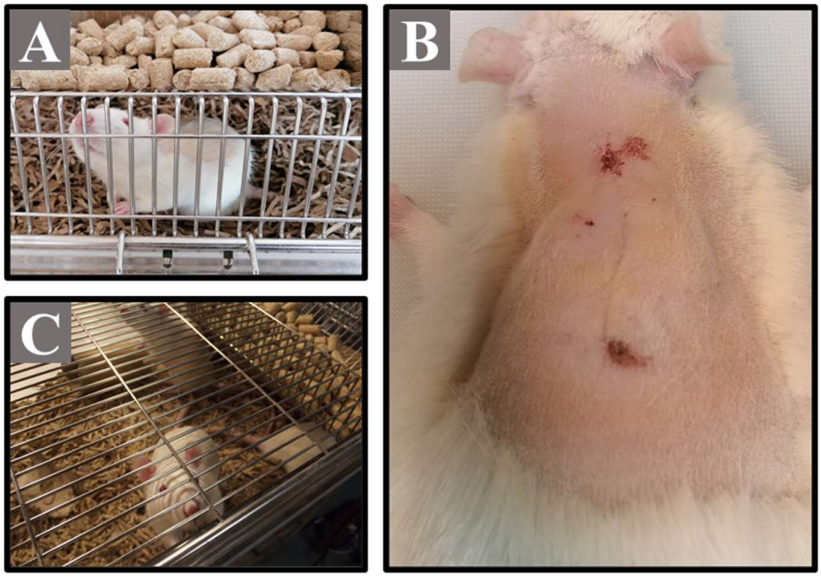

Figure 52. A. Grimace scale examination, B. Active animal behaviour (nest making), C. Incision wound (14th day)

Hemocompatibility

Regarding hemocompatibility, as expected a slight leukocyte (total white cell count) and granulocyte increase was documented (Table 17). Erythrocytes, thrombocytes were in normal range (Table 17).

Table 17. Haematological examination results for PSI and PSI/PVA composite meshes
Note: Presented values are average results along with their standard deviation

	PSI+PSI/DAB	**Co-spun PSI/PVA-GDA + PSI-DAB/PVA-GDA**	**Reference Values**
Leukocytes (10^9/L)	10.63 ±1.97	10.84 ±3.13	1.96-8.25
Granulocyte (%)	37.79 ± 15.90	33.13 ±11.02	6.20-26.70
Monocytes (%)	7.46 ± 3.98	7.47 ± 4.90	0.8-3.80
Lymphocytes (%)	54.75 ±17.42	59.40 ±12.50	66.6-90.30
Erythrocytes (10^9/L)	7.10 ±0.59	6.94 ±0.56	7.27-9.65
Haemoglobin (g/L)	140.5 ±6.3	140.42 ±10.2	130.70-170.60
Haematocrit (%)	43.01 ±2.08	41.46 ±3.09	39.60-52.50
Thrombocytes (10^9/L)	947.125 ±166.59	719 ±300.38	638-1177

Macroscopic Results

During sample retrieval PSI samples were not found. In contrast PSI-DAB were found swollen surrounded by granulation tissue (Figure 53A, B). PSI/PVA-GDA samples decreased approximately 25% in size while PSI-DAB/PVA-GDA remained unaltered (Figure 533C). PVA-GDA were the most inert out of all the meshes showing no sign of swelling, only being surrounded by a loosely attached granulation tissue (Figure 533D). Serious complication (infection, seroma, haematoma were not found in any of the animals. A healthy granulation tissue was found encompassing the samples containing newly formed vessels.

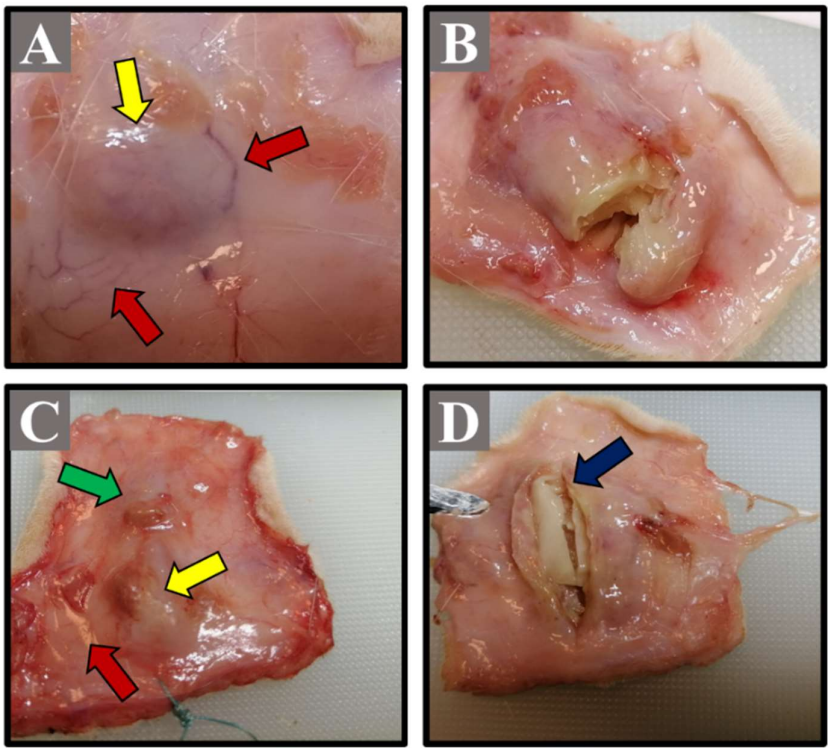

Figure 53. Macroscopical findings during sample retrieval: A., B. PSI-DAB (yellow arrow), C. PSI/PVA-GDA (green arrow) + PSI-DAB/PVA-GDA (yellow arrow), D. PVA-GDA (blue arrow), Newly formed vessels (neovascularisation) (red arrows).

Microscopic Results

With the exclusion of the PSI samples, the rest of the implanted samples were found.At the implantation site a minimal to mild inflammatory reaction can be seen in all the samples. In the case of the PSI-DAB (Figure 54 A), PSI/PVA-GDA (Figure 54 B) and PSI-DAB/PVA-GDA (Figure 54 C), the exact border between the sample and the

surrounding granulation tissue was not well demarcated. In comparison, the PVA-GDA sample had typically better demarcation. In the granulation tissue, a mild amount of leukocytes (macrophages, lymphocytes) can be found along with newly formed vessels. At this point newly formed collagen can be seen but a definitive capsule formation has not occurred yet. Haematoma, necrosis, fatty infiltrates, or giant foreign body cells were not found either.

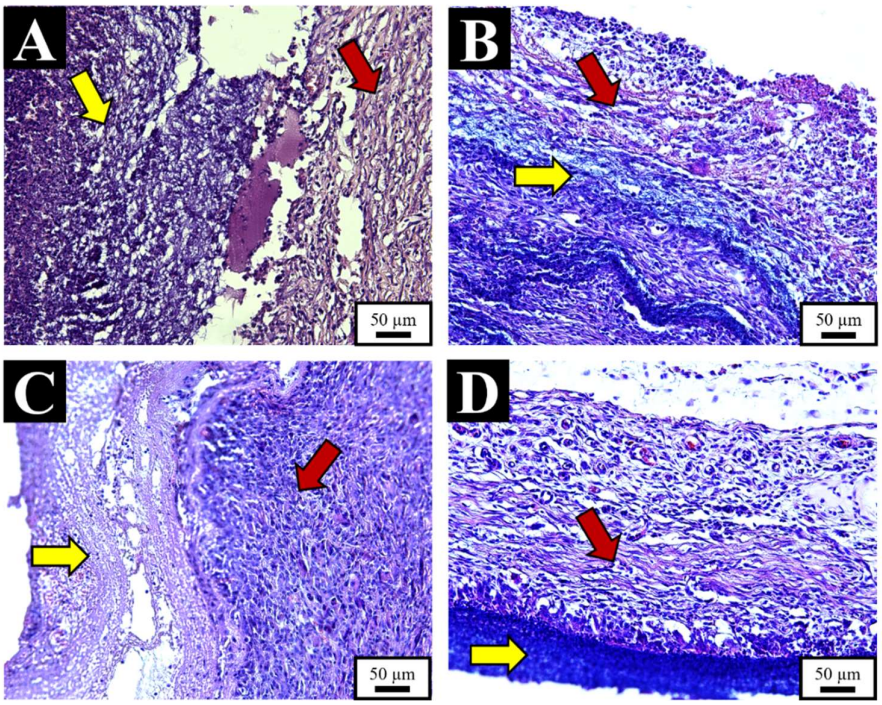

Figure 54. Histopathology examination of: A. PSI-DAB, B.PSI/PVA-GDA, C. PSI-DAB/PVA-GDA, D. PVA-GDA.

Note: Yellow Arrow: Implant, Red Arrow: Granulation Tissue

4.4 Polysuccinimide/ Polycaprolactone composite meshes

4.4.1 PSI/PCL Layer, Co- and Blend electrospinning

No issues were documented in any of the electrospinning configurations. Layer electrospinning is the most straightforward process while blend electrospinning has a fabrication electrospinning window of 48 hours (time that the polymer solution is miscible and blend electrospinning is feasible and reproducible). All composite meshes are macroscopically identical (Figure 55), there seems to be a difference only in texture. PSI meshes are fleecy, fluffy, and easily adhere to surfaces due to being charged, PCL meshes on the contrary lack any of these features. Out of all the composite meshes, blend-spun PSI/PCL meshes exhibit the most fleecy/fluffy nature. In addition, after the chemical treatment, blend-spun PSI/PCL seems to swell at least visually the most.

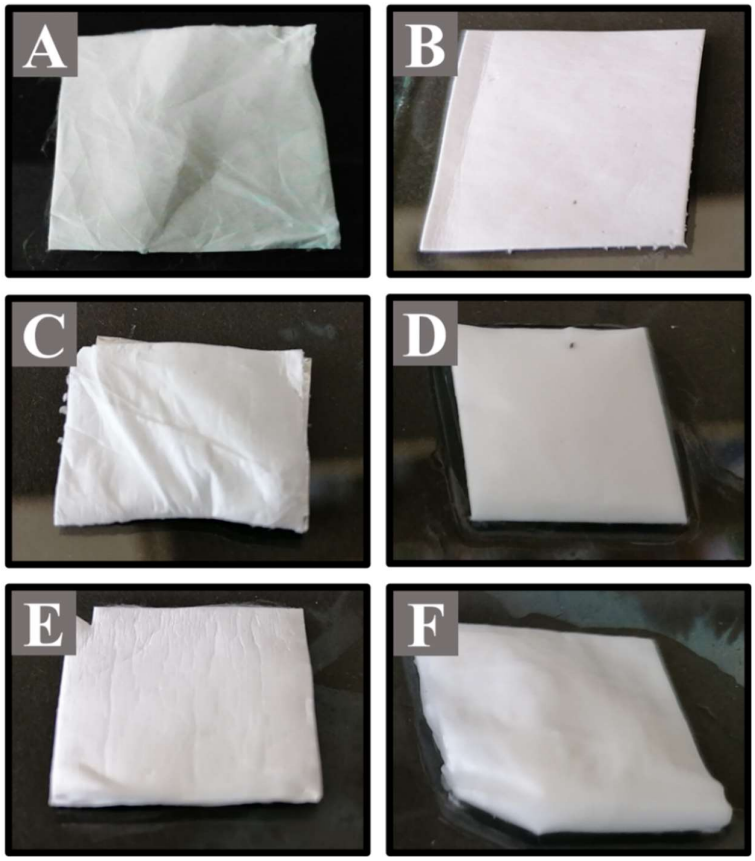

Figure 55. Macroscopical differences among PSI/PCL composite meshes A. PSI, B. PCL, C. Co-spun PSI/PCL D. Co-spun PSI-DAB/PCL, E. Blend-spun PSI/PCL, F. Blend-spun PSI-DAB/PCL

Note: Sample size 1.5 x 1.5 cm

4.4.2 Microstructure and Nanofibre Diameter

The fibrous microstructure was present in all the composite meshes (layer-spun, co-spun and blend-spun PSI/PCL) and remained unaltered throughout the mechanical and chemical treatment. The microscopic pictures showed a homogenous fibrous structure without any defect in all cases including the chemical treatment (Figure 56-57). PCL fibres were thicker ($p < 0.005$) than PSI ones measuring 610 ±210 and 550 ±120 respectively (

Table 18). The co-spun PSI/PCL meshes composed two polymer fibre types resulted in an average diameter of 560 ±180 nm (calculations were performed regarding the two fibres composing the mesh as one system). Blend-spun PSI/PCL had the thickest fibres measuring 620 ±140 nm. The chemical treatment as previously documented with PSI-DAB meshes, decreased the average fibre diameter of all the composite meshes.

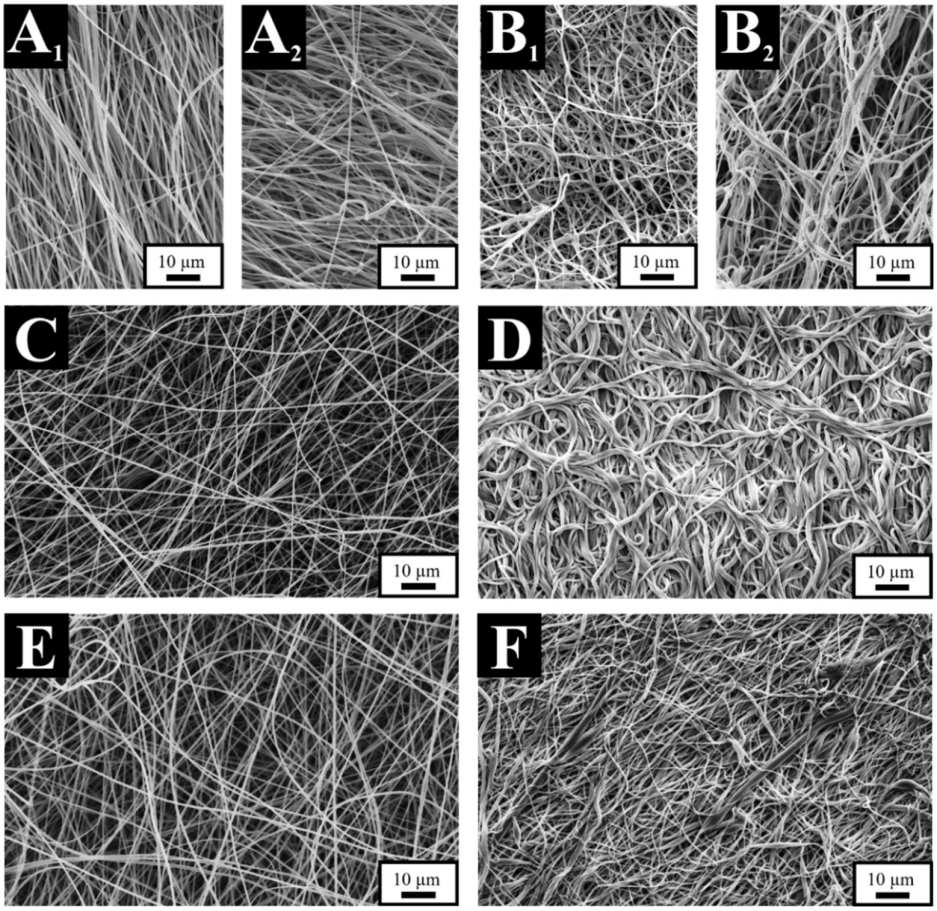

Figure 56. Microstructure of PSI/PCL composite meshes A1. layer-spun PSI/PCL (PSI side), A2. layer-spun PSI/PCL (PCL side), B1. layer-spun PSI-DAB/PCL (PSI side), B2. layer-spun

PSI-DAB/PCL (PCL side), C. Co-spun PSI/PCL D. Co-spun PSI-DAB/PCL, E. Blend-spun PSI/PCL, F. Blend-spun PSI-DAB/PCL

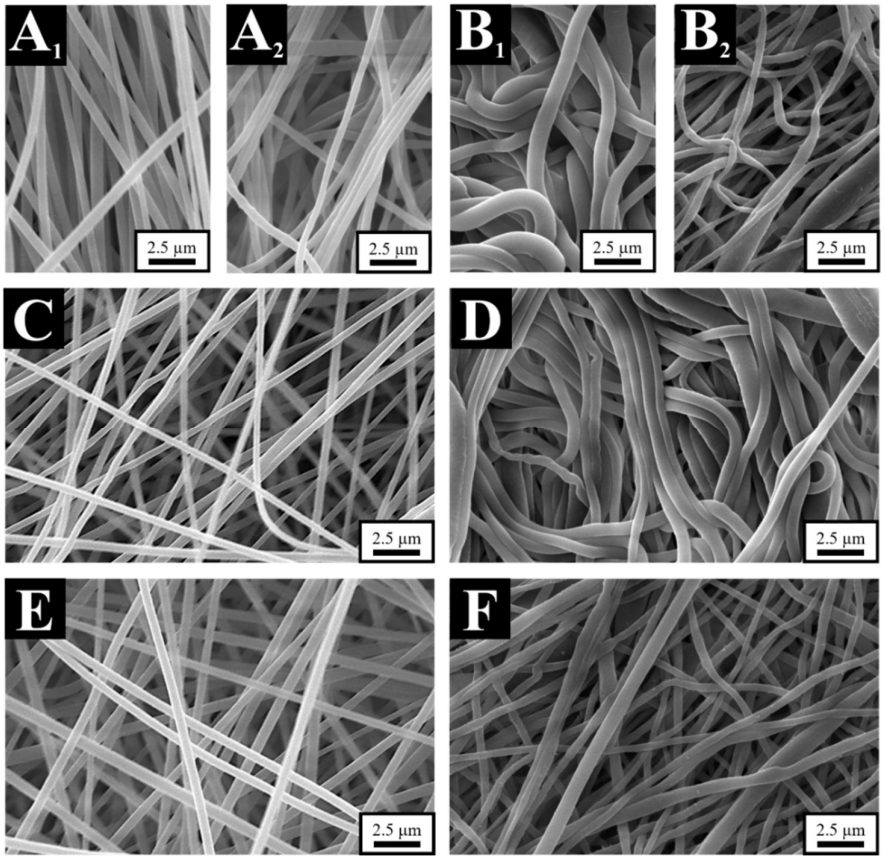

Figure 57. Fibre quality differences among PSI/PCL composite meshes A_1. layer-spun PSI/PCL (PSI side), A_2. layer-spun PSI/PCL (PCL side), B_1. layer-spun PSI-DAB/PCL (PSI side), B_2. layer-spun PSI-DAB/PCL (PCL side), C. Co-spun PSI/PCL D. Co-spun PSI-DAB/PCL, E. Blend-spun PSI/PCL, F. Blend-spun PSI-DAB/PCL

Table 18. Average Fibre diameters of PSI/PCL composite meshes

Mesh Type	Average Diameter (nm)
Layer-spun PSI/PCL (PSI side /PCL side/)	550 ±120 / 610 ±210
Layer-spun PSI-DAB/PCL (PSI side /PCL side/)	440±130 / 600 ±200
Co-spun PSI/PCL	560 ±180
Co-spun PSI-DAB/PCL	450 ±100
Blend-spun PSI/PCL	620 ±140
Blend-spun PSI-DAB/PCL	560±180

Fluorescent Microscopy was successfully utilised to visually confirm the main difference between the co-electrospun and blend-electrospun PSI/PCL meshes. Firstly,

compared to PSI-based ones (Figure 58 A, B), PCL were not visible through the 380 or 480 nm detector channel (Figure 58 C, D). In contrast, Nile Blue stained PCL fibres were visible and easily observable through either channel (Figure 58 E, F). Subsequently, examining co-electrospun PSI/PCL sample, the two different polymer fibres are visible, as PCL fibres apart from green also emit red (Figure 599 B-E). In comparison, the two polymers are found within one fibre in the case of the blend-electrospun PSI/PCL meshes as fibres emit in both green and red through the 380 and 480 nm channel respectively (Figure 599 C-F).

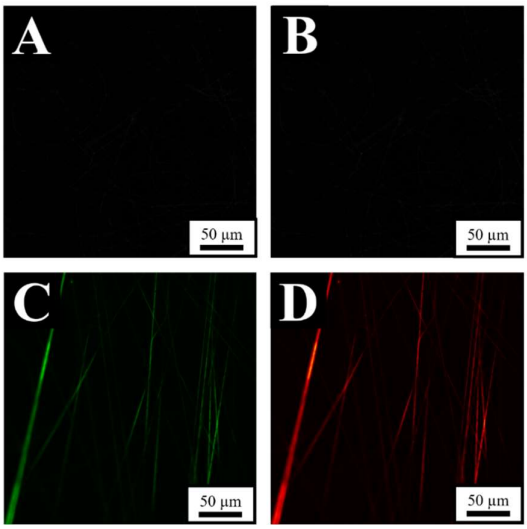

Figure 58. Fluorescent microscopy images of: A. Unstained PCL - 380nm, D. Unstained PCL - 480 nm, Stained PCL - 380 nm, F.-Stained PCL - 480nm

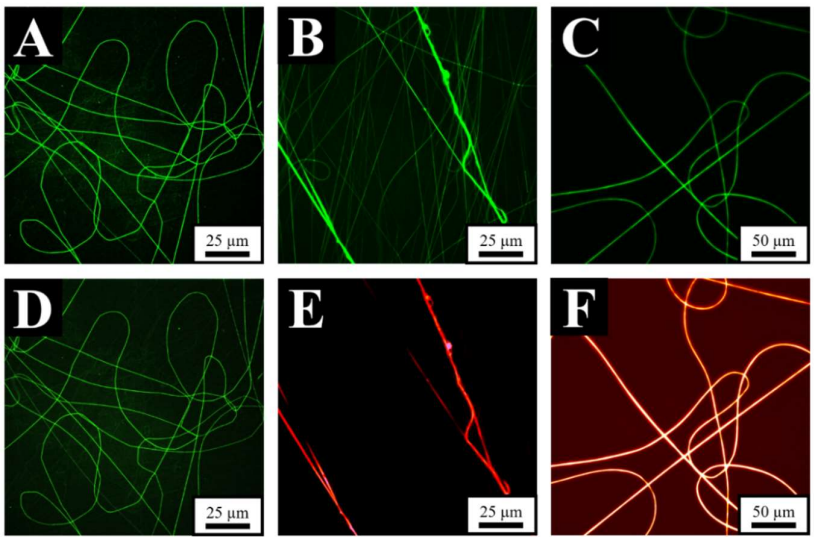

Figure 59. Fluorescent microscopy images of: A. Co-electrospun Unstained PSI/PCL - 380 nm, B. Co-electrospun stained PSI/PCL 380 nm, C Blend-spun PSI/PCL stained - 380 nm, D. Co-

electrospun Unstained PSI/PCL - 480 nm, E. Co-electrospun stained PSI/PCL - 480 nm, F. Blend-electrospun stained PSI/PCL - 480 nm

4.4.3 Chemical Composition Differences and Changes

As in the case of the co-spun PSI/PVA meshes, chemical characterisation was performed for all the PSI/PCL composite meshes before and after the cross-linking process (Figure 60). Typical PCL peaks at approximately 2950 cm^{-1} and 2860 cm^{-1} marking the asymmetric and symmetric CH2 stretching, the peak at 1730 cm^{-1} marking the carbonyl stretching, the peak at 1190 cm^{-1} marking the OC–O stretching and the peak at approximately 800 cm^{-1} for the C–H bending are visible in both the PCL control and PSI/PCL meshes along with the main PSI peaks at 3596 cm^{-1} for the O–H groups, 2961 cm^{-1} for the C–H bonds c. 1709 cm^{-1} (asymmetric stretching vibration) and 1393 cm^{-1} (stretching bending vibration) for the imide-ring. and at approximately 1200 cm^{-1} for the C–N (stretching vibration), the C=C (835 cm^{-1}) and C-H (697 cm^{-1}) bending vibration.

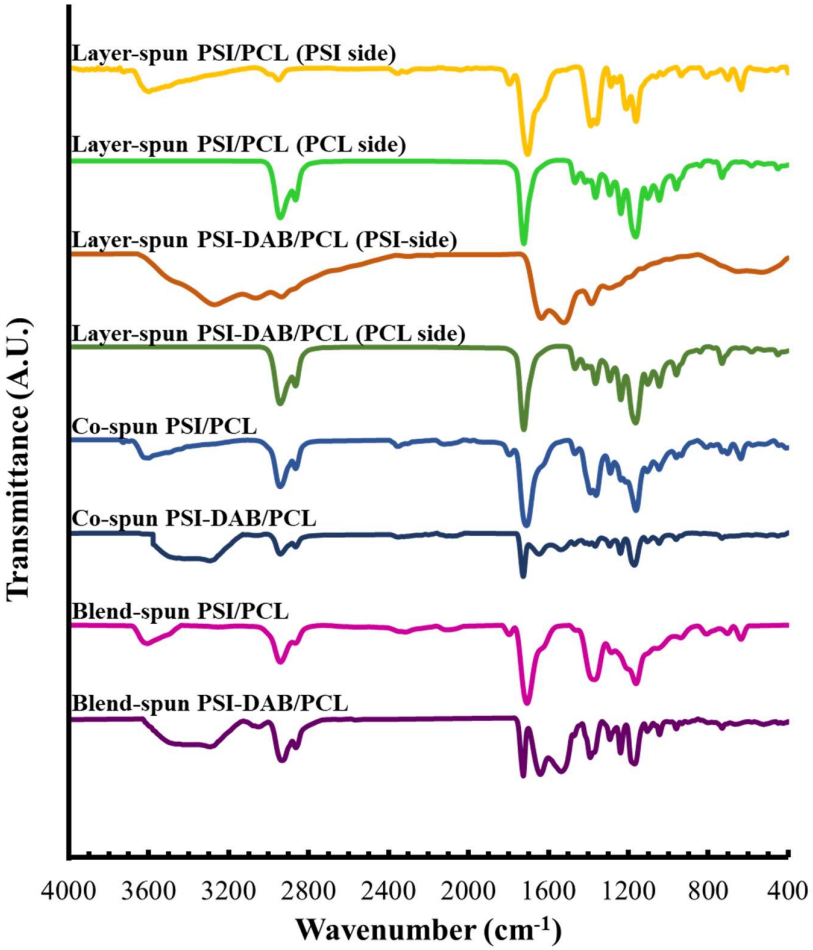

Figure 60. ATR/FTIR characterisation of PSI/PCL composite meshes

4.4.4 Wettability

The layered electrospun PCL/PSI mesh exhibited a dual nature as the PCL side is hydrophobic while the PSI side exhibits pseudo hydrophilic properties (capillary effect)(Figure 61). After the cross-linking as before PSI-DAB contact angle and absorption time slightly increases while no significant change is documented on the PCL side (Table 19). The initial water angle measured on the co-electrospun meshes (θ = 129.2°, t = 3.22 s;) is quite different from the one measured for blend electrospinning (θ = 109.5°, t = 7.55 s) and so was the absorption time (less than half) (Table 19). The cross-linking surprisingly decreased the water angle of both co- and blend electrospun meshes (Table 19).

Table 19. Wettability of PSI/PCL composite meshes
Note: Presented values are average results along with their standard deviation

Mesh	Contact angle, θ (°)	Absorption time, t (s)
Layered-spun PSI/PCL_PSI Side	31.7 ± 2.0	1.41 ± 2.37
Layered-spun PSI/PCL_PCL Side	131.8 ± 6.1	Not relevant
Layered-spun PSI-DAB/PCL_PSI Side	28.7 ± 6.1	28.7 ± 14.4
Layered-spun PSI-DAB/PCL_PCL Side	130 ± 7.2	Not relevant
Co-electrospun PSI/PCL	129.2 ± 5.8	3.22 ± 10.37
Co-electrospun PSI-DAB/PCL	104.9 ± 45.9	8 ± 1.2
Blend-electrospun PSI/PCL	109.5 ± 3.2	7.55 ± 5.5
Blend-electrospun PSI-DAB/PCL	30 ± 4.6	1.1 ± 0.5

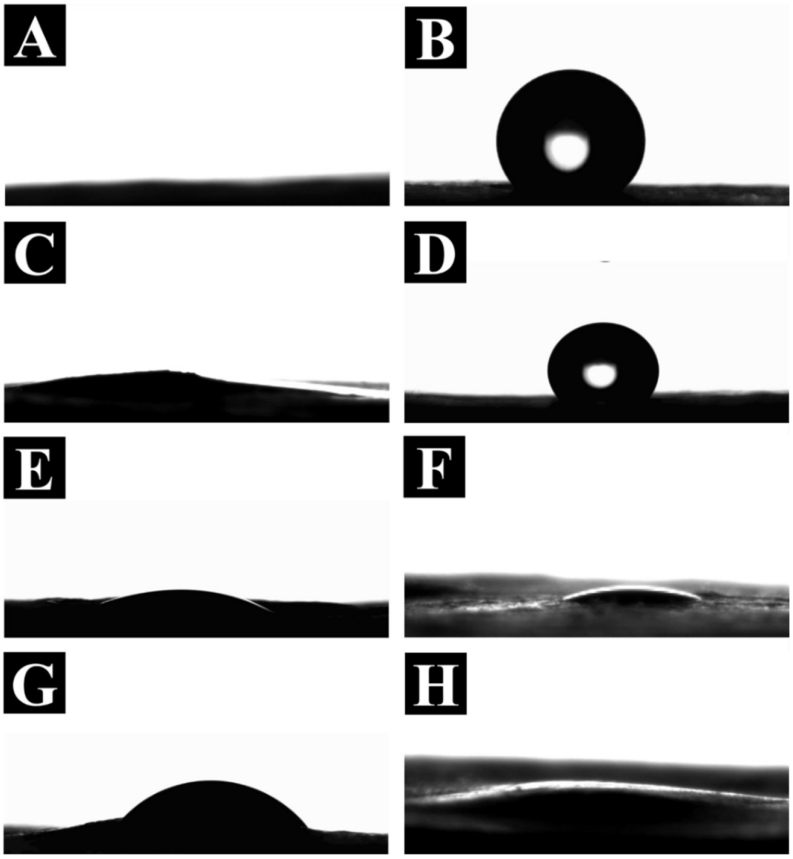

Figure 61. Wettability of PSI/PCL composite meshes: A. Layer-spun PSI/PCL_PSI side, B. Layer-spun PSI/PCL_PCL side, C. Layer-spun PSI-DAB/PCL_PSI-DAB side, D. Layer-spun PSI-DAB/PCL_PCL side, E. Co-spun PSI/PCL, D. Co-spun PSI-DAB/PCL, E. Blend-spun PSI/PCL, Blend-spun PSI-DAB/PCL

4.4.5 Mechanical Properties

According to the uniaxial mechanical assessment PCL meshes are significantly stronger than PSI ones. PCL significantly increased the mechanical performance of PSI meshes (Table 20). Out of the composite meshes, layer spun was the strongest and blend-spun the weakest (Table 20). Due to the significant tensile strength difference, the tearing of the PSI fibres can be seen visually on the samples and on the stress-strain curves as peaks. Un-treated samples (not cross-linked) suffered a decrease of specific loading capacity under liquid, the decrease can be compensated partly by DAB cross-linking (Table 20). Representative stress-strain curves (not incorporating sample mass) of the PSI/PCL composite meshes can be found in Figure 62.

Table 20. Specific loading capacities of PSI/PCL composite meshes
Note: Presented values are average results along with their standard deviation

c	Specific Loading Capacity (N m^2/g)	
	Vertical	**Horizontal**
PSI (in air)	0.310 ±0.500	0.240 ±0.500
PSI (under liquid)	0.08 ±0.500	0.01 ±0.007
PSI-DAB (under liquid)	0.037 ±0.008	0.005± 0.001
PCL (in air)	0.927 ±1	0.191 ±0.039
PCL (under liquid)	0.336 ±0.065	0.070 ±0.005
PSI/PCL layer-spun (in air)	0.366 ±0.017	0.059 ±0.011
PSI/PCL layer-spun (under liquid)	0.455 ±0.155	0.025 ±0.030
PSI-DAB/PCL layer-spun (under liquid)	0.332 ±0.063	0.031 ±0.010
PSI/PCL co-spun (in air)	0.352 ±0.070	0.135 ±0.008
PSI/PCL co-spun (under liquid)	0.259 ±0.064	0.102 ±0.048
PSI-DAB/PCL co-spun (under liquid)	0.303 ±0.013	0.082 ±0.005
PSI/PCL blend-spun (in air)	0.277 ±0.011	0.151 ±0.014
PSI/PCL blend-spun (under liquid)	0.054 ±0.012	0.025 ±0.001
PSI-DAB/PCL blend-spun (under liquid)	0.162 ±0.022	0.070 ±0.004

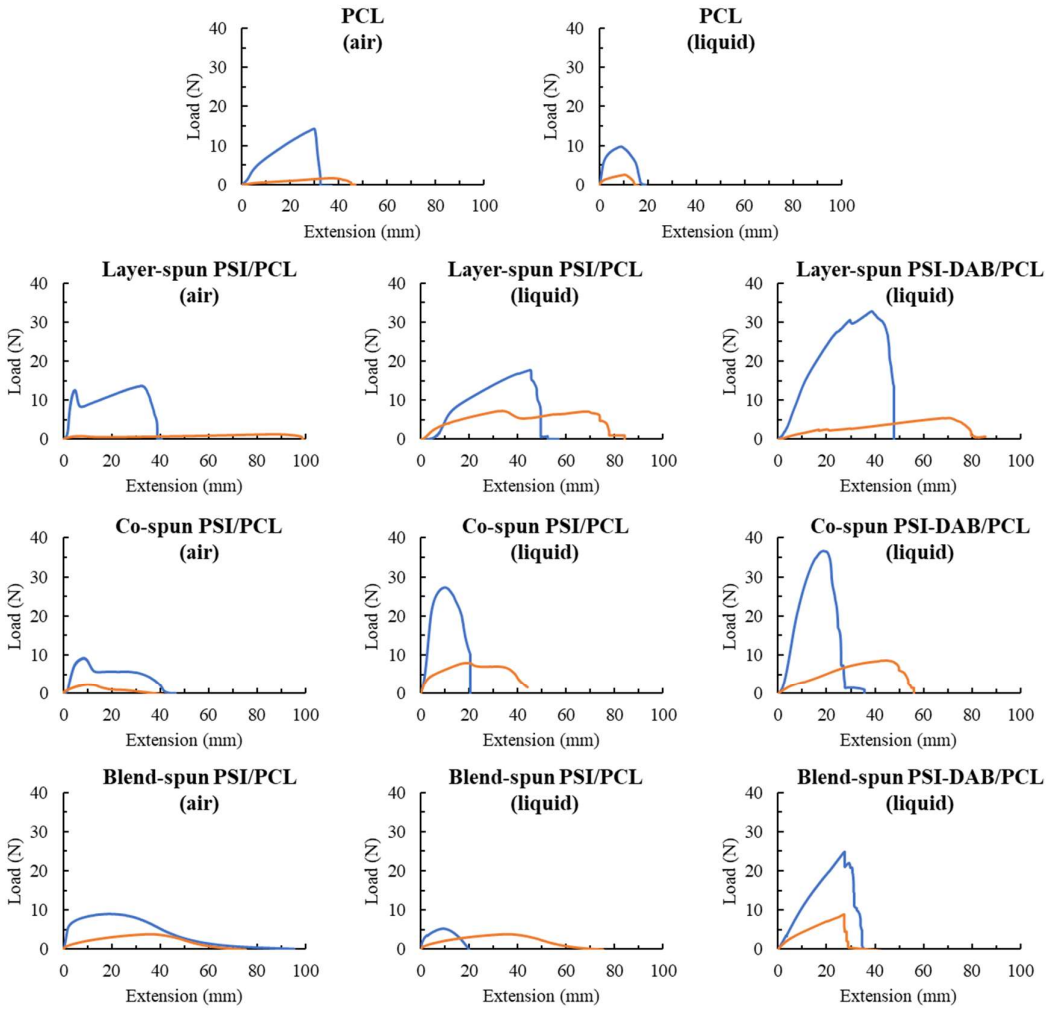

Figure 62. Stress-Strain curves of PSI/PCL composite meshes

Note I.: blue curves indicate vertical samples, orange curves indicate horizontal samples

Note II: The curves do not take surface density into account

4.4.6 Cytotoxicity, Morphology and Cell Adhesion

Cytotoxicity

According to the cell studies PCL meshes are not cytotoxic. On the contrary PSI meshes did not perform as well. Cell viability of the PSI meshes decreased after 24 and 72 hours and the pattern was similar for in the case of composite PSI/PCL meshes (Figure 63-64). After cross-linking the PSI, the issue once again resolves as PSI-DAB and PSI-DAB/PCL meshes exhibited a non-cytotoxic nature as cell viability largely increases after 72 hours.

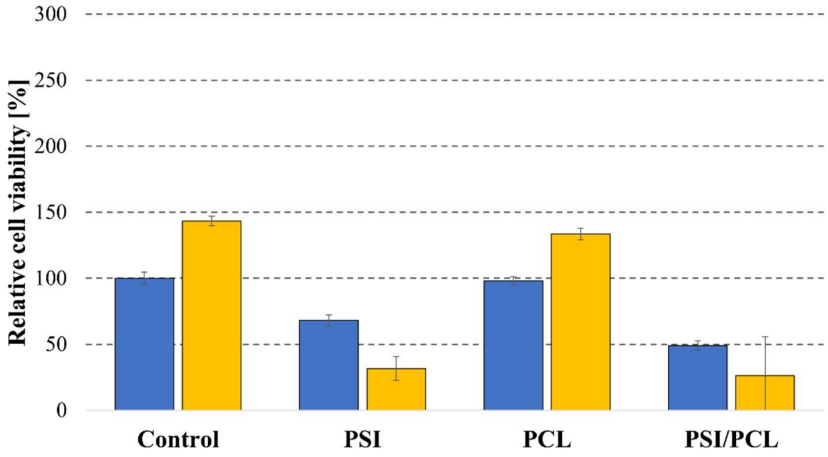

Figure 63. Cell viability of PSI, PCL and PSI/PCL meshes
Note: Blue – 24 hours, Yellow – 72 hours

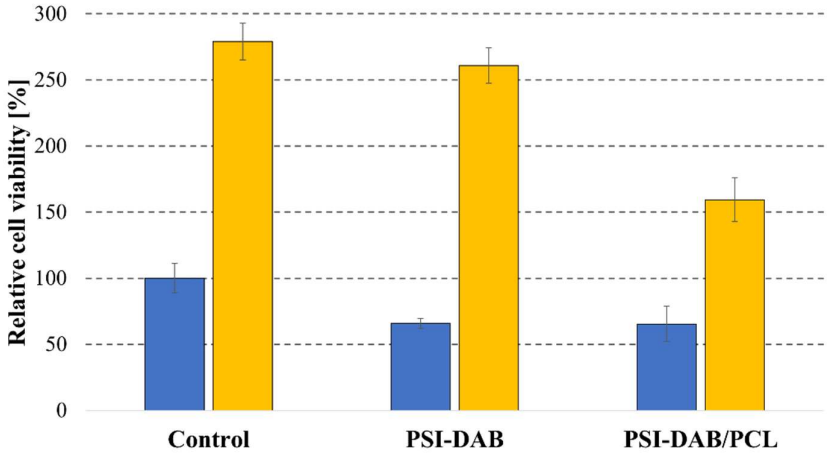

Figure 64. Cell viability of PSI-DAB and PSI-DAB/PCL meshes
Note: Blue – 24 hours, Yellow – 72 hours

Morphology

In terms of cell, morphology, cell retained their fibroblast shape with no evidence of differentiation. A few apoptotic cells can also be seen in the control and almost every sample (Figure 65, Figure 66).

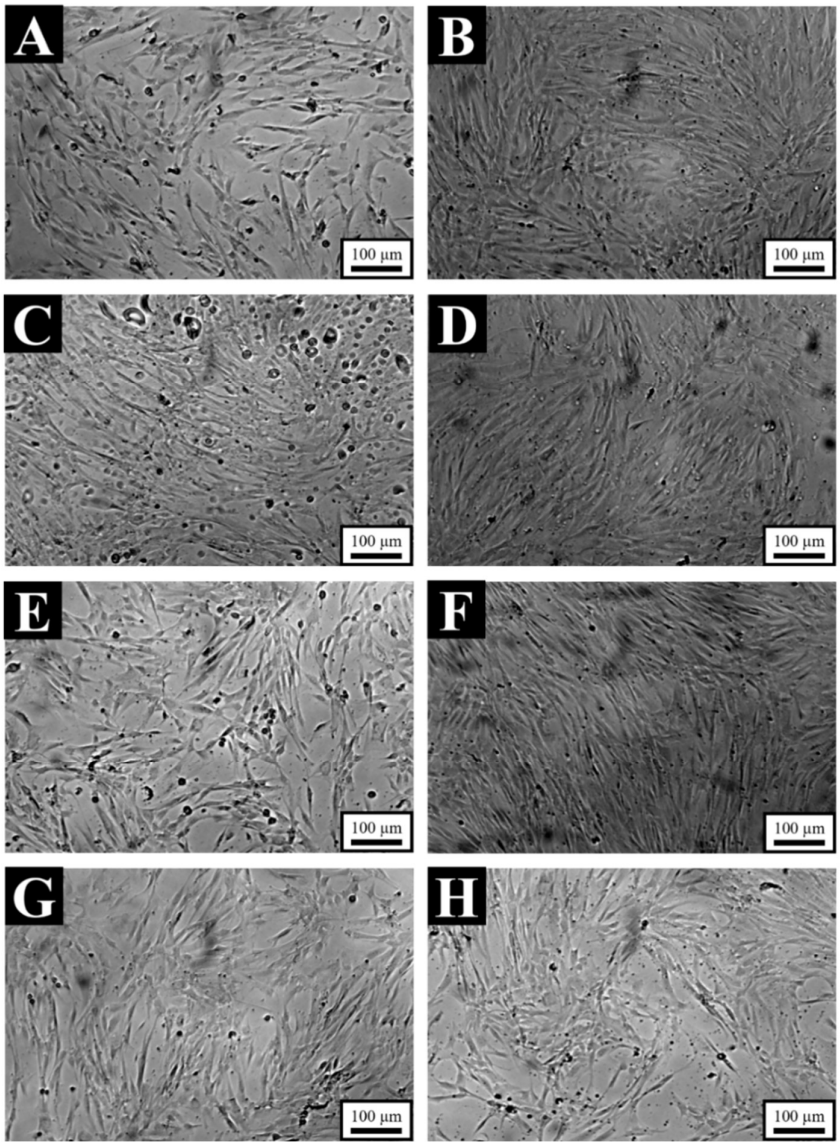

Figure 65. Phase contrast microscopy A. 24h Control, B. 72h Control, C. 24h PSI, D. 72h PSI, E. 24h PCL, F. 72h PCL, G. 24h Co-spun PSI/PCL , F.72h Co-spun PSI/PCL

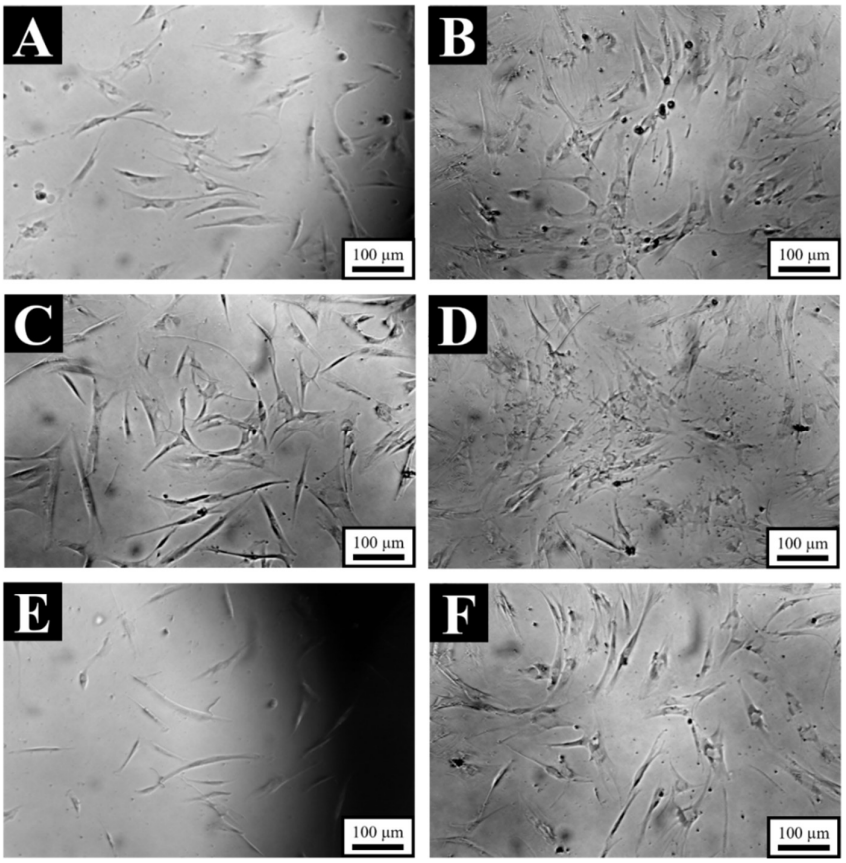

Figure 66. Phase contrast microscopy A. 24h Control, B. 72h Control, C. 24h PSI-DAB, D. 72h PSI-DAB, E. 24h Co-spun PSI-DAB/PCL, F.72h Co-spun PSI-DAB/PCL

Cell adhesion

Regarding cell adhesion, compared to PSI-DAB, every meshes containing PCL (PCL, Co-spun PSI-DAB, Blend-spun PSI-DAB/PCL) performed better. Cells (red) are evidently seen on the surface of PCL containing meshes (green) (Figure 67).

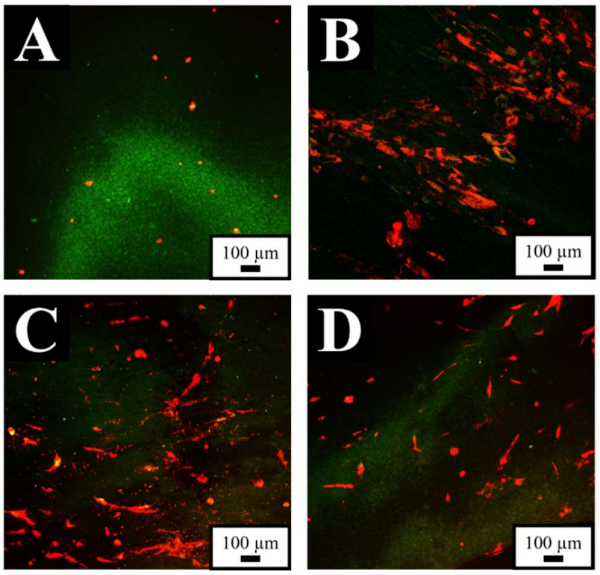

Figure 67. Two photon excitation microscopy imaging of cells placed on A. PSI-DAB, B. PCL, C. Co-spun PSI-DAB/PCL, D. Blend-spun PSI-DAB/PCL
Note: Red: Cells, Green: Mesh surface

4.4.7 Animal Experiments and Biocompatibility Study

Operative Experience

During the surgical procedure, no difficulties were experienced in either surgical handling or fixation. Samples were easily fixated and sample tearing due to suturing was not observed.

Animal Monitoring

During the postoperative period, two animals exhibited signs of mild postoperative discomfort while the rest did not demonstrate pain or irritation scoring low on the grimace scale (
Table 21, Figure 69 A). Animals as expected lost some of their appetite for 1-2 days (Figure 68) after which they regained normal habitual behaviour (i.e., food intake, bowl movement, mobility) (Figure 69B) and weight (Figure 68) but also showed curious

behaviour about the environment enrichment (Figure 69 B). Animals exhibited a physiological wound healing (Figure 69C, Figure 52 C).

Table 21. Post-operative Grimace scale
Note: Points are given in the following manner: 0 – Not present, 1 Moderately present, 2. Obviously present

Day	Average Orbital Tightening	Average Nose/Cheek Flattening	Average Ear Changes
Day 1	0.14 ±0.34	0.07 ±0.25	0.07 ±0.25
Day 2	0.14 ±0.34	0.07 ±0.25	0.00
Day 3	0.00	0.00	0.00
Day 4	0.00	0.00	0.00
Day 5	0.00	0.00	0.00

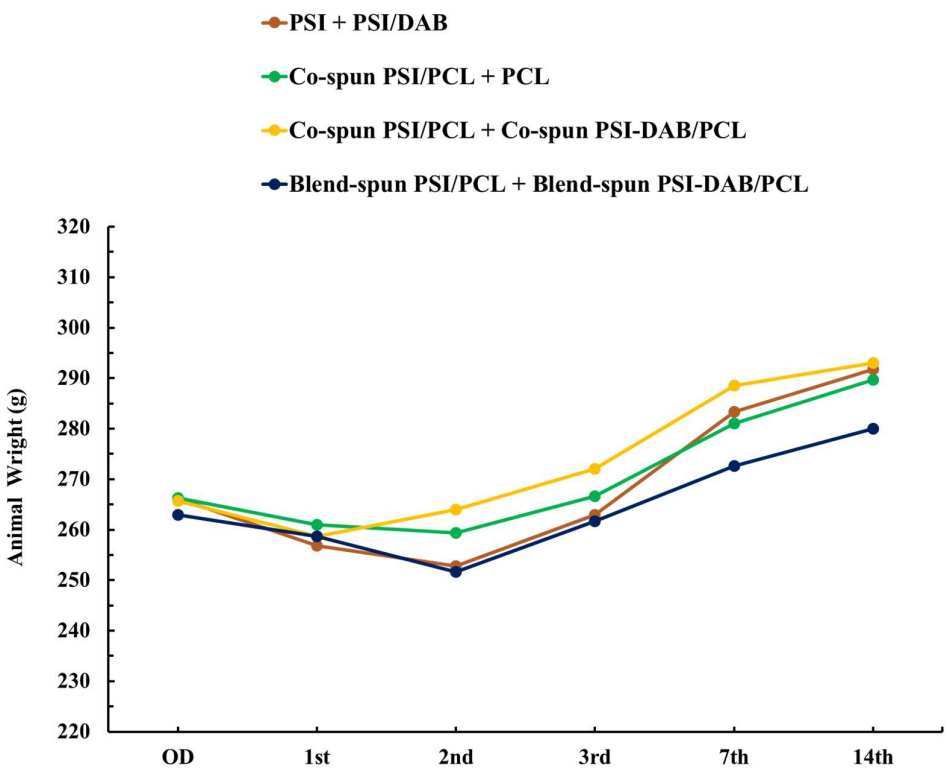

Figure 68. Animal weight changes during the post-operative period

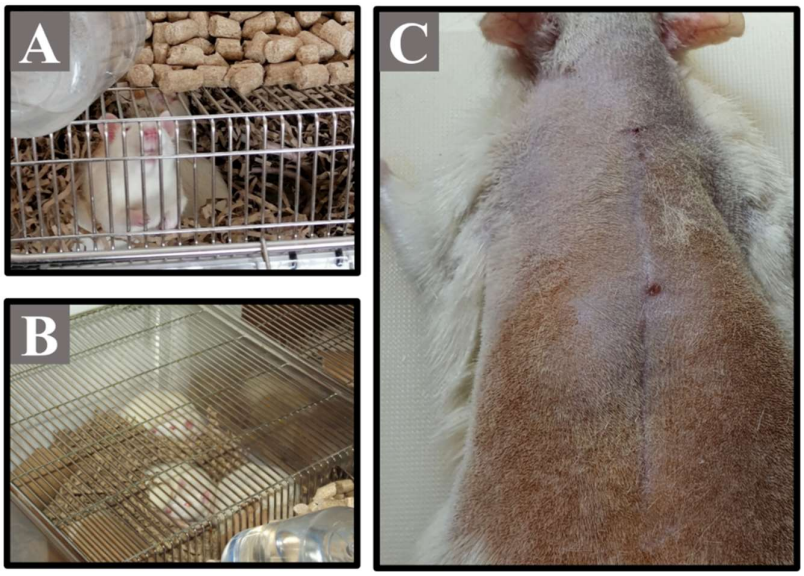

Figure 69. A. Grimace scale evaluation example, B. Animal active behaviour (sleeping in nests), C. Incision wound after 2 weeks

Hemocompatibility

Regarding hemocompatibility, as expected a slight leukocyte (total white cell count) and granulocyte increase was documented (Table 22). Erythrocytes, thrombocytes were in normal range.

Table 22. Haematological examination results for PSI/PCL composite meshes
Note: Presented values are average results along with their standard deviation

	Co-spun PSI/PCL + PSI-DAB/PCL	**Blend-spun PSI/PCL + PSI-DAB/PCL**	**Reference Values**
Leukocytes (10^9/L)	9.22 ±2.16	9.78 ±1.62	1.96-8.25
Granulocyte (%)	32.25 ±5.35	36.8 ±8.35	6.20-26.70
Monocytes (%)	7.58 ±4.87	2.01 ±1.66	0.8-3.80
Lymphocytes (%)	60.17 ±6.93	61.18 ±3.46	66.6-90.30
Erythrocytes (10^9/L)	7.149 ±0.46	7.25 ±0.32	7.27-9.65
Haemoglobin (g/L)	144 ±9.30	145.83 ±4.42	130.70-170.60
Haematocrit (%)	42.61 ±2.06	45.56 ±2.32	39.60-52.50
Thrombocytes (10^9/L)	759 ±277.27	535.66 ±313.83	638-1177

Macroscopic Results

All samples were found incorporating in a healthy granulation tissue. Serious complications (infection, seroma, haematoma) were not found in any of the animals. When comparing co-spun and blend spun PSI/PCL samples, it evident that blend-spun samples induced a thinner and almost transparent granulation tissue/capsule formation. In both samples nevertheless, neovascularisation was also quite visible (Figure 70).

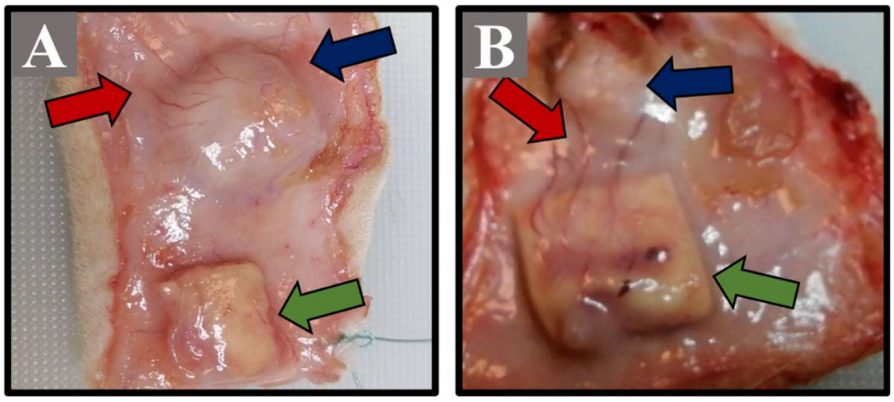

Figure 70. Macroscopical findings during sample retrieval: A. Co-spun PSI/PCL (blue arrow), Co-spun PSI-DAB/PCL (green arrow), B. Blend-spun PSI/PCL (blue arrow), Blend-spun PSI-DAB/PCL (green arrow), Newly formed vessels (neovascularisation) (red arrows)

Microscopic Results

A mild inflammation was found around all the samples (Figure 71). As expected, a granulation tissue formation, leukocyte infiltration and neovascularisation were found as well. At this 2 week point no significant difference can be seen when comparing the different samples. Comparing PSI/PVA and PSI/PCL samples the granulation tissue seem to incorporate a larger number of fibroblasts and newly formed collagen at least visually. Haematoma, necrosis, fatty infiltrates, or giant foreign body cells were not found in any of the samples.

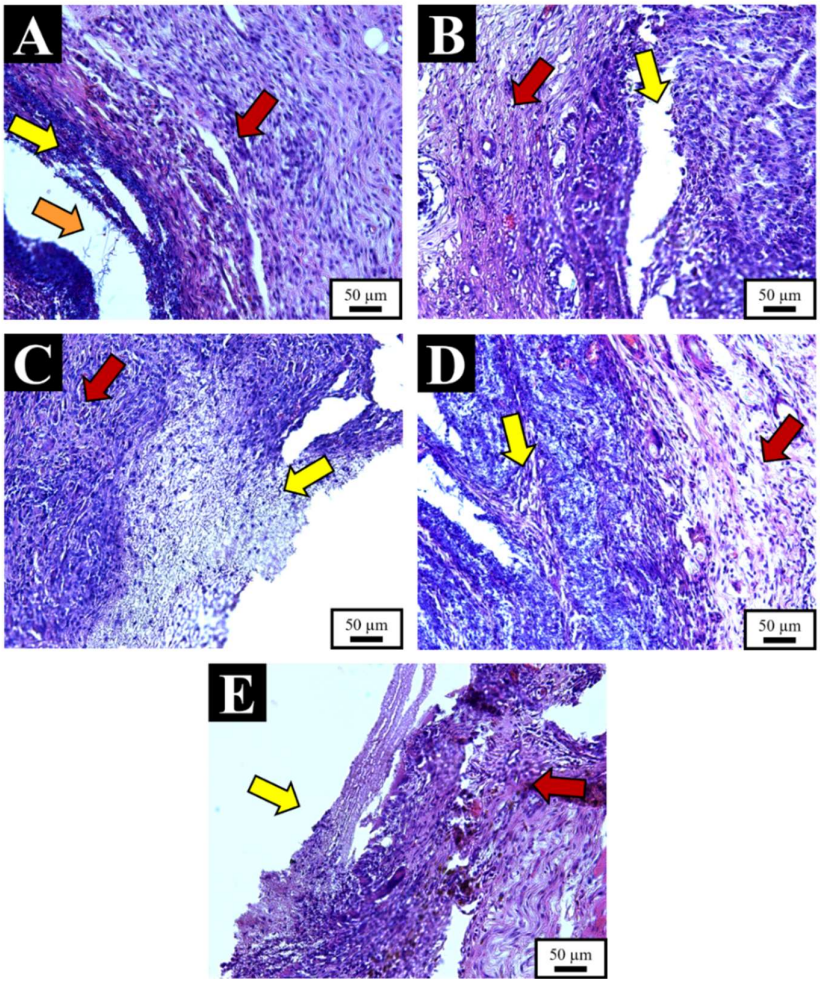

Figure 71. Histopathology examination of: A. Co-spun PSI/PCL, B. Co-spun PSI-DAB/PCL, C. Blend-spun PSI/PCL, D. Blend-spun PSI-DAB/PCL, E. PCL

Note: Yellow Arrow: Implant, Red Arrow: Granulation Tissue Orange Arrow: Visible Nanofibre

4.5 Functionalised PSI and PSI Composite meshes

4.5.1 Macroscopic Results

After the cross-linking and incorporation of the magnetic nanoparticles the meshes change dramatically. From an initial thin fleecy paper-thin sheet (PSI) they first swelled (PSI-DAB) then became black. The meshes retain their original shape while immersed in liquid media. After removing them from an aqueous medium meshes soon lose their shape (not exhibiting self-support) and structural integrity. More importantly, PSI-DAB-Magn samples responded to external magnetic field, evidently exhibiting the presence of magnetite (Figure 72).

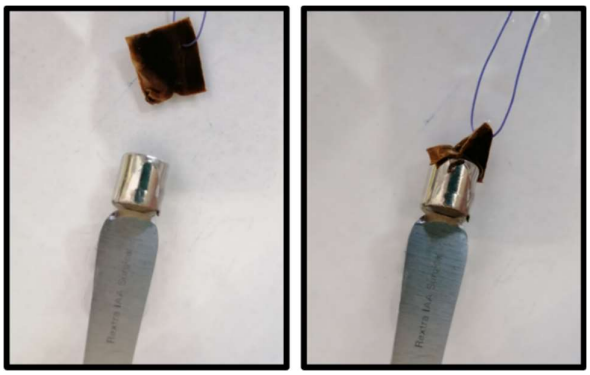

Figure 72. Sutured PSI-DAB-Magn sample exhibiting it magnetic properties.
Note: Sample size: 1 x 1 cm

4.5.2 Physical Characterisation

Scanning electron microscopy confirmed that the fibrous microscstructure was unaltered after the chemical procedure involving the nanoparticle incorporation (Figure 73 A,B). Fibre surface is definitely not smooth anymore as nanoprticles of various sizes are present along the entire surface. Transmission electron microscopy studies confirmed that magnetite was present in the sample (Figure 73 C,D). The average particle size ranged between 8-10 nm.

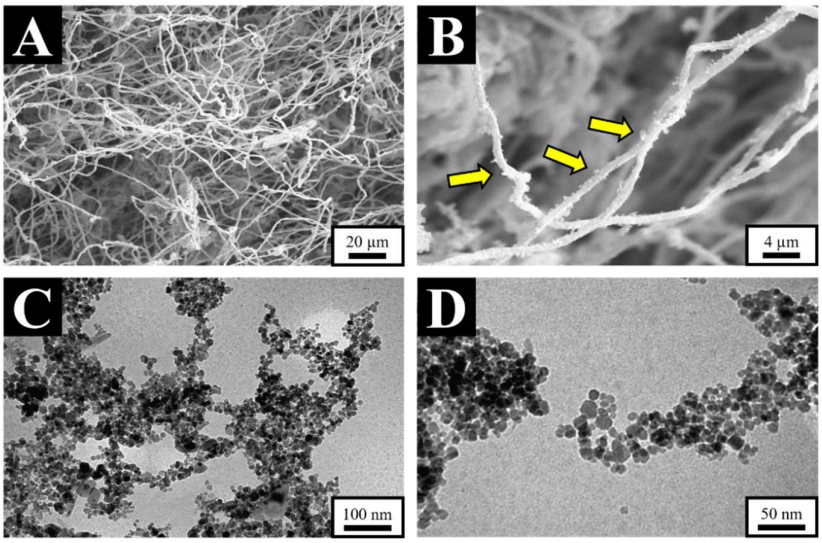

Figure 73. SEM (A, B) and TEM (C D)analysis of PSI-DAB-Magn meshes.
Note: Yellow arrows indicate the magnetite nanoparticles found on the PSI fibres

4.5.3 Chemical Characterisation

The most important peaks on PSI mesh spectrum (Figure 74), namely, the asymmetric stretching vibration of the C=O group (1705 cm^{-1}), the stretching bending vibration of the C-O group (1385 cm^{-1}) and the stretching bending vibration (1385 cm^{-1}) for the imide ring disappeared on the spectrum of the PSI-DAB and PSI-DAB-Magn samples, since all imide rings were cross-linked during NaOH treatment. Moreover, PSI-DAB-Magn also showed an absorption at 580 cm^{-1} (magnetite Fe-O stretch), proving that magnetite is present as the pure magnetite has the absorption peak at the same position.

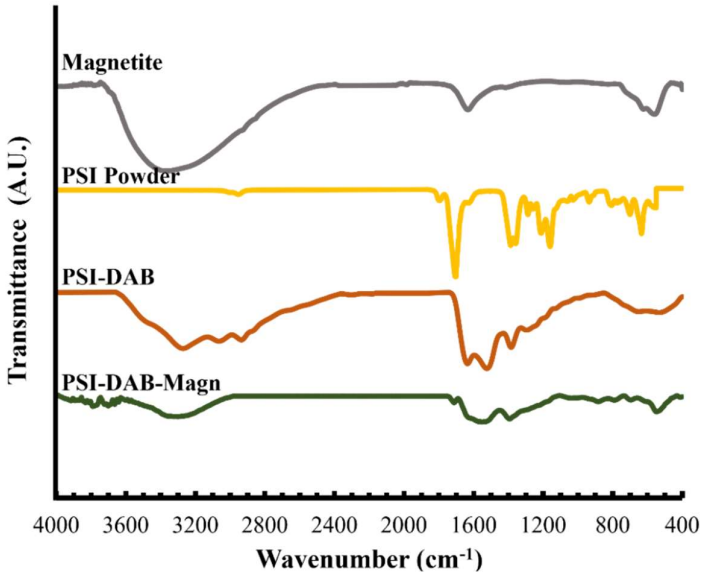

Figure 74. Chemical Characterisation of PSI-DAB and PSI-DAB-Magn meshes

4.5.4 Animal Experiments and Biocompatibility Study

Operative Experience

The surgical procedure was carried out without issues or difficulties. The samples were not damaged by the use of traumatic surgical instruments while suturing and surgical fixation was easily performed. Throughout the entire postoperative period animals behaved normally (food intake, bowl movement, mobility) with no sign of postoperative pain or irritation and no macroscopic complications at the surgical site.

MRI Imaging

On the MRI images taken on the 1st post-operative day the samples can be seen, with clear dimensions and borders without observable surrounding inflammation (Figure 75a). Samples have been only slowly losing their magnetite content. Samples demonstrated excellent contrast properties even after 8 days following implantation According to the MRI images taken on the 8th day the samples can be clearly seen while their dimensions did not change (Figure 75 b). Furthermore, after 8 days inflammation was still not observed.

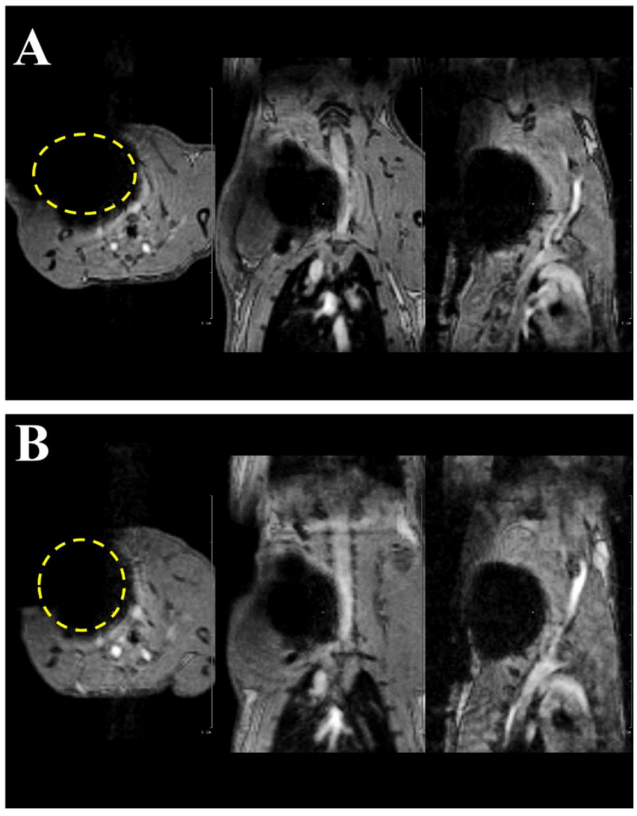

Figure 75. MRI from the 1st (A) and 8th (B) post-operative day (T2 relaxation)

Macroscopic Results

After 8 days, the animals were terminated (Figure 76). No inflammatory signs or other complications were macroscopically observed on the meshes themselves or in the surrounding tissue. Samples were carefully removed and dissected to retain the samples intact while preserving the surrounding newly formed granulation tissue and the underlying muscle layer. Compared to the implantation time, samples have swelled to almost twice their original size.

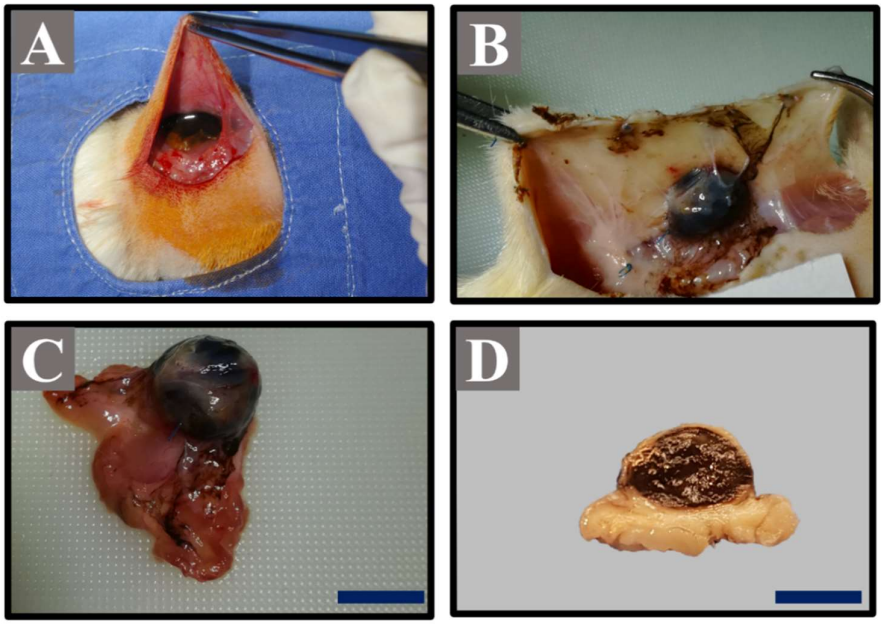

Figure 76. Macroscopic results of animal experiments: PSI-DAB-Magn meshes during implantation (A), during sample extraction (B), Extracted PSI-DAB-Magn samples (C,D). Note: Scale bar set at 2 cm

Microscopic Results

According to the histopathologic evaluation only a mild inflammatory reaction and no serious complications were observed. The sample and the surrounding granulation tissue can be identified clearly. The granulation tissue can be considered thin, while leukocytes mainly granulocytes) are present (Figure 77 A,B). A capsule has not formed at this point while a mild neovascularisation within the granulation tissue is also observable. Giant foreign body type cells were not found. The Berlin blue staining was very efficient in visualizing the iron nanoparticles which seem to migrate further away from the sample, which suggests that tissue integration is in progress (Figure 77 C,D).

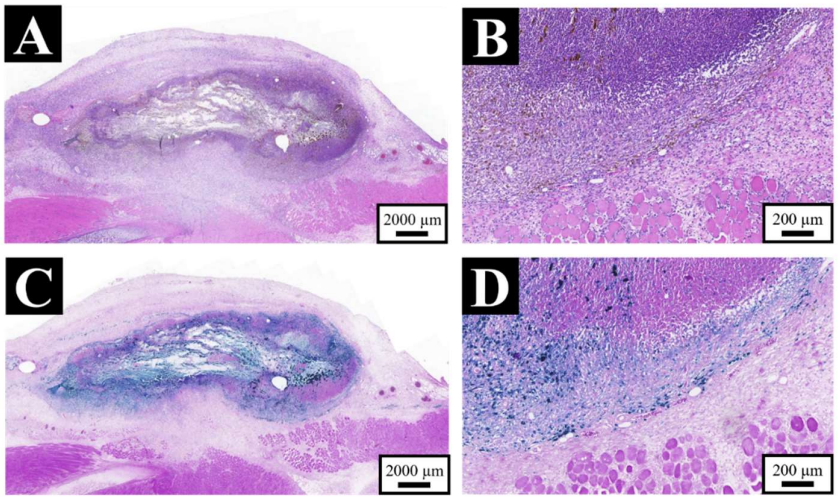

Figure 76. Sample stained with: Haematoxylin-Eosin (A, B) and Berlin Blue (C, D), Border between PSI-DAB-Magn sample, and the surrounding granulation tissue. (B) (D)

4.5.5 Functionalised Composite PSI/PCL Meshes

In the same manner as PSI-DAB-Magn meshes, incorporation of iron oxide nanoparticles was carried out for every PSI/PCL composite mesh. Macroscopically the samples underwent the same texture and colour transformation as seen with the PSI-DAB-Magn meshes making them undistinguishable from each other (Figure 78). The presence of magnetite nanoparticles was confirmed qualitatively via scanning electron microscopy (Figure 79) and qualitatively by ATR/FTIR (Figure 79).

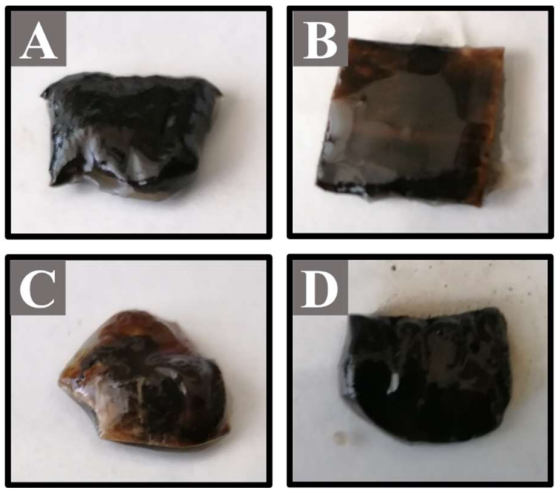

Figure 77. A. PSI-DAB-Magn, B. Layer-spun PSI-DAB/PCL-Magn, C. Co-spun PSI-DAB/PCLMagn,
D. Blend-spun PSI-DAB/PCL-Mag.
Note: Sample size: 1.5 x 1.5 cm

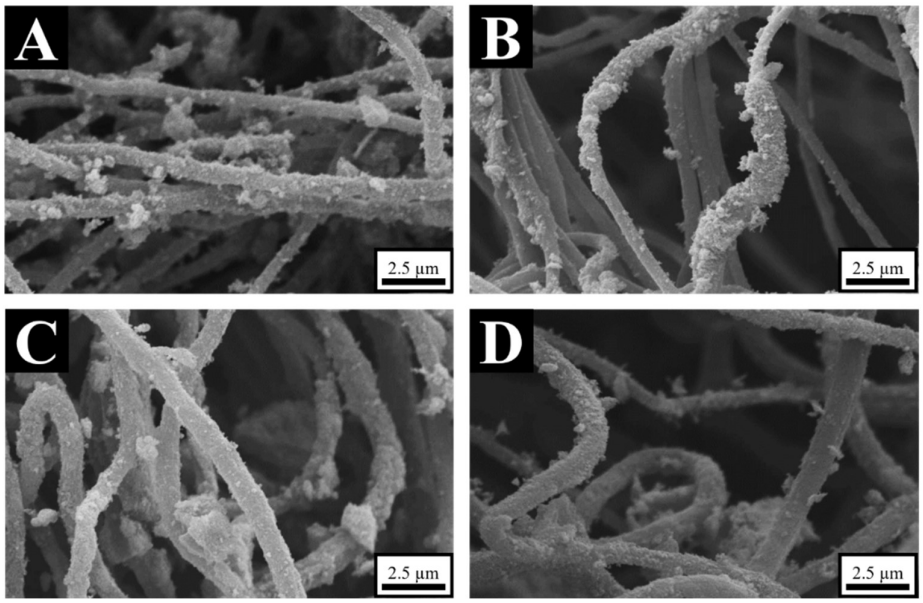

Figure 789. A. PSI-DAB-Magn, B. Layer-spun PSI-DAB/PCL-Magn, C. Co-spun PSI-DAB/PCL -Magn, D. Blend-spun PSI-DAB/PCL -Magn.

The presence of nanoparticles along the surface of the fibres is evident on the SEM images taken from all the composite meshes. Furhtermore, the magnetite peak at 600 cm^{-1} can be found in all the PSI-DAB/PCL meshes regardless of fabrication configuration (layer-spun, co-spun or blend-spun).

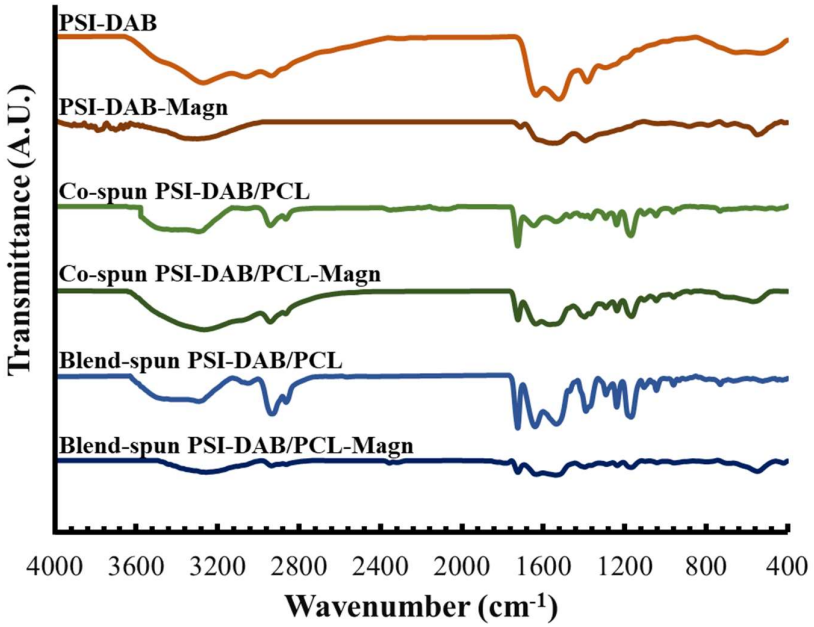

Figure 79. ATR/FTIR analysis of PSI-DAB/PCL-Magn meshes.

5. Discussion

5.1 Polysuccinimide based meshes

5.1.1 Electrospinning, Fibre Quality and Size

Polysuccinimide synthesis was first reported by Hugo Schiff in 1897 (74). At the time the synthesised polysuccinimide was of rather low polymerization degree. Almost a century later, Paolo Neri documented PSI synthesis via thermal polycondensation in the presence of phosphoric acid reaching another milestone (75). Polysuccinimide recently gained the interest of the biomedical field as due its reactive nature as it can be easily modified making it a versatile component for functionalisation of different tissue engineering or drug carrier systems. PSI nanoparticles and hydrogels are documented in the literature (72,76–78) yet manuscripts regarding electrospun polysuccinimide meshes are extremely limited (ranging in the single digits). Therefore, the first objective of this thesis was a comprehensive investigation and optimisation regarding electrospinning parameters and their effects. Electrospinning parameters can affect the quality and size of the produced fibres and therefore the parameters and characteristics of the resulted meshes (79–81).

According to the solubility study (Section 5.1.1) PSI was dissolved in DMAc, DMF and DMSO (Figure 24) as also described in literature (82). Among the three solvents, DMF produced the best quality fibres (Figure 27). Although DMAc and DMSO produced fibres with defects (yellow arrows, Figure 27). Bead formation is a controversial topic in the relevant literature. Until recently, they have been considered as a disadvantage to the system (80,83–85) occurring due to instability in the electrospinning jet (caused by too low voltage, low viscosity etc.). Recently however, the topic has been re-examined (84) and beads may have some value for specific applications (e.g. drug delivery, filters). However, the largest issue is that bead formation cannot be regulated. Moreover, electrospun fibres due to electrospinning's nature itself exhibit a diameter distribution which typically follows a normal distribution. The size distribution can be decreased after optimisation, but it can never be eliminated. Thus, introducing an additional component (beads) which cannot be regulated in an already difficult to regulate system is troublesome. Furthermore whether beads are an advantage always depends on the

polymer used, for example, mechanical performance issues have been documented in their presence (80).

DMF being the best solvent was rather unexpected as it neither was the most conductive (DMSO) or the fastest to evaporate (DMAc) (Table 10, Table 11). As suggested by Juhasz et al. (86) an additional relationship between PSI and DMF seems to be present on a molecular level which makes PSI/DMF electrospinning effortless and easy. Nevertheless, in the future DMAc and DMSO could be of importance as they could be utilised in binary solvents or in combining other polymers.

The smallest fibre diameter was achieved by optimising needle diameter, flow rate, polymer concentration, and voltage. The most crucial parameter was polymer concentration (or more accurately polymer solution viscosity) along with voltage. While fibre formation is possible at a 22.5 w/w % without a high enough voltage, bead formation can occur (Figure 31). Following viscosity and voltage, the combined effect of needle size and flow rate were the second most important parameter (Figure 30). Collector distance and speed did not have any significant effect on fibre diameter. Environmental parameters were not examined as all meshes were fabricated under the same conditions, in this case, room temperature and humidity (Temperature: 25 C ±1 ºC, Humidity: 25 ±5 %) which did not change throughout the experiments. Nevertheless, it has been reported that ambient humidity may have a significant role in fibre formation and structure (83). In addition, temperature affects the viscosity of the solution and the evaporation rate of the electrospinning jet while humidity affects the solidification process of the formed fibres. The degree that ambient temperature and humidity can affect fibre formation depends on the polymer used. For example systems composed of water-soluble systems like poly(vinyl alcohol) (PVA), polyvinylpyrrolidone (PVP) exhibited a decrease in fibre diameter when humidity levels were elevated (87,88) on the contrary in the case of polycaprolactone, water-insoluble system increase of humidity increased fibre diameter (89). Increase of ambient temperature, typically decreases fibre diameter as seen with polyacrylonitrile (PAN), polycaprolactone and cellulose (88,90,91).

The average PSI fibre diameter was successfully reduced from an initial 615 nm (Figure 32) to 280 nm without any quality aberrations (Figure 31). With fibres of this diameter range, literature reports significantly better results regarding biomedical applications. According to several studies, cell adhesion, proliferation and differentiation

was higher on scaffold composed of thinner fibres (≈ 300 nm) (92–95). As PSI is an anhydrous form of a poly(amino acid) and a biocompatible and biodegradable polymer, PSI fibrous systems with advantageous fibre sizes would greatly complement an already promising candidate for tissue engineering (64,66,72,96).

The only drawback of the fibre reduction is the production or fabrication speed as decreasing the flow rate by 75 % it will of course increase the production time. This issue can be circumvented nevertheless, with the use of additional needles, multi-needle spinnerets or even needles electrospinning (97–99), tactics commonly applied in industrial settings.

5.1.2 Mechanical Properties of PSI meshes

Relatively speaking PSI-based meshes are not as strong as polypropylene, polyurethane, or other synthetic polymer-based meshes used in surgery (100,101). However, this is a rather expected disadvantage as most biodegradable meshes are typically mechanically weaker (100,101). In order to improve the performance of the meshes, mechanically induced fibre alignment as well as multi-layer stacking and compression was used.

As with other polymers, fibre alignment was evident at a 2000 rpm collector speed (81,102,103). The alignment of the fibres significantly increased loading capacities on one axis. Multi-layer stacking and compression successfully enhanced the biaxial resistance of the meshes. This is especially important as meshes are most resistant and can resist better potential forces during their *in vivo* implementation. The strongest polymer meshes used in medical applications are surgical hernia meshes used in abdominal hernia treatment. These meshes are typically produced by plastic extrusion followed by a weaving or knitting process. The meshes are composed of microfibres and are microporous. Mechanical properties and depending on the polymer used maximum force sustained vary (104). For example a pure PP mesh e.g., Prolene® by Johnson and Johnson with 0.508 mm thickness and area density of 80–85 g/m^2 tears at approximately 85 N/cm (105). To compare a co-spun PSI/PCL mesh with surface density of 21.6 g/m^2 teared at 10.4 N. However, the PSI/PCL is fully biodegradable whereas PP is not. A few fully biodegradable hernia meshes exist (e.g., TIGR matrix, PHASIX mesh), but they are not commonly used in the daily practice, because of their extremely high prices. The TIGR matrix has similar mechanical performance to Prolene® at least initially (as no data

is provided regarding mechanical performance decrease after implantation). These are quite expensive and clinical data is limited however they are fully absorbed after 3 years (106) and present the era of new surgical hernia meshes. Although the mechanical properties of these electrospun meshes is not on par with current hernia meshes, improvements can still be made utilising fibre alignment as performed with the PSI meshes. For example, a mesh (produced at 4000 rpm) with surface density of 28.4 g/m^2 teared at 20N.

Comparing thick (615 nm) and thin (215 nm) fibre mechanics surprisingly thinner fibres performed worse (Figure 34,

Figure *35*). This is rather an anomaly as literature typically documents that thinner fibres perform mechanically better due to the large surface are contact between the fibres as in the case of Polyvinylidene fluoride (PVDF) and PCL (102,107). In the future, systems composed of two different fibres could be examined as they could potentially provide enhanced cell adhesion while not sacrificing more mechanical strength than desired.

5.1.3 PSI-DAB Meshes

Cross-linking of PSI is necessary as PSI will be hydrolysed into polyaspartic acid (PASP) and will be absorbed after 2-3 days. This property of PSI has a huge potential for drug carrier systems, yet for tissue scaffolds the bioabsorption period is extremely short. Diaminobutane (DAB) cross-linking provides a permanent bond that is not pH or redox labile thus provides stability to the system and can be used for long-term applications(69).

After the chemical treatment, PSI-DAB meshes definitely performed significantly worse than PSI ones, at least in absolute terms (Table 15). PSI performance under liquid is quite poor. This is expected as due to being continuously hydrolysed fibre constitution and therefore mechanical properties diminish (108,109). Although not improving mechanical strength as much as desired, DAB cross-linking significantly decreases the specific loading capacities (Table 15). Literature on mechanical properties of electrospun and cross-linked fibres (hydrogel fibres) is limited. Perhaps the only real example is PVA (40). While PVA hydrogels outperform PSI ones, currently, PVA electrospun and glutaraldehyde (GDA) cross-linked fibrous mesh exhibiting biodegradation does not occur. Therefore, although PSI is outperformed, mechanical strength was never the primary objective when utilising this polymer, as PSI component advantages in these

systems are rapid biodegradability and versatile modifications, making it a functionalisation component.

PSI cross-linking is definitely required if the intended application is surgical tissue regeneration. PSI meshes were not found after the 2-week time period. During a normal wound healing the collagen proliferation phase ends by the 3rd week. In other words, PSI meshes are degraded and absorbed before being able to provide a proper template for the fibroblast cells in the granulation tissue. PSI meshes could be utilised however as drug carrier systems. They have several features that should make them quite advantageous for this type of application including easy modification, biocompatibility, and rapid biodegradation. Although according to the cytotoxicity studies PSI meshes did not perform well (Figure 46), perhaps the parameters of the study were not suitable. The drop in pH occurs as the PSI is hydrolysed and the imide ring opens. This phenomenon has been previously documented (110,111) and is what most likely influences cell viability. In contrast PSI-DAB meshes performed far better (Figure 47), as the pH drop was circumvented due to the cross-linking (less imide rings opened in the cell media, thus less protons appeared in the solution to influence the pH).

During the *in vivo* animal experiments, only the PSI-DAB meshes performed very well. Animals soon gained their weight back (Figure 51) after the procedure, no serious haematological alteration (Table 17) were documented and no macroscopic (Figure 53) or microscopic (Figure 54) complications were found making PSI-DAB meshes highly promising.

5.2 Polysuccinimide/Poly(vinyl alcohol) composite meshes

PSI/PVA co-electrospinning and mesh fabrication was successfully performed. The reason for the combination of these two polymers was triple; to increase the mechanical performance of PSI under liquid, to make composite meshes with tuneable wettability and combine a water and non-water-soluble polymer fibre components. The presence of the two polymer fibres was confirmed by chemical (ATR/FTIR - Figure 43) and physical characterisation methods (SEM - Figure 41). In addition, two photon excitation microscopy (Figure 42) confirmed the random distribution of the PSI and PVA polymer fibres.

Throughout the entire mechanical and chemical post-electrospinning treatment (Section 4.6, and Section 4.7) the fibrous microstructure of the mesh remained relatively

intact (Figure 41). After the chemical treatment and crosslinking (Section 4.6, 4.7) average PSI fibre diameter decreased while PVA fibre increased (Table 13). In some cases, fibre fusion was found which is an already documented phenomenon (40,59). PVA cross-linking is essential as PVA being water-soluble will readily dissolve in an aqueous medium. In the case of the double cross-linking PSI-DAB/PVA-GDA issues were not documented.

For tissue engineering applications measuring the water contact angle of tissue scaffolds is essential as wettability highly influences cell adhesion and therefore tissue integration (112). PSI wettability has not been published before. Surprisingly while PSI itself is non-water soluble the electrospun meshes absorbed the droplets placed on them (Figure 38). This is due to a capillary effect induced by the fibrous microstructure of the mesh. The cross linking definitely increased the absorption time from 1.4 to 28.7 seconds (Table 12) and the initial contact angle however in practical terms (*in vivo* applications) this difference can be considered as irrelevant. Compared to PSI, PVA had a definitive contact angle ($\theta = 60^o \pm 10.9$) although still being hydrophilic (Table 13).

Regarding mechanical parameters, while PSI/PVA-GDA (Specific loading capacity: 0.164 Nm^2/g) meshes did indeed perform significantly better than PSI (Specific loading capacity: 0.08 Nm^2/g) and PSI-DAB (Specific loading capacity: 0.03 Nm^2/g) ones (Table 15), but they were still weaker than pure PVA-GDA meshes (Specific loading capacity: 0.418 Nm^2/g). Unfortunately, a synergistic relationship as seen in other systems as previously described in section 2.6 (Table 1) is not present, even more so DAB cross-linking seems to decrease the mechanical properties of the composite meshes. Nevertheless, the meshes possess mechanical properties suitable for implantation and surgical tissue regeneration. Future work is needed to assess whether the meshes could be used for example as hernia meshes. As demonstrated increasing the fibre alignment is a feasible and quite simple method to enhance mechanical properties which could be used in future if needed.

The cell studies confirmed that the PSI/PVA meshes are not cytotoxic, however DAB crosslinking greatly benefits the meshes as the pH drop does not happen therefore cell viability is not affected (Figure 47).

Cell adhesion and differentiation was not visible. Although retaining their fibroblast structure (Figure 47) cells were not able to adhere on the mesh surface (Figure

50). On the other hand, anti-adhesive surfaces can be utilised in surgical tissue regeneration as surgical hernia meshes or even wound dressings (22,40,113). The objective could potentially be to either prevent adhesion formation in the intraperitoneal cavity after a hernia repair or prevent the wound dressing for adhering to a fresh wound and causing damage on the newly formed tissue during its removal.

For this very purpose *in vivo* examinations were performed. The hypothesis was that a mesh composed of a rapidly biodegradable component (PSI) will enhance tissue integration of the non-degradable counterpart (PVA). In this regard, animal studies had highly promising results (Section 5.3.7) Animals gained weight, were socially active and presented with no issues during the haematological examinations. No macroscopic or microscopic complications were documented while physiological wound healing and new tissue formation was visible. When looking at both the macroscopical (implant size, shape, Figure 53) and microscopical findings (Figure 54) PSI/PVA-GDA and PSI-DAB/PVA-GDA meshes seem to be degrading faster by incorporating better in the surrounding tissue compared to the rather inert PVA-GDA. The 2-week period is definitely not long enough however, and long duration animal studies are needed (experiments are already in progress).

5.3 Polysuccinimide/Polycaprolactone composite meshes

Fabrication of PSI/PCL composite meshes had exciting and interesting results. In contrast to cross-linked PVA, PCL does not require cross-linking while is also biodegraded in the body in a two-phase process (first hydrolysis then enzymatic degradation) (114,115). Possessing quite favourable mechanical properties, the PCL can add robustness to the system but also provide stability as its biodegradation typically lasts 6 months (depending on the molecular weight). The aim of this frame was to fabricate a composite mesh with an early and a late biodegrading component which provides a regulated and mechanically stable tissue regeneration. As tissue regenerates on the rapidly bioreading PSI, PCL provides mechanical support in the background until finally after 6 months when the collagen proliferation has long reached its peak and the collagen fibres are mature (35,116,117), PCL will also be absorbed (102,118,119).

In contrast to PVA, PCL is dissolved in more than a few organic solvents therefore its well suited for the fabrication of composite meshes (Table 2). Three electrospinning configurations were examined. Wettability (Section 5.4.4), mechanical properties

(Section 5.4.5) even cell adhesion (Section 5.4.6) can be tuned according to the electrospinning configuration. In terms of mechanical strength, the layer-electrospun meshes are the strongest (In air: 0.455 ±0.155, in liquid: 0.332 ±0.063 Nm^2/g) while blend-spun ones the weakest (in air: 0.277, in liquid: 0.054 Nm^2/g) (Table 20). On the contrary, in terms of wettability, blend-spun meshes had the smallest contact angle. Contact angle decreased significantly from 131° (PCL) to 109 ° (Blend-spun PSI/PCL) to 30 ° (Blend-spun PSI-DAB/PCL).

PSI/PCL cell viability (Figure 63, Figure 64) was similar to the co-spun PSI/PVA meshes (Figure *46*, Figure 47) exhibiting a non-cytotoxic nature. Interestingly, regarding cell adhesion, PSI/PCL meshes performed better than PSI and PCL meshes (Figure 50 , Figure 67).

Animal studies also demonstrated similar results to the PSI/PVA composite meshes with no evident complications. Weight gain (Figure 677), haematological parameters (Table 22) and wound healing (Figure 69-69) were similar. Histopathology (Figure 71) revealed minimal inflammation with granulation tissues rich in fibroblasts and collagen compared. Although these are preliminary results, they are quite promising. As in the PSI/PVA meshes, PSI having a short biodegradation time increases tissue integration. PCL having a longer biodegradation long term animal experiment is needed for comprehensive assessment.

PCL has been regularly utilized as a tissue scaffold being biodegradable and mechanically robust yet its major disadvantage is the poor cellular infiltration due to its high hydrophobicity (118). Some tactics (15,112,120,121) have been already utilized in the endeavour of circumventing this issue yet they seem to always have disadvantages (additional or complicated processing steps, alteration of the original system, higher production costs). On the contrary, the PSI/PCL meshes not only circumvent this issue without requiring additional processing but can also be further modified (increasing collector speed, PSI/PCL ratio, PSI cross-linking) to further adjust these parameters but have the potential to be additionally functionalized as both polymers have been modified in the past (e.g., nanoparticle addition, drug encapsulation) providing further advantages to the system.

Therefore, according to the desired application, whether it requires mechanical strength and robustness (hernia mesh, pelvic mesh) or wettability for cell adhesion or

functionality the mesh can be fine-tuned. Furthermore, while the thesis presents composite meshes, these materials can be further optimised by altering the polymer ratios during electrospinning. For example, increasing PCL will increase tensile strength, increasing PSI while increase wettability, functionalisation possibilities and biodegradation time.

5.4 Functionalised PSI-DAB-Magn Meshes

Biomaterial research is certainly popular and exciting. In recent years the trend and focus of this discipline is not just synthesise and fabricate biomaterials but rather functional or even multi-functional biomaterials (e.g., mechanical, support, drug delivery, anti-microbial etc.). Incorporating nanoparticles in a fibrous mesh seem rather fitting. Nanofibres are an exceptionally well-suited medium for nanoparticle. Nanoparticles and nanofibres alike have a huge surface area to volume ratio. however, When combined however, one major issue of nanoparticles namely aggregation can be decreased or even eliminated and thus these materials can accentuate each other's properties. Magnetite was successfully incorporated in PSI meshes. PSI-DAB-Magn meshes were magnetically responsive (Figure 72). Additionally, the presence of magnetite was confirmed not only by chemical but by physical characterisation methods as well (Section 5.5.2 and 5.5.4). ATR/FTIR peaks were consistent, and the presence of Magnetite can be observed by the peak at 580 cm^{-1} (magnetite Fe-O stretch) (Figure 74). In addition, utilising SEM, fibres and the magnetite nanoparticles along their surface were observed (Figure 73). As PSI-DAB are hydrogel meshes (composed of hydrogel fibres) small molecules can diffuse freely into the fibres themselves and not just between the fibres. After the chemical treatment with NaOH, magnetite nanoparticles precipitated between but also within the PSI-DAB fibres. This method has been documented before (122–124). The combination of Magnetite and PSI has also been documented before (125,126) however these systems were nano-aggregates and nano-hydrogels. As aforementioned, nanofibrous meshes highly complement nanoparticles. The advantage of a nanofibrous mesh as a nanoparticle medium is that nanoparticle aggregation is limited and diffusion of the nanoparticles won't be as rapid *in vivo* (65). As the main objective of these meshes is localised hyperthermia treatment for cancer, the more localised the magnetite the more efficient it will be. In addition, compared to bulk hydrogels, meshes have the potential to be surgically fixated with sutures or other surgical equipment and therefore can be used in

the management of larger and laterally progressing tumours e.g., mesothelioma. This can be confirmed by the MRI imaging. Meshes exhibited excellent contrast even on 8th post-operative day making them a promising candidate for in vivo hyperthermia applications (Figure 75). During the animal experiments no complications were identified macroscopically or microscopically. Eight days is definitely a short period for a comprehensive biocompatibility and biodegradability profile evaluation, yet these preliminary results (minimal inflammation, no foreign body type giant cells) are highly promising indicating the biocompatible nature of the PSI-DAB-Magn meshes. Further examination is definitely needed, and perhaps a large animal model (e.g., swine) would also provide the opportunity to investigate surgical applicability and mesh functionality.

In this regard to provide mechanical support for a potential longer treatment PCL was incorporate as well. Functionalised PSI-DAB/PCL meshes were successfully fabricated (Section 5.5.6). Out of the composite meshes the co-spun PSI-DAB/PCL seems to be the most reproducible and consistent. PCL did indeed provide mechanical stability making the implant suturable and stable for longer periods of time. While the main objective for these meshes is to utilise these meshes for magnetic hyperthermia treatment as an alternative management option in cancer treatment, the incorporation of PCL provides an opportunity for a double functionalisation system. Thus as next step, a combined nanocomposite can be created, while magnetite nanoparticles are incorporated to the PSI component, drugs could be incorporated to PCL making a multi-functional nanocomposite material (118,127).

6. Conclusion

In this era of medicine, long-term complications of frequent and common diseases and disorders are evidently increasing. In this regard, tissue damage and subsequent loss is one of the typical issues. In a surgical ward these could range from diabetic wounds to abdominal defects. One of medicine's ultimate objectives always was the regeneration of damaged or lost tissues. While transplantation has been performed for decades, it has strict requirements, and it is performed after several clinical and compatibility examinations, furthermore resources are often limited. To provide a solution, biomedical science has turned towards the fabrication of synthetic tissues and tissue engineering.

Tissue engineering scaffolds can be produced via several methods and techniques however polymer based meshes have been shown to be quite advantageous for this purpose. Electrospinning is a method to produce membranes, meshes and mats composed of nanofibres. These meshes provide a perfect template for cell adhesion, proliferation, and differentiation as they resemble the innate extracellular matrix found almost around every cell in the body. In addition, having a high surface to volume ratio they have additional advantageous features which can be exploited for numerous applications.

In this thesis electrospun nanofibrous meshes have been fabricated using different polymer sources, optimised and examined as biomaterials intended for surgical tissue regeneration. The main polymer utilised was the anhydrous form of a synthetic poly(amino acid) with a high functionalisation profile namely polysuccinimide.

Through the work of this thesis, the following new scientific results have been achieved:

T1. Polysuccinimide meshes were successfully optimised in terms of fibre size and mechanical properties. The starting average fibre diameter measuring 615 ± 105 nm was reduced to 280 ± 50 nm via the optimisation of polymer concentration, needle size, flow rate and voltage. Mechanical enhancement was also successful improving the specific loading capacity of the meshes uniaxially from 0.3 to 0.7 Nm^2/g due to fibre alignment but also biaxially using the multilayer stacking technique. **(I./III.)**

T2. PSI was successfully combined with PVA to fabricate co-electrospun composite meshes, for the first time in current literature. ATR-FTIR proved the presence of the two polymer fibres in the samples while the two-photon excitation microscopy further

confirmed their random distribution along the sample surface. The PVA component improved the mechanical performance of the meshes under liquid reaching a specific loading capacity of 0.164 Nm^2/g. On the other hand, the PSI component increased wettability. Compared to pure PVA-GDA meshes which although hydrophilic did not let water pass through, PSI/PVA meshes evidently exhibited a definitive and measurable absorption time. **(II.)**

T3. Biocompatibility of the co-electrospun PSI/PVA meshes was examined *in vitro* with a fibroblast cell line and *in vivo* on small animals, specifically Wistar rats. Meshes proved to be cyto-, haemo- and biocompatible. As pure PVA and PSI/PVA meshes provided poor cell adhesion thus they can be described as antiadhesive. During the animal studies macroscopical and microscopical biocompatibility was evident while enhanced tissue integration after 2 weeks is highly suggestive.

T4. Three different PSI/PCL composite meshes were successfully fabricated for the first time in current literature by utilising three different electrospinning configurations: layer-electrospinning, co-electrospinning and blend-electrospinning. While ATR-FTIR demonstrated no difference in the chemical composition of these composite meshes, fluoresce microscopy confirmed that in the case of co-electrospun meshes two different polymer fibres are present (PSI and PCL) while in the case of the blend-electrospun meshes both polymers are present within the electrospun fibres. In term of mechanical performance layer-electrospun meshes proved the strongest both in air and under liquid exhibiting a specific loading capacity of 0.455 ± 0.155 and 0.332 ± 0.063 Nm^2/g respectively. Regarding wettability blend-electrospun PSI/PCL meshes exhibited the smallest contact angle ($\theta = 109.5^o \pm 3.2$) and shortest absorption time ($t = 7.55 \pm 5.5$ s.). Overall, PCL addition improved the mechanical performance of all the meshes both in air and under liquid while PSI once again increased wettability. **(IV.)**

T5. Biocompatibility of meshes was examined with in vitro cell and in vivo studies. Meshes proved to be cyto-, haemo- and biocompatible. According to the cell studies, PSI/PCL meshes fabricated in all three setups (layer-, co-, blend-spun) are cytocompatible and exhibiting excellent cell adhesion properties. During the animal studies macroscopical and microscopical biocompatibility was evident while enhanced tissue integration after 2 weeks is highly suggestive.

T6. Incorporation of magnetite nanoparticles was performed in PSI and PSI/PCL meshes. Magnetite presence was confirmed by physical (SEM, TEM) and chemical characterisation methods (ATR-FTIR). The magnetic property of the meshes was evident. Animal experiments demonstrated how PSI-DAB-Magn meshes exhibit excellent MRI contrast properties even after 8 days. Histopathology revealed no complications while nanoparticle diffusion was also documented in the surrounding local tissue.

7. Summary

The aim of the thesis was to investigate biomaterials intended for surgical tissue regeneration. For this purpose, a promising polymer, namely polysuccinimide was investigated as well as two combinations with already utilised polymers in this field (PVA and PCL).

In the first frame of this work, PSI meshes were optimised. The average nanofibre diameter was successfully decreased to less than half the initial diameter (from 615 to 280 nm) without compromising the quality of the microstructure or the fibres. To improve the mechanical properties of these meshes, mechanically induced orientation using a rotating collector and multi-layer stacking was utilised. These methods proved successful in enhancing the uniaxial and biaxial mechanical performance of the meshes, respectively.

In the second frame PSI was co-electrospun with PVA. These meshes exhibited increased specific loading capacities under liquid, increased wettability and proved as cytocompatible and biocompatible composite meshes.

Subsequently in the third frame the PSI was combined with PCL in three different electrospinning configurations. PCL complements PSI well by increasing its overall mechanical performance (both in air and under liquid) but also providing a stable frame for cell adhesion. On the other hand, PSI increased wettability and tissue integration. The features of these composite meshes can be adjusted according to which electrospinning configuration (layer-electrospinning, co-electrospinning or blend electrospinning) is utilised. Similarly, to co-spun PSI/PVA meshes, PSI/PCL meshes proved cytocompatible and biocompatible as well.

Finally, magnetite nanoparticles were incorporated with PSI meshes. The ultimate objective here will be an alternative cancer treatment option (magnetic hyperthermia) although this direction exceeds the theme of the thesis. The presence of the magnetite nanoparticles was confirmed by physical chemical characterisation methods while meshes exhibited magnetic properties. PSI-DAB-Magn meshes were also investigated *in vivo.* Similarly, biocompatibility is evident even at this early stage, while more importantly the meshes proved to be an excellent MRI contrast agent. PCL was subsequently also incorporated to provide mechanical support, however its role in the functionality of this system is yet to be examined.

8. Összefoglalás (Summary in Hungarian)

Munkám célja sebészeti szövetregenerációra alkalmas bioanyagok fejlesztése és vizsgálata volt. Ennek érdekében elektrosztatikus szálképzéssel nanoszálakból felépülő hálókat készítettem többféle polimer felhasználásával. Az elektrosztatikus szálhúzás körülményeit optimalizáltam, a hálókat széleskörűen vizsgáltam. A hálók fő polimere a poliszukcinimid (PSI) volt, mely egy könnyen funkcionalizálható szintetikus poli(aminosav)-származék, melyet további, bioanyagként használt polimerekkel - polivinil alkohollal (PVA) és polikaprolaktonnal (PCL) - kombináltam.

A munkám első lépéseként PSI hálókat állítottam elő, a szálátmérő és a mechanikai tulajdonságok szempontjából optimalizáltam a rendszert. A kezdeti átlagos szálátmérő a felére (615 nm-ről 280 nm-re) csökkent a polimerkoncentráció, a tűátmérő, az áramlási sebesség és a feszültség változtatásával, míg a hálók fajlagos terhelhetőségét sikeresen növeltük először egy kitűntetett irány mentén a szálak orientáltságának növelésével, majd a többrétegű elrendezésnek köszönhetően biaxiálisan is.

Ezt követően a PSI-t sikeresen kombináltam PVA-val ko-elektrosztatikus szálképzés segítségével. A PVA komponens jelentősen javította a hálók mechanikai teljesítményét folyadék alatt (mely orvosi alkalmazások szempontjából releváns), másrészt a PSI komponensnek köszönhetően a hálók nedvesíthetősége nőtt. A hálók haemo-, cito-, és biokompatibilisnek bizonyultak az állatkísérletek során, míg a sejtes kísérletekben antiadhezív tulajdonságot mutattak.

Ezt követően a PSI-t három különböző szálképzési konfiguráció (réteg- , ko- és keverék szálhúzás) alkalmazásával PCL-el kombináltuk. A PCL jelenléte javította a mechanikai terhelhetőséget (levegőben folyadékban is), és stabil vázként szolgált a humán fibroblaszt sejtek letapadásához. Másrészt a PSI jelenléte a kompozit hálókban javította a nedvesíthetőséget és a szöveti integrációt az állatkísérletek alapján.

Végül magnetit nanorészecskéket tartalmazó PSI és PSI/PCL hálók előállítását is megvalósítottuk. A magnetit jelenlétét fizikai és kémiai jellemzési módszerekkel igazoltuk. Bizonyítottuk a hálók mágneses tulajdonságait illetve az állatkísérletek bizonyították, hogy a PSI-DAB-Magn hálók 8 nap után is kiváló MRI kontraszt tulajdonságokat mutatnak. A szövettani vizsgálat nem tárt fel szövődményeket, míg a nanorészecske diffúzió a környező lokális szövetekben is dokumentálható volt.

9. Bibliography

1. Mathur S, Sutton J (2017): Personalized medicine could transform healthcare (Review). *Biomed Reports* 7: 3–5.

2. Goetz LH, Schork NJ (2018): Personalized medicine: motivation, challenges, and progress. *Fertil Steril* 109: 952–963.

3. Ntege EH, Sunami H, Shimizu Y (2020): Advances in regenerative therapy: A review of the literature and future directions. *Regen Ther* 14: 136–153.

4. Grounds MD (2018): Obstacles and challenges for tissue engineering and regenerative medicine: Australian nuances. *Clin Exp Pharmacol Physiol* 45: 390–400.

5. Quint C, Niklason L (2009): Tissue Engineering and Regenerative Medicine. *Rossi's Principles of Transfusion Medicine: Fourth Edition*. https://doi.org/10.1002/9781444303513.ch61

6. Alarcin E, Bal-Ozturk A, Avci H, Ghorbanpoor H, Guzel FD, Akpek A, *et al.* (2021): Current Strategies for the Regeneration of Skeletal Muscle Tissue. *Int J Mol Sci* 22. https://doi.org/10.3390/ijms22115929

7. Xie C, Ye J, Liang R, Yao X, Wu X, Koh Y, *et al.* (2021): Advanced Strategies of Biomimetic Tissue-Engineered Grafts for Bone Regeneration. *Adv Healthc Mater*. https://doi.org/10.1002/adhm.202100408

8. Abdulghani S, Mitchell GR (2019): Biomaterials for in situ tissue regeneration: A review. *Biomolecules* 9. https://doi.org/10.3390/biom9110750

9. Di Gesù R, Amato G, Gottardi R (2019): Electrospun scaffolds in tendons regeneration: A review. *Muscles, Ligaments and Tendons Journal*, vol. 9. pp 478–493.

10. Nemati S, Kim S jeong, Shin YM, Shin H (2019): Current progress in application of polymeric nanofibers to tissue engineering. *Nano Converg* 6. https://doi.org/10.1186/s40580-019-0209-y

11. Liu Y, Wang C (2019): Advanced Nanofibrous Materials Manufacture Technology Based on Electrospinning. *Advanced Nanofibrous Materials Manufacture Technology Based on Electrospinning*. https://doi.org/10.1201/9780429085765

12. Wang F, Hu S, Jia Q, Zhang L (2020): Advances in Electrospinning of Natural Biomaterials for Wound Dressing. *J Nanomater* 2020. https://doi.org/10.1155/2020/8719859

13. Saini M (2015): Implant biomaterials: A comprehensive review. *World J Clin Cases* 3: 52.

14. Tang, Ben Zhong, Alaa S. Abd-El-Aziz SC (2014): *Electrospinning: Principles, Practice and Possibilities*. Retrieved from , www.rsc.org

15. Bosworth LA, Hu W, Shi Y, Cartmell SH (2019): Enhancing Biocompatibility without Compromising Material Properties: An Optimised NaOH Treatment for Electrospun Polycaprolactone Fibres. *J Nanomater* 2019. https://doi.org/10.1155/2019/4605092

16. Begum, Hosne Ara and Khan MKR (2017): Study on the Various Types of Needle Based and Needleless Electrospinning System for Nanofiber Production - Google Search. *Int J Text Sci* 6: 110–117.

17. Europeean Union (2017): Regulation (EU) 2017/745 OF The European Parlament and of the Council of 5 April 2017 on medical devices. *Off J Eur Union*. https://doi.org/10.1177/2165079915576935

18. Williams D, Xingdong Z (2019): Chapter II - Biomaterials and biomedical materials. In: Williams D, Zhang XBT-D of B for the T-FC, editors. *Definitions of Biomaterials for the Twenty-First Century*. Elsevier, pp 15–23.

19. Vert M, Doi Y, Hellwich K-H, Hess M, Hodge P, Kubisa P, *et al.* (2012): Terminology for biorelated polymers and applications (IUPAC Recommendations 2012). *Pure Appl Chem* 84: 377–410.

20. Wong JY, Bronzino JD, Peterson DR (2013): *Biomaterials Principles and*

Practices.

21. Banoriya D, Purohit R, Dwivedi RK (2017): Advanced Application of Polymer based Biomaterials. *Mater Today Proc* 4: 3534–3541.

22. Gruber-Blum S, Brand J, Keibl C, Fortelny RH, Redl H, Mayer F, Petter-Puchner AH (2017): Abdominal wall reinforcement: biologic vs. degradable synthetic devices. *Hernia* 21: 305–315.

23. Zhu L-M (2015): Mesh implants: An overview of crucial mesh parameters. *World J Gastrointest Surg* 7: 226.

24. Nava MB, Rancati A, Angrigiani C, Catanuto G, Rocco N (2017): How to prevent complications in breast augmentation. *Gland Surg* 6: 210–217.

25. Williams DF (2008): On the mechanisms of biocompatibility. *Biomaterials* 29: 2941–2953.

26. Anderson JM (2001): Biological responses to materials. *Annu Rev Mater Sci* 31: 81–110.

27. Carnicer-Lombarte A, Chen ST, Malliaras GG, Barone DG (2021): Foreign Body Reaction to Implanted Biomaterials and Its Impact in Nerve Neuroprosthetics. *Front Bioeng Biotechnol* 9: 1–22.

28. Chandorkar Y, Ravikumar K, Basu B (2019): The Foreign Body Response Demystified. *ACS Biomater Sci Eng* 5: 19–44.

29. Shishatskaya EI, Volova TG, Puzyr AP, Mogilnaya OA, Efremov SN (2004): Tissue response to the implantation of biodegradable polyhydroxyalkanoate sutures. *J Mater Sci Mater Med* 15: 719–728.

30. Schoen FJ, Levy RJ, Tam H, Vyavahare N (2020): 2.4.5 - Pathological Calcification of Biomaterials. In: Wagner WR, Sakiyama-Elbert SE, Zhang G, Yaszemski MJBT-BS (Fourth E, editors. Academic Press, pp 973–994.

31. Labuda J, Bowater RP, Fojta M, Gauglitz G, Glatz Z, Hapala I, *et al.* (2018):

Terminology of bioanalytical methods (IUPAC Recommendations 2018). *Pure Appl Chem* 90: 1121–1198.

32. Barczikai D, Kacsari V, Domokos J, Szabó D, Jedlovszky-Hajdu A (2021): Interaction of silver nanoparticle and commonly used anti-inflammatory drug within a poly(amino acid) derivative fibrous mesh. *J Mol Liq* 322. https://doi.org/10.1016/j.molliq.2020.114575

33. Simões D, Miguel SP, Ribeiro MP, Coutinho P, Mendonça AG, Correia IJ (2018): Recent advances on antimicrobial wound dressing: A review. *Eur J Pharm Biopharm* 127: 130–141.

34. Zhang CL, Yu SH (2014): Nanoparticles meet electrospinning: Recent advances and future prospects. *Chem Soc Rev* 43: 4423–4448.

35. Okur ME, Karantas ID, Şenyiğit Z, Üstündağ Okur N, Siafaka PI (2020): Recent trends on wound management: New therapeutic choices based on polymeric carriers. *Asian J Pharm Sci* 15: 661–684.

36. Oliveira A, Simões S, Ascenso A, Reis CP (2020): Therapeutic advances in wound healing. *J Dermatolog Treat* 0: 1–21.

37. Pamu D, Tallapaneni V, Karri VVSR, Singh SK (2021): Biomedical applications of electrospun nanofibers in the management of diabetic wounds. *Drug Deliv Transl Res*. https://doi.org/10.1007/s13346-021-00941-6

38. Bates NM, Puy C, Jurney PL, McCarty OJT, Hinds MT (2020): Evaluation of the Effect of Crosslinking Method of Poly(Vinyl Alcohol) Hydrogels on Thrombogenicity. *Cardiovasc Eng Technol* 11: 448–455.

39. Deskins DL, Ardestani S, Young PP (2012): The polyvinyl alcohol sponge model implantation. *J Vis Exp* 1–6.

40. Molnár K, Voniatis C, Fehér D, Ferencz A, Fónyad L, Reiniger L, *et al.* (2018): Biocompatibility study of poly(Vinyl alcohol)-based electrospun scaffold for hernia repair. *Express Polym Lett* 12: 676–687.

41. Hirsch E, Vass P, Démuth B, Pethő Z, Bitay E, Andersen SK, *et al.* (2019): Electrospinning scale-up and formulation development of PVA nanofibers aiming oral delivery of biopharmaceuticals. *Express Polym Lett* 13: 590–603.

42. Lu T, Zou Q, Zhu KZ, Yuan DZ, Ma MX, Ye C (2021): Electrospun egg white/polyvinyl alcohol fiber dressing to accelerate wound healing. *J Polym Res* 28. https://doi.org/10.1007/s10965-021-02422-3

43. Hirsch E, Nacsa M, Ender F, Mohai M, Nagy ZK, Marosi GJ (2018): Preparation and characterization of biocompatible electrospun nanofiber scaffolds. *Period Polytech Chem Eng* 62: 510–518.

44. Duan B, Yuan XY, Zhu Y, Zhang YY, Li XL, Zhang Y, Yao KD (2006): A nanofibrous composite membrane of PLGA-chitosan/PVA prepared by electrospinning. *Eur Polym J* 42: 2013–2022.

45. Sipos E, Csatári T, Kazsoki A, Gergely A, Bitay E, Szabó Z-I, Zelkó R (2020): Preparation and Characterization of Fenofibrate-Loaded PVP Electrospun Microfibrous Sheets. *Pharmaceutics* 12: 612.

46. Sayed MM, Mousa HM, El-Aassar MR, El-Deeb NM, Ghazaly NM, Dewidar MM, Abdal-hay A (2019): Enhancing mechanical and biodegradation properties of polyvinyl alcohol/silk fibroin nanofibers composite patches for Cardiac Tissue Engineering. *Mater Lett* 255. https://doi.org/10.1016/j.matlet.2019.126510

47. Alharbi HF, Luqman M, Khalil KA, Elnakady YA, Abd-Elkader OH, Rady AM, *et al.* (2018): Fabrication of core-shell structured nanofibers of poly (lactic acid) and poly (vinyl alcohol) by coaxial electrospinning for tissue engineering. *Eur Polym J* 98: 483–491.

48. Cao L, Zhang F, Wang QG, Wu XF (2017): Fabrication of chitosan/graphene oxide polymer nanofiber and its biocompatibility for cartilage tissue engineering. *Mater Sci Eng C-MATERIALS Biol Appl* 79: 697–701.

49. Chahal S, Hussain FSJ, Yusoff MM, Rasad M, Kumar A (2017): Nanohydroxyapatite-coated hydroxyethyl cellulose/poly (vinyl) alcohol

electrospun scaffolds and their cellular response. *Int J Polym Mater Polym Biomater* 66: 115–122.

50. Wu ZJ, Kong B, Liu R, Sun W, Mi SL (2018): Engineering of Corneal Tissue through an Aligned PVA/Collagen Composite Nanofibrous Electrospun Scaffold. *NANOMATERIALS* 8. https://doi.org/10.3390/nano8020124

51. Afrash H, Nazeri N, Davoudi P, FaridiMajidi R, Ghanbari H (2021): Development of a Bioactive Scaffold based on NGF Containing PCL/Chitosan Nanofibers for Nerve Regeneration. *BIOINTERFACE Res Appl Chem* 11: 12606–12617.

52. Lan XZ, Liu YR, Wang YQ, Tian F, Miao XM, Wang H, Tang YD (2021): Coaxial electrospun PVA/PCL nanofibers with dual release of tea polyphenols and e-poly (L-lysine) as antioxidant and antibacterial wound dressing materials. *Int J Pharm* 601. https://doi.org/10.1016/j.ijpharm.2021.120525

53. Wang XS, Yang JM, Ding RJ, Liu XZ, Jiang XB, Yang ZJ, *et al.* (2021): Fabrication of a Polylactide-Glycolide/Poly-E-Electrospinning for Annulus Fibrosus Regeneration. *J Biomed Nanotechnol* 17: 873–888.

54. Wang CY, Wang H, Guo QP, Ang X, Li B, Han FX, *et al.* (2021): Bladder muscle regeneration enhanced by sustainable delivery of heparin from bilayer scaffolds carrying stem cells in a rat bladder partial cystectomy model. *Biomed Mater* 16. https://doi.org/10.1088/1748-605X/abf08b

55. Rezk AI, Kim KS, Kim CS (2020): Poly(epsilon-Caprolactone)/Poly(Glycerol Sebacate) Composite Nanofibers Incorporating Hydroxyapatite Nanoparticles and Simvastatin for Bone Tissue Regeneration and Drug Delivery Applications. *Polymers (Basel)* 12. https://doi.org/10.3390/polym12112667

56. Tao FH, Cheng YX, Tao H, Jin L, Wan ZH, Dai FF, *et al.* (2020): Carboxymethyl chitosan/sodium alginate-based micron-fibers fabricated by emulsion electrospinning for periosteal tissue engineering. *Mater Des* 194. https://doi.org/10.1016/j.matdes.2020.108849

57. Yang DC, Song ZC, Lin YJ, Dong WP, Fu SJ, Yang JJ, *et al.* (2020): Prevention of

intestinal adhesion and regeneration of abdominal wall tissue with meshes containing an electrostatically spun acellular dermal matrix (ADM)/silk fibroin (SF) fiber composite polypropylene mesh. *J Mech Behav Biomed Mater* 112. https://doi.org/10.1016/j.jmbbm.2020.104087

58. Molnar K, Jedlovszky-Hajdu A, Zrinyi M, Jiang S, Agarwal S (2017): Poly(amino acid)-Based Gel Fibers with pH Responsivity by Coaxial Reactive Electrospinning. *Macromol Rapid Commun* 38: 1–5.

59. Molnar K, Juriga D, Nagy PM, Sinko K, Jedlovszky-Hajdu A, Zrinyi M (2014): Electrospun poly(aspartic acid) gel scaffolds for artificial extracellular matrix. *Polym Int* 63: 1608–1615.

60. Nguyen MP, Nguyen MH, Kim J, Kim D (2020): Encapsulation of superparamagnetic iron oxide nanoparticles with polyaspartamide biopolymer for hyperthermia therapy. *Eur Polym J* 122: 109396.

61. Krisch E, Gyarmati B, Szilágyi A (2017): Preparation of pH-responsive poly(Aspartic acid) nanogels in inverse emulsion. *Period Polytech Chem Eng* 61: 19–26.

62. Xin X, He Z, Hill MR, Niedz RP, Jiang X, Sumerlin BS (2018): Efficiency of Biodegradable and pH-Responsive Polysuccinimide Nanoparticles (PSI-NPs) as Smart Nanodelivery Systems in Grapefruit: In Vitro Cellular Investigation. *Macromol Biosci* 18: 1–8.

63. Jalalvandi E, Shavandi A (2018): Polysuccinimide and its derivatives: Degradable and water soluble polymers (review). *Eur Polym J* 109: 43–54.

64. Molnar K, Varga R, Jozsa B, Barczikai D, Krisch E, Nagy KS, *et al.* (2020): Investigation of the cytotoxicity of electrospun polysuccinimide-based fiber mats. *Polymers (Basel)* 12: 1–11.

65. Lu C, Wang X, Wu G, Wang J, Wang Y, Gao H, Ma J (2014): An injectable and biodegradable hydrogel based on poly(α,β- aspartic acid) derivatives for localized drug delivery. *J Biomed Mater Res - Part A* 102: 628–638.

66. Cho W (2020): A new biocompatible coating for bioanalytical devices based on PSI (polysuccinimide). *ETD Collect Purdue Univ*.

67. Gyarmati B, Mammadova A, Barczikai D, Stankovits G, Misra A, Alavijeh MS, *et al.* (2021): Side group ratio as a novel means to tune the hydrolytic degradation of thiolated and disulfide cross-linked polyaspartamides. *Polym Degrad Stab* 188. https://doi.org/10.1016/j.polymdegradstab.2021.109577

68. Németh C, Gyarmati B, Gacs J, Salakhieva D V., Molnár K, Abdullin T, *et al.* (2020): Fast dissolving nanofibrous matrices prepared by electrospinning of polyaspartamides. *Eur Polym J* 130. https://doi.org/10.1016/j.eurpolymj.2020.109624

69. Molnar K, Voniatis C, Feher D, Szabo G, Varga R, Reiniger L, *et al.* (2021): Poly(amino acid) based fibrous membranes with tuneable in vivo biodegradation. *PLoS One* 16: e0254843.

70. Molnár K (2018): *Development of Biocompatible Polymer Based Fibrous Materials for Medical and Biological Use*. Semmelweis University.

71. Németh C (2021): *Poly(Aspartic Acid) Derivatives for Gastrointestinal Drug Delivery*. Budapest University of Technology and Economics.

72. Jalalvandi E, Shavandi A (2018): Polysuccinimide and its derivatives: Degradable and water soluble polymers (review). *Eur Polym J* 109: 43–54.

73. Tudorachi N, Chiriac AP (2011): TGA/FTIR/MS study on thermal decomposition of poly(succinimide) and sodium poly(aspartate). *Polym Test* 30: 397–407.

74. Schiff H (1897): Ueber Polyaspartsäuren. *Berichte der Dtsch Chem Gesellschaft* 30: 2449–2459.

75. Neri P, Antoni G, Benvenuti F, Cocola F, Gazzei G (1973): Synthesis of .alpha.,.beta.-poly [(2-hydroxyethyl)-DL-aspartamide], a newplasma expander. *J Med Chem* 16: 893–897.

76. Chai C, Xu Y, Shi S, Zhao X, Wu Y, Xu Y, Zhang L (2018): Functional polyaspartic acid derivatives as eco-friendly corrosion inhibitors for mild steel in 0.5 M H2SO4 solution. *RSC Adv* 8: 24970–24981.

77. Fu L, Lv J, Zhou L, Li Z, Tang M, Li J (2020): Study on corrosion and scale inhibition mechanism of polyaspartic acid grafted β-cyclodextrin. *Mater Lett* 264: 127276.

78. Zakharchenko S, Sperling E, Ionov L (2011): Fully biodegradable self-rolled polymer tubes: A candidate for tissue engineering scaffolds. *Biomacromolecules* 12: 2211–2215.

79. Cipitria A, Skelton A, Dargaville TR, Dalton PD, Hutmacher DW (2011): Design, fabrication and characterization of PCL electrospun scaffolds - A review. *J Mater Chem* 21: 9419–9453.

80. Asvar Z, Mirzaei E, Azarpira N, Geramizadeh B, Fadaie M (2017): Evaluation of electrospinning parameters on the tensile strength and suture retention strength of polycaprolactone nanofibrous scaffolds through surface response methodology. *J Mech Behav Biomed Mater* 75: 369–378.

81. Beachley V, Wen X (2009): Effect of electrospinning parameters on the nanofiber diameter and length. *Mater Sci Eng C* 29: 663–668.

82. John Wiley & Sons (2016): *Ullmann's Polymers and Plastics : Products and Processes.*

83. Haider A, Haider S, Kang IK (2018): A comprehensive review summarizing the effect of electrospinning parameters and potential applications of nanofibers in biomedical and biotechnology. *Arab J Chem* 11: 1165–1188.

84. Zhao H, Chi H (2018): Electrospun Bead-on-String Fibers: Useless or Something of Value? *Nov Asp Nanofibers*. https://doi.org/10.5772/intechopen.74661

85. Zuo W, Zhu M, Yang W, Yu H, Chen Y, Zhang Y (2005): Experimental study on relationship between jet instability and formation of beaded fibers during

electrospinning. *Polym Eng Sci* 45: 704–709.

86. Juhasz AG, Molnar K, Idrissi A, Jedlovszky-Hajdu A (2020): Salt induced fluffy structured electrospun fibrous matrix. *J Mol Liq* 312: 113478.

87. Huan S, Liu G, Han G, Cheng W, Fu Z, Wu Q, Wang Q (2015): Effect of experimental parameters on morphological, mechanical and hydrophobic properties of electrospun polystyrene fibers. *Materials (Basel)* 8: 2718–2734.

88. Yang GZ, Li HP, Yang JH, Wan J, Yu DG (2017): Influence of Working Temperature on The Formation of Electrospun Polymer Nanofibers. *Nanoscale Res Lett* 12. https://doi.org/10.1186/s11671-016-1824-8

89. Ghobeira R, Asadian M, Vercruysse C, Declercq H, De Geyter N, Morent R (2018): Wide-ranging diameter scale of random and highly aligned PCL fibers electrospun using controlled working parameters. *Polymer (Guildf)* 157: 19–31.

90. Hardick O, Stevens B, Bracewell DG (2011): Nanofibre fabrication in a temperature and humidity controlled environment for improved fibre consistency. *J Mater Sci* 46: 3890–3898.

91. Ramazani S, Karimi M (2014): Investigating the influence of temperature on electrospinning of polycaprolactone solutions. *E-Polymers* 14: 323–333.

92. Noriega SE, Hasanova GI, Schneider MJ, Larsen GF, Subramanian A (2012): Effect of fiber diameter on the spreading, proliferation and differentiation of chondrocytes on electrospun chitosan matrices. *Cells Tissues Organs* 195: 207–221.

93. Chen M, Patra PK, Warner SB, Bhowmick S (2007): Role of fiber diameter in adhesion and proliferation of NIH 3T3 fibroblast on electrospun polycaprolactone scaffolds. *Tissue Eng* 13: 579–587.

94. Christopherson GT, Song H, Mao HQ (2009): The influence of fiber diameter of electrospun substrates on neural stem cell differentiation and proliferation. *Biomaterials* 30: 556–564.

95. Yu C, Xing M, Wang L, Guan G (2020): Effects of aligned electrospun fibers with different diameters on hemocompatibility, cell behaviors and inflammation in vitro. *Biomed Mater* 15. https://doi.org/10.1088/1748-605X/ab673c

96. Adelnia H, Blakey I, Little PJ, Ta HT (2019): Hydrogels Based on Poly(aspartic acid): Synthesis and Applications. *Frontiers in Chemistry*, vol. 7. pp 1–14.

97. Jiang J, Zheng G, Wang X, Li W, Kang G, Chen H, *et al.* (2020): Arced Multi-Nozzle Electrospinning Spinneret for High-Throughput Production of Nanofibers. *Micromachines* , vol. 11. https://doi.org/10.3390/mi11010027

98. Wei L, Sun R, Liu C, Xiong J, Qin X (2019): Mass production of nanofibers from needleless electrospinning by a novel annular spinneret. *Mater Des* 179: 107885.

99. Ranjbari E, Bazgir S, Shirazi MMA (2020): Needleless electrospinning of poly(acrylic acid) superabsorbent: Fabrication, characterization and swelling behavior. *Polym Test* 84: 106403.

100. Acik G, Altinkok C (2019): Polypropylene microfibers via solution electrospinning under ambient conditions. *J Appl Polym Sci* 136: 48199.

101. Pedicini A, Farris RJ (2003): Mechanical behavior of electrospun polyurethane. *Polymer (Guildf)* 44: 6857–6862.

102. Wong SC, Baji A, Leng S (2008): Effect of fiber diameter on tensile properties of electrospun poly(ε-caprolactone). *Polymer (Guildf)* 49: 4713–4722.

103. Nitti P, Gallo N, Natta L, Scalera F, Palazzo B, Sannino A, Gervaso F (2018): Influence of nanofiber orientation on morphological and mechanical properties of electrospun chitosan mats. *J Healthc Eng* 2018. https://doi.org/10.1155/2018/3651480

104. Deeken CR, Lake SP (2017): Mechanical properties of the abdominal wall and biomaterials utilized for hernia repair. *J Mech Behav Biomed Mater* 74: 411–427.

105. Pott PP, Schwarz MLR, Gundling R, Nowak K, Hohenberger P, Roessner ED

(2012): Mechanical Properties of Mesh Materials Used for Hernia Repair and Soft Tissue Augmentation. *PLoS One* 7: 1–10.

106. Hjort H, Mathisen T, Alves A, Clermont G, Boutrand JP (2012): Three-year results from a preclinical implantation study of a long-term resorbable surgical mesh with time-dependent mechanical characteristics. *Hernia* 16: 191–197.

107. Zhu G, Zhao LY, Zhu LT, Deng XY, Chen WL (2017): Effect of Experimental Parameters on Nanofiber Diameter from Electrospinning with Wire Electrodes. *IOP Conf Ser Mater Sci Eng* 230. https://doi.org/10.1088/1757-899X/230/1/012043

108. Hong Y, Huber A, Takanari K, Amoroso NJ, Hashizume R, Badylak SF, Wagner WR (2011): Mechanical properties and in vivo behavior of a biodegradable synthetic polymer microfiber-extracellular matrix hydrogel biohybrid scaffold. *Biomaterials* 32: 3387–3394.

109. Costa A, Naranjo JD, Turner NJ, Swinehart IT, Kolich BD, Shaffiey SA, *et al.* (2016): Mechanical strength vs. degradation of a biologically-derived surgical mesh over time in a rodent full thickness abdominal wall defect. *Biomaterials* 108: 81–90.

110. Hegedus O, Juriga D, Sipos E, Voniatis C, Juhász Á, Idrissi A, *et al.* (2019): Free thiol groups on poly(aspartamide) based hydrogels facilitate tooth-derived progenitor cell proliferation and differentiation. *PLoS One* 14: 1–20.

111. Juriga D, Sipos E, Hegedus O, Varga G, Zrínyi M, Nagy KS, Jedlovszky-Hajdú A (2019): Fully amino acid-based hydrogel as potential scaffold for cell culturing and drug delivery. *Beilstein J Nanotechnol* 10: 2579–2593.

112. Chakrapani VY, Sampath Kumar TS, Raj DK, Kumary T V. (2017): Electrospun cytocompatible polycaprolactone blend composite with enhanced wettability for bone tissue engineering. *J Nanosci Nanotechnol* 17: 2320–2328.

113. Teodorescu M, Bercea M, Morariu S (2019): Biomaterials of PVA and PVP in medical and pharmaceutical applications: Perspectives and challenges. *Biotechnol*

Adv 37: 109–131.

114. Malikmammadov E, Tanir TE, Kiziltay A, Hasirci V, Hasirci N (2018): PCL and PCL-based materials in biomedical applications. *Journal of Biomaterials Science, Polymer Edition*, vol. 29. Taylor & Francis. https://doi.org/10.1080/09205063.2017.1394711

115. Permyakova ES, Kiryukhantsev-Korneev P V., Gudz KY, Konopatsky AS, Polčak J, Zhitnyak IY, *et al.* (2019): Comparison of different approaches to surface functionalization of biodegradable polycaprolactone scaffolds. *Nanomaterials* 9. https://doi.org/10.3390/nano9121769

116. Dreifke MB, Jayasuriya AA, Jayasuriya AC (2015): Current wound healing procedures and potential care. *Mater Sci Eng C* 48: 651–662.

117. Jones K (2015): Fibrotic Response to Biomaterials and all Associated Sequence of Fibrosis. In: Badylak SF, editor. *Host Response to Biomaterials: The Impact of Host Response on Biomaterial Selection*. Oxford: Academic Press, pp 189–237.

118. Guarino V, Gentile G, Sorrentino L, Ambrosio L (2017): Polycaprolactone: Synthesis, Properties, and Applications. *Encyclopedia of Polymer Science and Technology*. https://doi.org/10.1002/0471440264.pst658

119. Díaz E, Sandonis I, Valle MB (2014): In vitro degradation of poly(caprolactone)/nHA composites. *J Nanomater* 2014. https://doi.org/10.1155/2014/802435

120. Akbarzadeh M, Pezeshki-Modaress M, Zandi M (2019): Biphasic, tough composite core/shell PCL/PVA-GEL nanofibers for biomedical application. *J Appl Polym Sci* 48713: 1–12.

121. Rubert M, Dehli J, Li YF, Taskin MB, Xu R, Besenbacher F, Chen M (2014): Electrospun PCL/PEO coaxial fibers for basic fibroblast growth factor delivery. *J Mater Chem B* 2: 8538–8546.

122. Hajdú A, Tombácz E, Illés E, Bica D, Vékás L (2008): Magnetite nanoparticles

stabilized under physiological conditions for biomedical application. *Prog Colloid Polym Sci* 135: 29–37.

123. Tombácz E, Illés E, Majzik A, Hajdú A, Rideg N, Szekeres M (2007): Ageing in the inorganic nanoworld: Example of magnetite nanoparticles in aqueous medium. *Croat Chem Acta* 80: 503–515.

124. Rashid H, Mansoor MA, Haider B, Nasir R, Abd Hamid SB, Abdulrahman A (2020): Synthesis and characterization of magnetite nano particles with high selectivity using in-situ precipitation method. *Sep Sci Technol* 55: 1207–1215.

125. Kim H, Kim D (2012): Polysuccinimide graft copolymer nano aggregates encapsulating magnetites for imaging probe. *Macromol Res* 20: 259–265.

126. Vega-Chacón J, Arbeláez MIA, Jorge JH, Marques RFC, Jafelicci M (2017): pH-responsive poly(aspartic acid) hydrogel-coated magnetite nanoparticles for biomedical applications. *Mater Sci Eng C* 77: 366–373.

127. Nejaddehbashi F, Hashemitabar M, Bayati V, Moghimipour E, Movaffagh J, Orazizadeh M, Abbaspour M (2020): Incorporation of silver sulfadiazine into an electrospun composite of polycaprolactone as an antibacterial scaffold for wound healing in rats. *Cell J* 21: 379–390.

10. Bibliography of the candidate's publications

Publications relevant to the Thesis

I. **C. Voniatis**, L. Balsevicius, D. Barczikai, D. Juriga, A. Takács, L. Kishida, K. Nagy, A. Jedlovszky-Hajdu*, Co-electrospun polysuccinimide/poly(vinyl alcohol) composite meshes for tissue engineering, J. Mol. Liq. 306 (2020). https://doi.org/10.1016/j.molliq.2020.112895. (Impact factor: 6.165)

II. **C. Voniatis**, D. Barczikai, G. Gyulai, A. Jedlovszky-Hajdu*, Fabrication and characterisation of electrospun Polycaprolactone/Polysuccinimide composite meshes, J. Mol. Liq. 323 (2021). https://doi.org/10.1016/j.molliq.2020.115094 (Impact factor: 6.165)

III. K. Molnar, **C. Voniatis**, D. Feher, G. Szabo, R. Varga, L. Reiniger, D. Juriga, Z. Kiss, E. Krisch, G. Weber, A. Ferencz, G. Varga, M. Zrinyi, K.S. Nagy, A. Jedlovszky-Hajdu*, Poly(amino acid) based fibrous membranes with tuneable in vivo biodegradation, PLoS One. 16 (2021) e0254843. https://doi.org/10.1371/journal.pone.0254843 (Impact factor: 3.240)

IV. **C. Voniatis**, R. Gottscháll, D. Barczikai, G. Szabó, A. Jedlovszky-Hajdu*, Enhancing critical features of poly(amino acid) based meshes, J. Appl. Polym. Sci. 139 (2022) 51933. https://doi.org/https://doi.org/10.1002/app.51933. (Impact factor: 3.125)

Publications not relevant to the Thesis

1. P. Ádám, O. Temesi, Z. Dankházi, **C. Voniatis**, J. Rohonczy, K. Sinkó*, Various colloid systems for drawing of aluminum oxide fibers, Ceram. Int. 48 (2022) 5499–5508. https://doi.org/https://doi.org/10.1016/j.ceramint.2021.11.094 (Impact factor: 4.527)

2. **C. Voniatis**, S. Bánsághi, A. Ferencz, T. Haidegger*, A large-scale investigation of alcohol-based handrub (ABHR) volume: hand coverage correlations utilizing an innovative quantitative evaluation system, Antimicrob. Resist. Infect. Control. 10 (2021) 1–10. https://doi.org/10.1186/s13756-021-00917-8 (Impact factor: 4.887)

3. D. Fehér*, A. Ferencz, G. Szabó, K. Juhos, D. Csukás, **C. Voniatis**, L. Reininger, K. Molnár, A. Jedlovszky-Hajdú, G. Wéber, Early and late effects of absorbable poly(vinyl alcohol) hernia mesh to tissue reconstruction, IET Nanobiotechnology. 15 (2021) 565–574. https://doi.org/https://doi.org/10.1049/nbt2.12015 (Impact factor: 1.847)

4. O. Hegedus, D. Juriga, E. Sipos, **C. Voniatis**, Á. Juhász, A. Idrissi, M. Zrínyi, G. Varga, A. Jedlovszky-Hajdú, K.S. Nagy*, Free thiol groups on poly(aspartamide) based hydrogels facilitate tooth-derived progenitor cell proliferation and differentiation, PLoS One. 14 (2019) 1–20. https://doi.org/10.1371/journal.pone.0226363 (Impact factor: 2.740)

5. K. Molnar, **C. Voniatis**, D. Feher, G. Szabo, R. Varga, L. Reiniger, D. Juriga, Z. Kiss, E. Krisch, G. Weber, A. Ferencz, G. Varga, M. Zrinyi, K.S. Nagy, A. Jedlovszky-Hajdu*, Poly(amino acid) based fibrous membranes with tuneable in vivo biodegradation, PLoS One. 16 (2021) e0254843. https://doi.org/10.1371/journal.pone.0254843 (Impact factor: 2.875)

Note: Bold: PhD Candidate:, Underlined: First author:, Star*: Corresponding author:

11. Acknowledgments

First of all, I would like to express an innumerable amount of gratitude to my supervisors Dr. Angéla Jedlovszky-Hajdú and Dr. Andrea Ferencz for the endless guidance and support, for their precious time they spend on me and showing me how to improve.

I am very much indebted to Dóra Barczikai for quite a number of things, amongst others the scanning electron microscopy, help with the statistical analysis, but more importantly her ability to challenge me in every way possible which always pushed me forwards.

I also would like to thank Ramóna Gottschall, Olivér Závoti and Lukas Balsevicius for helping test my hypotheses and performing the follow up experiments. I also would like to thank Tamás Veres without whom, nanoparticle synthesis and incorporation would not have been possible.

I am especially grateful to Krisztina Toth and Kristina S. Nagy, as without them the cell studies wouldn't be in this work.

I would also like to thank Ibolya Schum and Karolina Csépke for all the help they provided during the animal studies, and for taking care of my animals when couldn't.

This work was possible with the help of experts from other departments and universities I am tremendously thankful.to Angéla Takacs and László Kőhidai form the Oral Biology Department, to Zoltán Varga and Andrea Kóvacs from the department of Pharmacology to Péter Adam and Gergő Gyulai from the Eötvös Loránd University and Kolos Mólnar from the Budapest University of Technology And Economics

Finally, I am so grateful to my family for the courage and persistence, the hopefulness and cheerfulness and for the love and support they gifted me since the very beginning.

Financial support

EFOP-3.6.3-VEKOP-16-2017-00009, Az orvos-, egészségtudományi- és gyógyszerészképzés tudományos műhelyeinek fejlesztése.